# Design and Control of a Large Modular Robot Hexapod

Matt Martone

CMU-RI-TR-19-79

November 22, 2019



The Robotics Institute
School of Computer Science
Carnegie Mellon University
Pittsburgh, PA

**Thesis Committee:**
Howie Choset, *chair*
Matt Travers
Aaron Johnson
Julian Whitman

*Submitted in partial fulfillment of the requirements*
*for the degree of Master of Science in Robotics.*

*To all my mentors:*
*past and future*

# Abstract

Legged robotic systems have made great strides in recent years, but unlike wheeled robots, limbed locomotion does not scale well. Long legs demand huge torques, driving up actuator size and onboard battery mass. This relationship results in massive structures that lack the safety, portability, and controllability of their smaller limbed counterparts. Innovative transmission design paired with unconventional controller paradigms are the keys to breaking this trend. The Titan 6 project endeavors to build a set of self-sufficient modular joints unified by a novel control architecture to create a spiderlike robot with two-meter legs that is robust, field-repairable, and an order of magnitude lighter than similarly sized systems. This thesis explores how we transformed desired behaviors into a set of workable design constraints, discusses our prototypes in the context of the project and the field, describes how our controller leverages compliance to improve stability, and delves into the electromechanical designs for these modular actuators that enable Titan 6 to be both light and strong.

# Acknowledgments

# Funding

x

# Contents

*When this thesis is viewed as a PDF, the page header is a link to this Table of Contents.*

# List of Figures

# List of Tables

# Chapter I

# Introduction

The invention of the wheel over five thousand years ago was a turning point in human civilization and technology, one that continues to drive the development of infrastructure to this day [1]. Even with vast road networks, half of the terrain on Earth is inaccessible to wheeled systems, which fail without traction, a consistent path of support, sufficient ground clearance, or in the presence of large obstacles [2]. Years of engineering and optimization in pressurized tires, passive suspensions, and tank treads have refined the wheel for rugged off-road mobility, but where wheels fail, walking succeeds.

Many of the benefits offered by limbed locomotion for automated exploration of unstructured terrain stem from the ability to choose advantageous footholds rather than requiring a continuous rolling path. The traversable terrain for a wheeled system is limited by the worst features along a given path; i.e. a single gap, ledge, or protruding obstacle larger than the wheel diameter will prevent forward motion. However, a legged system can opportunistically choose its ground contacts, so it is limited by the best possible features along a given path [3]. This means that a legged system can straddle chasms, climb stairs, and step over hazards to reach its goal much better than a wheeled system of the same size. As long as there are enough discrete footholds within the reachable workspace of the legs, arbitrarily complex terrain becomes navigable. Additionally, when crossing terrain with fragile formations or vegetation, rolling locomotion can be mutually destructive to the environment and the drivetrain. By choosing foot placement to avoid plant life or interesting ground

1

features, legged explorers are much more valuable in minimally-invasive study of densely populated ecosystems.

Modern field robotics are generally wheeled or tracked systems, but after four decades of development, platforms that instead rely on legged locomotion are beginning to leave the laboratory. These walking robots have shown resilience to obstacles through mechanically intelligent design [4] or robust control architecture [5], but can still be stymied by obstacles larger than the leg or flooded areas expected at disaster sites or remote biomes. Navigating these conditions requires high ground clearance, and a wide base of support, and an expansive leg workspace to reach for sparsely available footholds; motivating the design of long-legged sprawled-posture hexapods such as AMBLER [6] and ATHLETE [7]. However, these behemoths weigh in at 2500 kg and 850 kg respectively, making their deployment impractically slow and dependent on vehicles to transport the robots to their starting points. Placing the robot as close as possible to the goal before deploying under its own power in a search and rescue scenario can save critically valuable time, so ease of transport and setup by available teams must be prioritized [8]. Yet even a robotic system optimized for rough terrain locomotion and deployability won't be selected for a rescue team's limited kit if there isn't a robust methodology for repairs in the field. Modular architectures such as those demonstrated on the Unified Snake [9] and RoboSimian [10] simplify field repairs with minimal time, expertise, and tooling required.

Here I present Titan 6 (a concept model of which is shown in Figure 1.1), a large, lightweight, modular hexapod designed for maximum terrain navigability which can be easily deployed and repaired deep in the field. By developing a long-legged system with such strict mass requirements, we introduce adverse mechanical properties such as flexible body structures and actuators working near saturation limits, thus invalidating certain assumptions fundamental to existing legged robot control. Titan 6 relies on dynamic controllers and specialized gait design to traverse complex environments and perform mapping or reconnaissance tasks with human supervision. Titan 6 was designed with a modular approach to improve field repairability and reconfigurability, even though a monolithic solution would be much easier to design. In this thesis I explore the advantages and disadvantages of such a system, delve into mechanical design and controls solutions, present results of experiments, and propose a path

forward for future generations of giant-spider walking robots.[1]
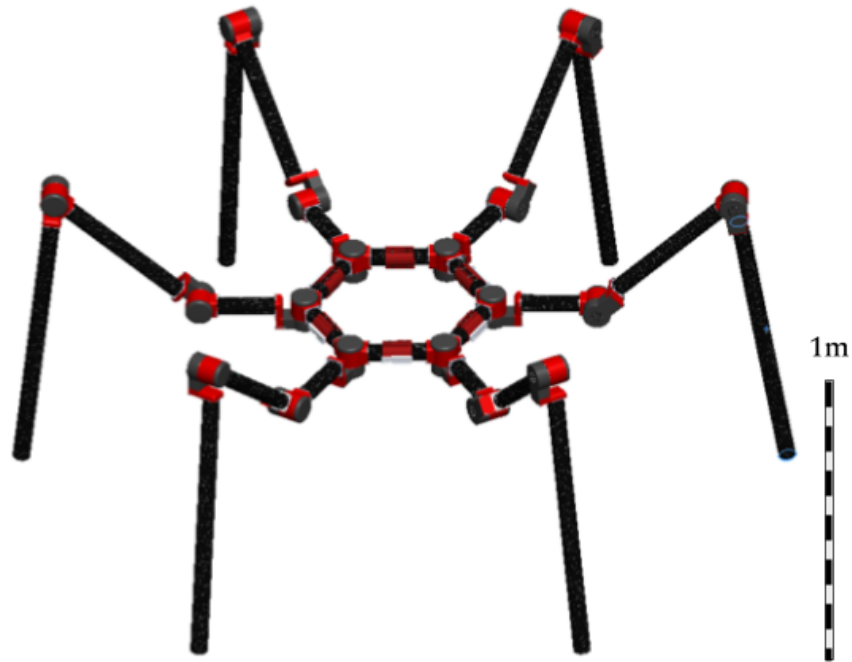


Figure 1.1: A conceptual model of the Titan 6 robot showing approximate scale and modular design.

# 1.    Survey of Legged Robotic Systems

Evolution has produced a plethora of biological legged systems optimized for a spectrum of locomotion strategies, inspiring roboticists to respond with a similarly diverse array of walking robots. Insects [4], birds [12], reptiles [13], and mammals [14] have all served as inspiration for robotic locomotion, and legged robots are showing potential for locomotion across natural and man-made surfaces. Now these robots in turn serve as inspiration for Titan 6, providing lessons learned and results to inform our design of the electromechanical system and the control architecture.

---

[1]While Titan 6 has six legs rather than eight, it is biomechanically most similar to a spider due to the ratio of limbs to body size and radial hips located on the cephalothorax. Bioinspiration for Titan 6 came from *Artema atlanta* of the Pholcid family of arachnids, commonly known as "cellar spiders" or "daddy long-legs" [11].

Legged robots are easily categorized by number of legs, intended use, weight class, or actuation method, but in the context of Titan 6, it is most prudent to classify these systems by the stability criteria of their motion. While most can walk with a variety of footfall patterns, their motions are inherently either statically stable or dynamically stable.

## Quasi-Static Walkers

Statically stable systems tend to have many points of ground contact that are spread over a wide area. This provides a large support polygon for stabilizing the body, even when some of the legs are in swing. These robots rely on the fundamental assumption that the support provided by the ground reaction force to the feet is constant over time and can be adequately resisted by the leg actuators. This leads to the conclusion that most gaits employed by these systems can be generated kinematically frame-by-frame, where the robot's state at any time is independent of prior time steps and the state is stable if the center of mass lies in the support polygon. While Titan 6 is geometrically akin to these systems (shown in Figure 1.2), early iterations use a fundamentally different control scheme because the suspended body is subject to destabilizing oscillations while a subset of the legs are in swing, making the motions time-dependent and quasi-dynamic.
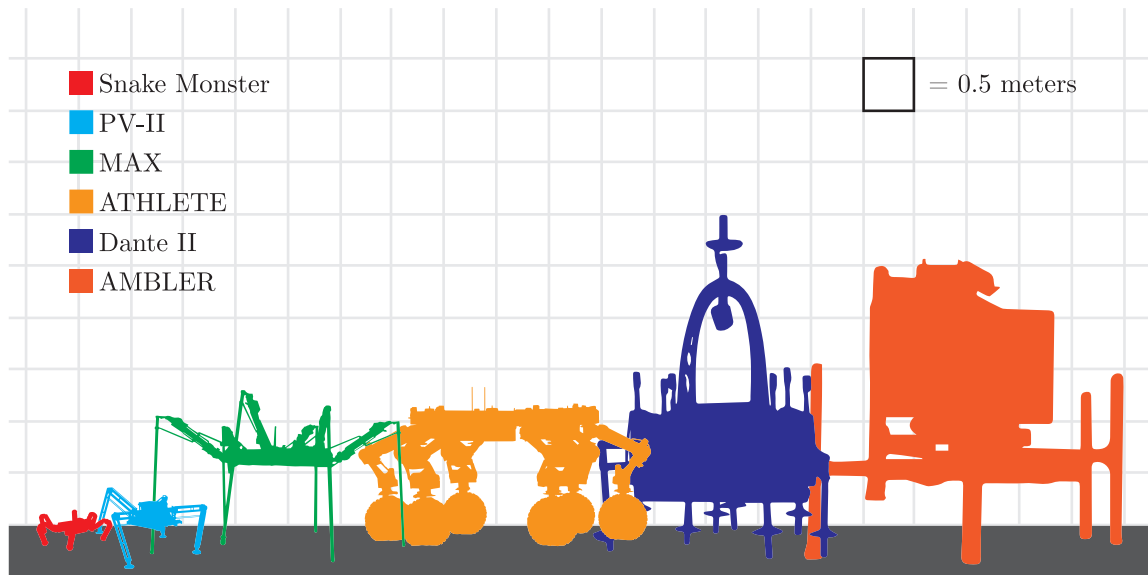


Figure 1.2: Size comparison of sprawled posture walking robots.

Table 1.1: Quasi-Static Walking Robots Considered During Titan 6 Design

| Name | Year | Legs | Length* (m) | Mass (kg) | Speed (m/s) | Use Case |
|---|---|---|---|---|---|---|
| PV-II [15] | 1979 | 4 | 0.9 | $10^\dagger$ | Unavailable | Climbing Stairs |
| AMBLER [6] | 1989 | 6 | 2.5 | 2500 | 0.0067 | Planetary Exploration |
| Dante II [16] | 1999 | 8 | 1.31 | 770 | 0.01 | Rappelling Slopes |
| ATHLETE [7] | 2009 | 6 | 2.08 | 850 | $0.9^\ddagger$ | Personnel Transport |
| Snake Monster [17] | 2015 | $6^\S$ | 0.43 | 8 | 0.05 | Modularity Research |
| MAX [18] | 2017 | 6 | 2.25 | 60 | 0.073 | Ultralight Locomotion |

* The lengths provided here represent the sum of the individual link lengths of each leg.
$\dagger$ PV-II uses a tether for off-board power and control so this figure does not account for the full mass.
$\ddagger$ ATHLETE uses wheeled feet to achieve this speed on flat ground, its ambulatory speed is significantly slower.
$\S$ Snake Monster has modular legs which can have variable multiplicity and length, the case considered here is its usual rough-terrain walking configuration.

## Dynamic Hoppers and Runners

Dynamic robots are in a constant state of falling over; executing gaits that take their inertial models into account to use their legs to push off and catch themselves repeatedly. These robots must be considered in the context of their prior actions and current velocities to determine the stability of a motion. Some dynamic systems are unable to form a stable support polygon in any upright configuration, so they must rely on in-place gaits to balance [19]. With dynamic balancing fewer legs are needed and the robot can use reactive control to reject disturbances or correct error. Additional legs improve payload capacity or allow for quasi-static gaits specific to the use case. Titan 6 has enough legs to maintain static stability, but requires a similar reactive control scheme while walking as it is executing a controlled fall during a step, discussed further in Chapter V.

Table 1.2: Dynamic Running Robots Considered During Titan 6 Design

| Name | Year | Legs | Length[*] (m) | Mass (kg) | Speed (m/s) | Use Case |
|---|---|---|---|---|---|---|
| Raibert Hopper [20] | 1983 | 1 | 0.5 | 17[†] | 2.2 | Balance and Hopping |
| BigDog [5] | 2008 | 4 | 1.2 | 109 | 2.0 | Superior Outdoor Locomotion |
| StarlETH [21] | 2012 | 4 | 0.49 | 23 | 0.7 | Versatile Locomotion |
| MIT Cheetah [14] | 2013 | 4 | 0.7 | 33[†] | 12.6 | Fast Running |
| Atlas [22] | 2015 | 2 | 0.94 | 155 | 0.4 | DARPA Robotics Challenge |
| ATRIAS [19] | 2015 | 2 | 1.25 | 62 | 5.7 | Simplified Bipedal Walking |
| Spot [23] | 2016 | 4 | 1.1 | 25 | 1.6 | Inspection and Security |

[*] The lengths provided here represent the sum of the individual link lengths of each leg.
[†] The Raibert Hopper and the MIT Cheetah used tethers for off-board power and control so this figure does not account for the full mass.

## Hybrid Systems

Rugged legged robots with low centers of mass are much less concerned with balancing in an upright posture and can fall outside of this classification model. RHex is a prime example of such a system; as a hexapod primarily utilizing an alternating tripod gait, RHex is statically stable [24]. Despite its sufficient polygon of support, periods of flight in the gait cycle and distinct landing and push off phases of contact make its motion markedly dynamic. The Spring Loaded Inverted Pendulum Model is similar to the dynamic control of the Raibert Hopper, and the six legs act in tripods as two virtual legs except when steering [25]. However, dynamic gaits are not always used in extremely rough terrain, where slower gait options use the low body for ground contact to scramble over obstacles [26]. The exhibition of dynamic gait behaviors with statically-stable body manipulability indicate that both RHex and Titan 6 are quasi-dynamic hybrids. Indeed, it is clear from the above prior work that both the large leg workspace of a sprawled-posture static system and the speed of a dynamic system are necessary to meet mobility requirements set for Titan 6.

# 2.   Titan 6 Project Requirements

Titan 6 was initially proposed with a set of outcome expectations ranging from critical to reach goals [27]. Based on results of early experiments, the team solidified these goals into a list of requirements, which narrowed the design space, but were key to realizing a large, fully-modular, deployable hexapod. Below is a summary of the most influential system requirements realized as technical specifications.

**Architecture:** The system must be a two meter tall, sprawled-posture hexapod capable of rough terrain locomotion with a small payload. The nominal height of the system can be less than two meters during locomotion, but must be able to raise the body up to this height to gain vantage of its surroundings. The robot must be capable of stepping over barriers at least one meter high and crouching behind barriers with all components fully hidden below one meter. This is largely a function of the leg kinematic design, discussed in Chapter II. The system must be strong enough to carry a set of cameras and LIDAR for observation, localization, and mapping, which is estimated to be 2.5 kg.

**Modularity:** The robot's actuation must be fully modular, with as few distinct components as possible to minimize number of spare parts needed to repair the robot in the field. The legs must be identical and symmetric and all actuators must be identical and self-sufficient. Each actuator must have its own computation and power source such that there are no central points of potential electrical failure. This distributed power and control ensures that a single failure in any actuator circuit would be contained to that joint without crippling the rest of the system. Actuator or leg replacement must take less than two minutes. A reach goal includes designing a quick-connect actuator that can be swapped with no tools required.

**Deployability:** In addition to robust locomotion at 1.5 $\frac{m}{s}$, the system must be field deployable by a team with intermediate technical knowledge and limited human carrying capacity. The system must disassemble or fold into containers with total volume less than 1.0 m$^3$ and mass less than 70 kg total. The system should be safe for nearby operators such that no exposed component should exceed 70 °C, generate live electrical current, or be sharp. Pinch points should be clearly annotated and avoided where possible. The system must be protected from expected outdoor hazards and rated at least IP52.

# 3.  Overview of Modular Actuators

Modular actuators are the key to building reconfigurable systems quickly and iterating rapidly towards an optimal solution [28]. This has been the philosophy of the Biorobotics Lab since the development of the modular architectures used in early snake robots; eventually leading to the Snake Monster robot[17]. A similar approach has been successfully employed by JPL's Robotic Vehicles Group to build RoboSimian [10], Surrogate [29], and Ice Worm [30] using interchangeable joint modules.

A highly articulated robotic system takes years to design and build using conventional, monolithic design principles, and mechanical augmentations or configuration updates take months. By developing a consistent set of modules that use a unifying electrical architecture, a common communication protocol, and a standardized Application Programming Interface (API), joints can be added or removed from a robot with minimal hassle, reducing reconfiguration or repair times from week scale to minute scale. Once an architecture is established, a library of both passive and active modules can be developed and integrated seamlessly into the system. While Titan 6 is modular primarily for expeditious repairs, reconfiguring the robot by altering link lengths for specific deployments could improve performance over the generalized form presented here.

| | USnake | Hebi X-Actuator | Titan 6 Joint |
|---|---|---|---|
| Actuation + Sensing | ✓ | ✓ | ✓ |
| Computation + Control | ✗ | ✓ | ✓ |
| Power | ✗ | ✗ | ✓ |
| Peak Torque | 13 Nm (115 lb-in) | 38 Nm (336 lb-in) | 100 Nm (885 lb-in) |

Figure 1.3: Comparison of existing modular actuator self-sufficiencies with desired capabilities for a Titan-6 joint.

The main drawback of modular architectures is the addition of redundant mass. Each module requires a mechanical connection and an electrical connection, which can cost more volume and weight than a streamlined system with integrated actuators. Modules can have varying degrees of self-sufficiency as illustrated in Figure 1.3, but the basic components that make up a module are a control board, motor, transmission, output shaft, internal sensor package, casing, and connector ports. These are discussed in detail in Chapter III and I present our designs in Chapter IV. As intrinsic capabilities of the modules become more extensive, the robot as a whole relies less on centralized infrastructure; Titan 6's modules require no central sensor network, computer, or power source.

# Chapter II

# System Specification

Titan 6 was designed using a top-down approach that first specified the leg and body geometries before exploring the individual module design space for the links and joints. By using the system requirements to generate the robot geometry and justify the required joint speeds and torques, it is guaranteed that the module design is capable of meeting the overall project goals. This chapter lays out the system-level and joint-level requirements specification processes used to navigate the design space.

## 1.  Leg Kinematics

For any walking robot, the leg kinematics determine the reachable end-effector workspace, the mass distribution for balance, and the torque profiles expected at the joints during motion. These factors must be considered while choosing the number and relative orientations of the joints in a leg and while optimizing the link lengths between them. With the exception of a small body structure to affix the hips together, Titan 6's long, modular legs make up the entire system's mass, power draw, and cost, making the leg structure even more critical for this robot.

Titan 6's legs are serial chains of actuators[1] and rigid links that transform input joint angles, $\vec{\theta} = [\theta_1 \dots \theta_n]^\top$, to foot positions, $\vec{x} = [x, y, z, \theta_x, \theta_y, \theta_z]^\top$. In the absence

---

[1]Parallel leg linkages have proven effective in smaller dynamic robots such as Minitaur [31] and GOAT [32], but these leg structures can seriously impede foot placement on rough terrain where the linkage beams may make unintentional ground contact. These were disqualified early in the design process because they are not suitable for sprawled posture legs.

of redundant joints or singularities, an $N$-degree of freedom (DoF) leg will have an $N$-DoF workspace for the foot, up to 6-DoF. For example, even with step-shaping linkages, Dante II's footstep locations are constrained along a 1-DoF path [16], and RoboSimian's 7-DoF legs can reach any position and orientation in a 6-DoF workspace [10].

Based on this fundamental reasoning, three rotary joints can be arranged to provide the largest possible workspace volume in which to find footholds with the minimum number of joints. The orientation of the foot in the workspace is largely unimportant for ball feet with assumed point contacts, so the 3-DoF kinematics only consider the position of the foot as $\vec{x} = [x, y, z]^\top$. The selected kinematic configuration, shown in Figure 2.1 is common and has been proven on many of the systems described in Chapter I.[2]
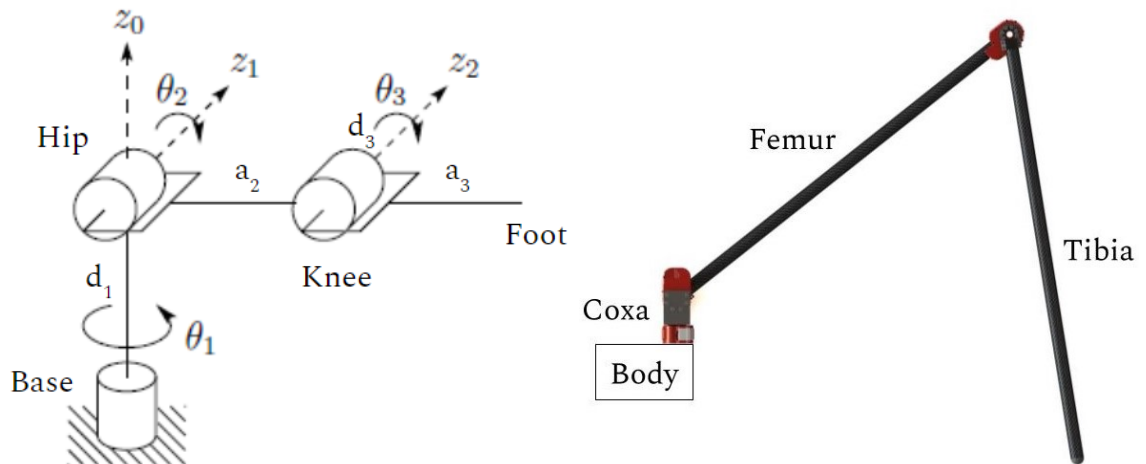


Figure 2.1: Generalized kinematic model of the Titan 6 legs with joint names and parameters called out, adapted from [33] (left) and an early CAD model of a Titan 6 leg with link names called out (right).

Notably, the base joint axis of rotation is parallel to gravity when the robot's body is level, so it is largely exempt from using power to maintain a standing position when level. Similarly, the knee joint's torques are kept low when the tibia is near vertical and the robot is standing still. The long tibia link keeps the body and all actuators with sensitive electronics suspended up to a meter above the footholds to prevent

---

[2]PV-II, Snake Monster, and MAX use this leg configuration in a sprawled posture; StarlETH and Spot use this configuration in an upright posture.

contact with floodwaters or debris. A full kinematic description of the various Titan 6 prototypes is provided in Appendix A.

# 2. Body Kinematics

The body of Titan 6 must provide a rigid structure to mechanically fix the base joints of each leg together and to mount a payload. The legs are arranged in a hexagonal pattern with the home position radially outward from the center (each 60° from its neighbors) to maximize reachable area and minimize workspace overlap between the legs. Unlike other systems with centralized sensor clusters, computation, and power, these components are distributed to each modular joint, keeping the suspended body mass low. Mass in the knee and tibia of a leg in stance is directly supported by the ground, reducing loads on hip and knee joints. This mass distribution does increase leg inertia, compounding the energy expended to swing the leg, but this factors in mostly for dynamic running gaits, which would not be required of Titan 6 to meet its speed requirements.

There are three important reference frames when considering the body kinematics of Titan 6; the world frame, the body frame defined as shown in Figure 2.2, and the leg frames centered at each numbered vertex. Each leg frame z-axis is aligned with the axis of rotation of the base joint (parallel to the body z-axis) and the x-axis aligned with the home position of the base joint.
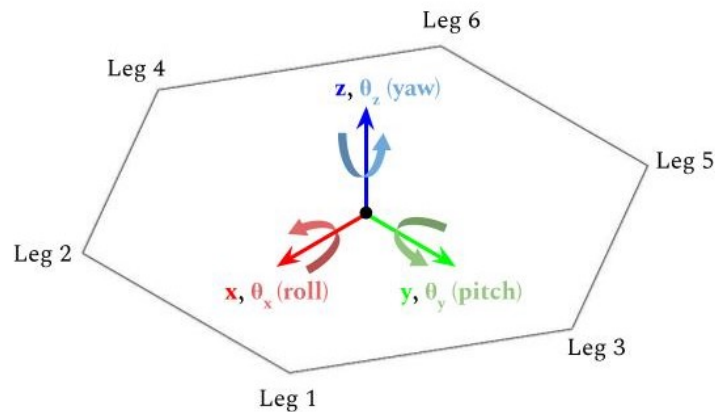


Figure 2.2: Titan 6's body layout with robot body frame and leg numbers called out.

# 3.  Joint Requirements Calculation Tool

Like any system, legged robots face design choices based on competing mass, speed, size, and torque trade-offs [34]. For example, with actuator power kept constant, joint speed and torque are inversely proportional, and raising actuator power requires increasing actuator mass, which in turn increases the torque requirements to resist gravity. Increasing walking speed can be accomplished by extending the femur link or reducing the transmission ratio of the actuator, but each solution drives up torque requirements. The viable design space shrinks drastically when considering larger legged robots; remaining designs often tend towards high-mass, low-speed designs not suitable for Titan 6. Navigating these relationships to find the optimal ratios is an underconstrained problem that can seem intractable without the aid of computational tools.

In order to more accurately determine the torques and rotational speeds Titan 6 needs at the joints to accomplish body-level tasks, a full kinematic study was performed in simulation and extended to form the codebase for the Hexapod Actuation Calculator App. This custom-developed tool allows a user to specify the physical parameters of a hexapod robot and a set of performance requirements, and it returns the torques and speeds needed for each joint to execute the desired behavior. It is intended to be used iteratively early in the design process to determine the viability of mass distributions and leg lengths, and was used extensively during the actuator selection process for Titan 6. Though the use case is constrained to hexapods with 3-DoF legs, it may prove useful in future robot development and is available from the MathWorks File Exchange or from the MATLAB Add-On Explorer.

## Assumptions, Inputs, and Outputs

The tool is designed for rapid iteration and approximate estimates of joint requirements; dynamic loads and inertial forces are not considered. These would require 3D component models or mass moment of inertia matrices, which are not available during early development. Instead, by assuming each defined component is a point mass with a gravitational force that acts downward at its centroid, the calculations are far simpler and can use a static model of the robot from Chapter I. The time-discretized

configurations are independent of one another, with current force entirely dependent on the current joint angles and robot geometry, not velocities or accelerations.

The preprogrammed gaits will always walk forward and keep the body level to the planar ground. When determining the step trajectory for a swing leg, the robot always takes the largest possible step while respecting the joint limits, and uses a minimum jerk trajectory to move between points. While a minimum jerk trajectory is not necessarily as time-efficient as ramp-up or uniform trajectories, it makes the quasi-static assumption more realistic by keeping the inertial effects minimized [35].

The tool expects a full geometric description of the robot leg via its Denavit-Hartenberg link lengths and offsets. The foot, tibia, knee, and femur are defined as distinct distal masses, and the body, payload, base, coxa, and hip are lumped into the aggregate body mass. The tool infers the properties of the robot from this single leg input assuming all legs are identical and the body is arranged as described above. The user can specify a desired walking speed, terrain grade, slope approach angle, body height, and gait. While the entire robot is taken into account for gait generation and mass effects, the outputs only describe the user-chosen leg. Outputs include the maximum angular velocity and torque expected from each joint to execute one gait cycle.

## Grasp Map Forces

The robot's foot locations are key factors in determining the ground forces each stance leg must react to hold the current body pose. These forces must counteract gravity and balance torques about the body to maintain static equilibrium, which can be solved as a linear system for $n$ stance legs with Eq. 2.1, where $[x_i]_r$ is the $x$ position of the $i$th foot in the robot's body frame, $F_i$ is the vertical force on the $i$th leg, and $m_r$ is the mass of the robot. This system has one solution with three stance legs sufficiently spread about the robot, and a least squares solution distributes the load in the case of $n > 3$ stance legs. This force calculation is known as a grasp map or force closure [36] and considers pose adjustment as self-manipulation using the legs as a hand would use fingers to manipulate an object. Early experiments with the Titan 6 robot verified that this provides a decent, computationally-inexpensive estimate of the gravity forces on each stance foot, but each leg has significant distal mass that

must be accounted for with Jacobian-based methods.

$$
\begin{bmatrix} [x_1]_r & \cdots & [x_n]_r \\ [y_1]_r & \cdots & [y_n]_r \\ 1 & \cdots & 1 \end{bmatrix} \begin{bmatrix} F_1 \\ \vdots \\ F_n \end{bmatrix} = \begin{bmatrix} 0 \\ 0 \\ m_r g \end{bmatrix} \tag{2.1}
$$

## Torque Calculations

The derivative of a leg's forward kinematic map yields the Jacobian, denoted $J(\theta)$, which maps joint velocities, $\dot{\theta}$, to foot position velocities, $\dot{x}$ (Eq. 2.2); its transpose maps end-effector forces, $f$, to joint torques, $\tau$ (Eq. 2.3). This relationship allows the simulator to apply the gravity reaction force from the grasp map, $F_k$, to the $k$th stance foot through the leg Jacobian by Eq. 2.4 ($F_k = 0$ for swing legs). Similarly, the distal weights of the leg components are applied at the appropriate locations along the legs via intermediate Jacobians, $J_0^i(\theta)$, where $i = [1, 2, 3, 4]$ corresponds to the femur, knee, tibia, and foot respectively. The slope geometry is incorporated via a rotation matrix, $R_r^w$, that describes the gravity vector in the body frame.

$$
\dot{x} = J(\theta)\dot{\theta} \tag{2.2}
$$

$$
\vec{\tau} = J(\theta)^\top \vec{f} \tag{2.3}
$$

$$
\vec{\tau}_k = -J(\theta)^\top R_r^w \begin{bmatrix} 0 \\ 0 \\ F_k \end{bmatrix} + \sum_{i=1}^{4} [J_0^i(\theta)]^\top R_r^w \begin{bmatrix} 0 \\ 0 \\ m_i g \end{bmatrix} \tag{2.4}
$$

The resulting vector, $\vec{\tau}_k$, yields the joint torques in the $k$th leg needed to support the robot's mass in the current pose with the given geometric definition. By passing through each set of joint angles in the automatically-generated discretized gait trajectory, a time-dependent torque function for each module is generated.

## Example

The Hexapod Actuation Calculator App was run hundreds of times to determine viable actuator masses, torques, and speeds. Since many behaviors and stances need to be considered to provide a complete picture of the robot's joint requirements, a suite of tests are required to fully evaluate a design. Figure 2.3 shows the Graphical User Interface (GUI) with a set of example input values for a Titan 6 prototype, and Figure 2.4 shows the returned plots and actuator specifications for that case.
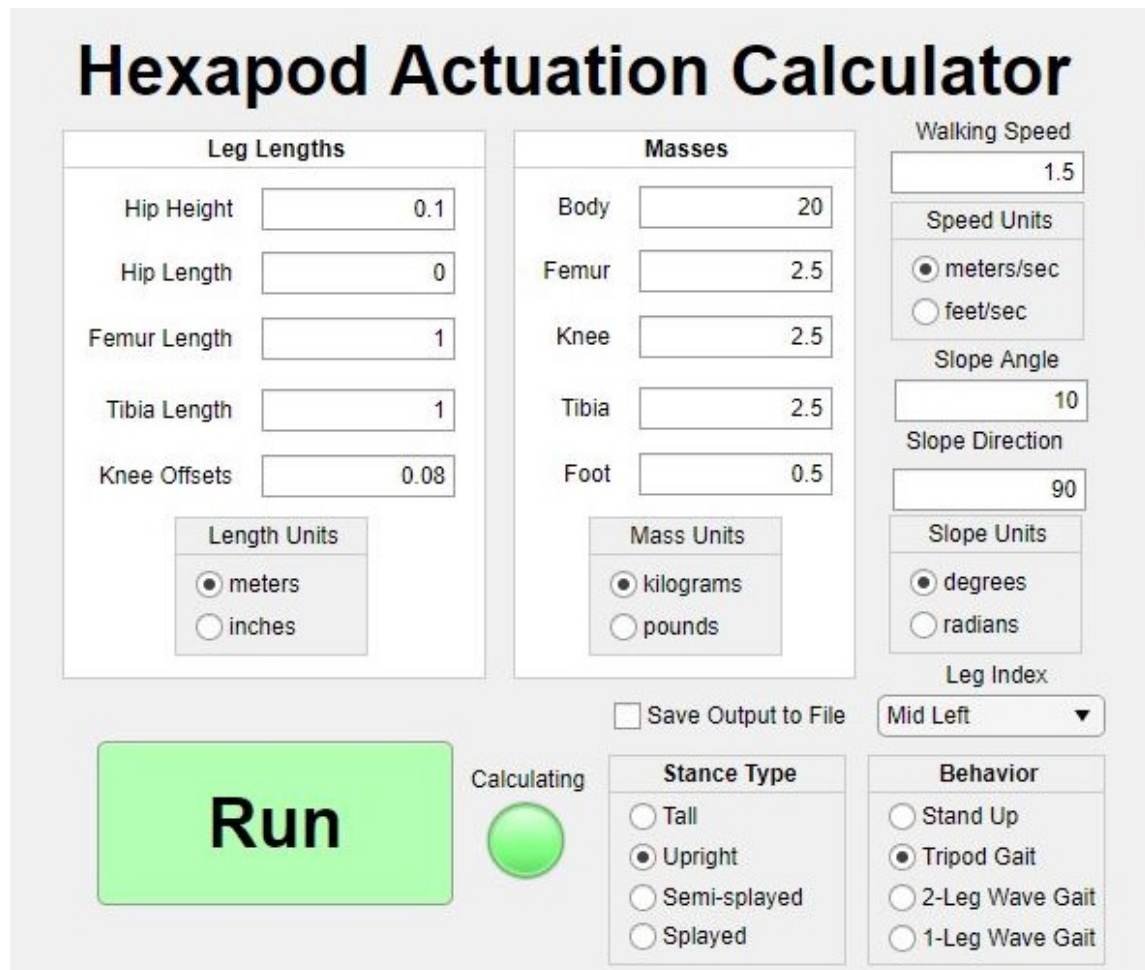


Figure 2.3: The application GUI that allows users to input geometric and behavioral parameters to a simulated hexapod.
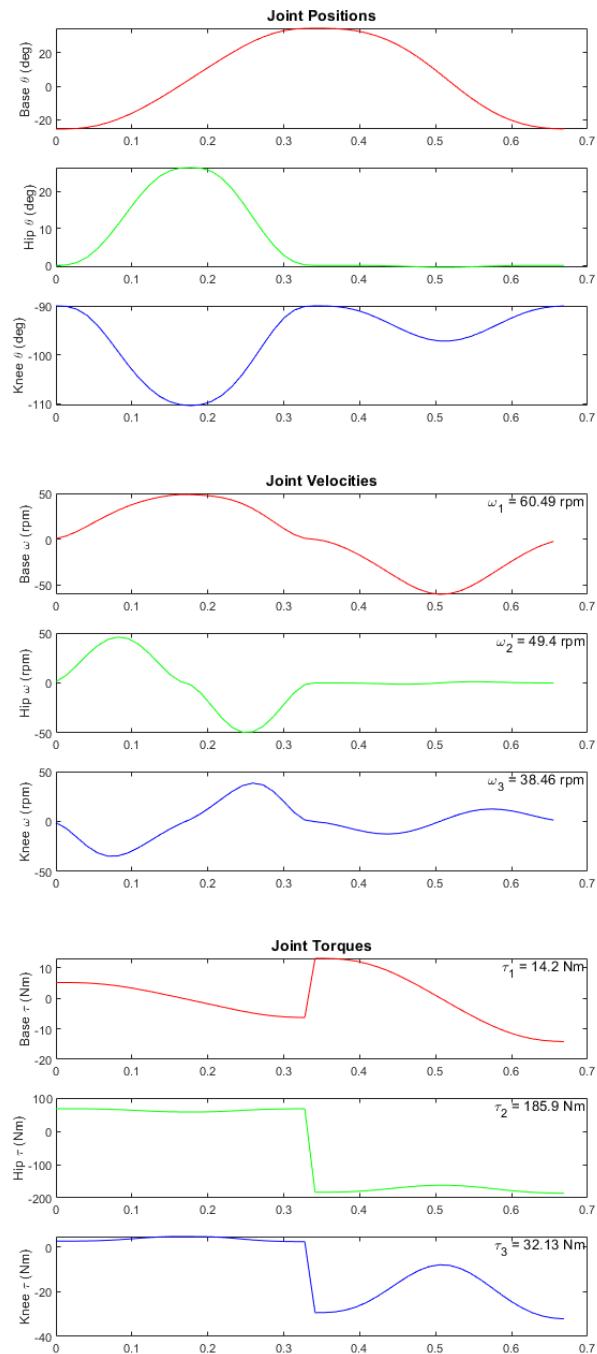
Figure 2.4: Output plots from the calculator showing the automatically-generated step trajectory in joint space, the required joint velocities though the gait, and the calculated joint torques to resist gravity.

# Chapter III

# Actuator Technology

Actuators embody one of the fundamental concepts of robotics; linking code and the physical world. They have been developed to use various physical driving forces, materials, and properties and exist at any size from smaller than a single cell [37] to larger than a building [38]. Some include sensors, computer interfaces, or linkage mechanisms, but at the core of an actuator is the power train: storage, conversion, and transmission. These components are the basic building blocks needed to make up a self-contained robotic actuator, and must be carefully designed for efficiency, cost, weight, and compatibility when building a robotic system. This is especially true for a modular system such as Titan 6, which uses a single actuator design for several joint applications with varying requirements. The following is a general survey of actuator technology studied for Titan 6 and the factors considered in context of a modular legged robot. The section follows the path of energy through the power train shown in Figure 3.1, identifying the options considered for each component and the associated benefits and drawbacks for Titan 6.

## 1. Energy Storage

An actuator exists to release energy in a controllable manner, but that energy can be stored effectively in several common mechanisms. Many modern field robots remain tethered to offboard power supplies for consistent control and easy retrieval [39], and microrobotic systems are often unable to store sufficient power onboard, preferring

external magnetic actuation [40]. However, these systems are not capable of free exploration without existing infrastructure, so we will only consider viable onboard storage solutions, especially those that are highly energy dense and realizable in distributed system. Key characteristics of such systems are discussed below.
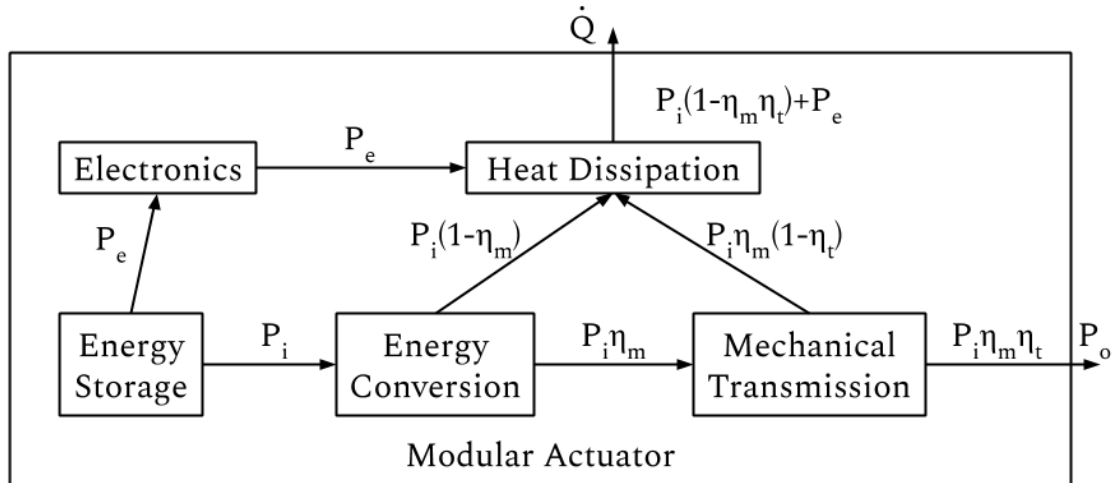


Figure 3.1: A block diagram showing the path of energy through a modular actuator where input power $P_i$, electronics power $P_e$, conversion efficiency $\eta_m$, transmission efficiency $\eta_t$, heat output rate $\dot{Q}$, and output power $P_o$ are all time-varying.

## Energy Storage Concepts

**Reusability:** Some means of energy storage can be reused indefinitely with no change in performance, such as a weight raised in a gravitational field, whereas burning gasoline to release chemical energy can only be done once. Most methods fall somewhere on this spectrum, with performance depreciation over time and use. Generally, it is important to consider the energy storage reusability in context of the robot lifetime as a whole and the acceptable upkeep costs to keep the system operational. Additionally, actuators that are easy to access with minimal system down-time may be able to tolerate single-use replaceable power storage, but Titan 6's limited deployment mass requirement includes replacement power storage.

**Discharge Rate:** Actuators usually have time-varying energy requirements based on their controllers and uses. An energy storage method must be compatible in both **Continuous** (the long-term draw of the actuator exerting its nominal force) and **Peak** (the short-term draw of the actuator during periods of high-exertion) cases.

A system that cannot release enough power at peak will be the limiting factor in actuator performance. Additionally, it is important to consider what happens when the actuator out-draws the energy storage mechanism; it could simply limit output, cause a brown-out that results in a system restart, or cause a dangerous reaction in volatile systems. An energy storage method's continuous and peak discharge rates must be well matched with the rest of the actuator - meeting or exceeding power draw expectations while remaining safe for components in the path of energy flow described in Figure 3.1.

**Capacity:** The capacity of an energy storage mechanism is simply the amount of energy stored when fully charged, which directly affects how long the system can operate. This can be generally measured in Joules or Watt-hours (or Amp-hours for batteries), but is often more useful in the context of the system, such as in hours of operation or range. Most power storage systems are easily scalable, such as batteries connected in parallel or fuel tanks, but adding capacity increases system mass, leading to nonlinear scaling in operation time. In a legged robot, increasing mass also increases actuator torque, drawing more power and increasing cost of transport, which may result in a poor return on investment for additional capacity.

**Volatility:** Storing large amounts of power is inherently dangerous, and systems with high capacity must be handled with care to avoid releasing that energy in an unsafe manner for either the system or nearby operators. It is often the case that the most power-dense or efficient methods of energy storage are the most volatile, as minimizing activation energy improves efficiency but increases the likelihood of unintended activation. Explosions and fires, as demonstrated in Figure 3.2, are often the result of energy storage systems that are allowed to discharge through unintended paths, such as a pressurized tank puncture, shorted battery cell, or spark in a fuel tank. Volatility encompasses the likelihood of these issues and the danger posed by byproducts of a compromised system, such as heat or toxic gases [41]. The working conditions of the robot must be compatible with the volatility of the storage system; disqualifying more volatile methods when the robot expects shock or heat exposure. The ideal power storage system is safe for the expected operation of the robot and resilient to minor operator error without catastrophic failure. Volatility concerns are important to consider for Titan 6, which experiences impact accelerations with each step and should survive in the case of a fall from its full two meter height.

Figure 3.2: The 2016 RoboSimian battery fire caused by thermal runaway that destroyed most of the robot body during unsupervised charging, an example of storage volatility in Li-Ion batteries, adapted from [42].

**Specific Energy:** When designing a power storage system for a legged robot, it is critical that the mass is minimized. Each method of energy storage has an associated specific energy, measured in $\frac{J}{kg}$, and energy density, measured in $\frac{J}{m^3}$. This characteristic is often steeply inversely related to those listed above as well as sharply correlated with cost [43]. Additional infrastructure for recharging, volatility safety, and energy conversion all contribute to the mass considered in an actuator's energy density. The goal of energy storage design should be to maximize specific energy such that volatility, reusability, discharge rate, and capacity requirements are met.

## Mechanical Storage

The most efficient actuators are ones that don't incur losses by converting from chemical or electrical energy to mechanical work, which can be achieved by harnessing potential or kinetic energy directly. These systems include energy stored in a gravitational field, compressed gas, wound spring, or the inertia of a flywheel, and can result in efficiencies near 100%. Fully mechanical power storage and actuation has been proposed where electrical alternatives are impossible, such as the surface of Venus

[44]. However, these storage solutions suffer from difficulty in controlling bidirectional motion since mechanical switches must be used to divert the flow of energy. For example: a wound clock spring can provide consistent power to a mechanism over time, but the transmission becomes prohibitively complicated for more controlled time-varying position output. Since most mechanical storage options have low specific energy, they are not well suited for bulk storage, but the ability demonstrated in Figure 3.3 - recovering and intelligently redirecting mechanical energy over time with minimal conversion losses - would be a useful augmentation in the joints of a legged robot.
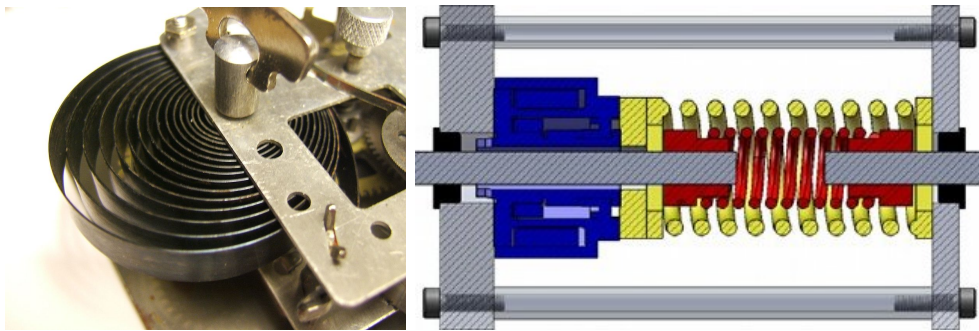


Figure 3.3: A wound clock-spring that can dissipate stored energy consistently over a long period of time, from [45] (left), and a combination series-spring and clutch-operated parallel spring mechanism that can store and release energy based on current applied joint forces, from [46] (right).

## Combustible Fuel Storage

Despite being highly volatile, not reusable, and polluting, combustible fuels are the clear winner among well-established methods when optimizing an energy source for specific energy. As shown in Table 3.1, conventional liquid fuels far surpass even the most advanced battery power in terms of how much energy can be stored in a given mass and volume. Though chemical bonds efficiently store energy, extracting that energy and converting to useful work via combustion is inefficient and requires significant heavy machinery. Unlike the high efficiencies of mechanical or electrochemical energy conversion, internal combustion engines are unable to harness most of that energy for useful work, releasing 60% to 80% as heat. The most efficient engines operate near 50% efficiency, but most are closer to 25% [47].

Combustible fuel energy storage has great potential in monolithic, centralized power systems, as demonstrated on BigDog [5] and ATHLETE [48], but does not distribute to multiple smaller systems well. Scaling down engine sizes results in further efficiency loss and quickly becomes impossible at the scales needed for individual robotic actuators. This means that a robot running on combustible fuel needs a central gas tank and engine that can generate electricity at a huge efficiency loss or must use distributed transmissions, such as hydraulics, to move the energy from storage to where it is needed.

Table 3.1: Energy Density of Storage Methods [49]

| **Storage Method** | **Specific Energy** $\left(\frac{MJ}{kg}\right)$ | **Energy Density** $\left(\frac{MJ}{L}\right)$ |
|---|---|---|
| Clock Spring | 0.0003 | 0.0006 |
| Lead-Acid Battery Cell | 0.14 | 0.36 |
| NiMH Battery Cell | 0.25-0.4 | 0.493-1.55 |
| Alkaline Battery Cell | 0.48 | 1.3 |
| Flywheel | 0.36-0.5 | Unavailable |
| Li-Ion Battery Cell | 0.46-0.72 | 0.83-3.6 |
| Jet A Fuel | 42.8 | 33 |
| Gasoline | 46.4 | 34.2 |

## Electrochemical Storage

Recent developments in battery chemistry have made cells cheaper, more scalable, less volatile, and extended their lifetimes [50]. It is now possible to design custom battery packs using well-characterized cells as building blocks to achieve desired voltage, discharge rate, and capacity. The convenience of a power storage system that is highly adaptable in form factor, reusable,[1] and maintains steady output voltage cannot be understated. Additionally, while electricity is not inherently required by actuators, it is required for onboard computation and computer-managed sensing and control. Unless a system is generating electricity by siphoning energy from the active power train, a battery is required to keep the robot's brain alive. Having a single power storage architecture for both actuation and control is mass-efficient and minimizes complexity.

[1]Only certain chemical cell compositions are rechargeable, such as Li-Ion, NiMH, and Lead-Acid. Alkaline and primary zinc-air cells are disposable after a single use.

Though battery cells come in many chemical compositions, Li-Ion cells[2] in particular have gained immense popularity in robotics for their high specific energy relative to other chemistries (see Figure 3.4). In addition to being lighter than NiMH or Lead-Acid cells, Li-Ion cells have low internal resistance, which allows them to discharge safely at much higher peak rates. Though these cells are volatile and extremely dangerous in thermal runaway, they are well studied and can be kept reasonably safe with standard safety equipment and careful handling. Optimized cells designed specifically for certain robot applications are reasonable in some cases, but standardized cells, such as 18650 and 21700, are mature technology and widely available. They can be combined in series or parallel to assemble custom battery packs with desired voltage and capacity with intermediate battery management circuitry. Titan 6's distributed power storage system would benefit from a customizable form factor to fit in available space in leg links rather than a bespoke body cavity for centralized power storage. Figure 3.5 compares the characteristics of batteries and other energy storage methods, summarizing the rationale for choosing Li-Ion cells.
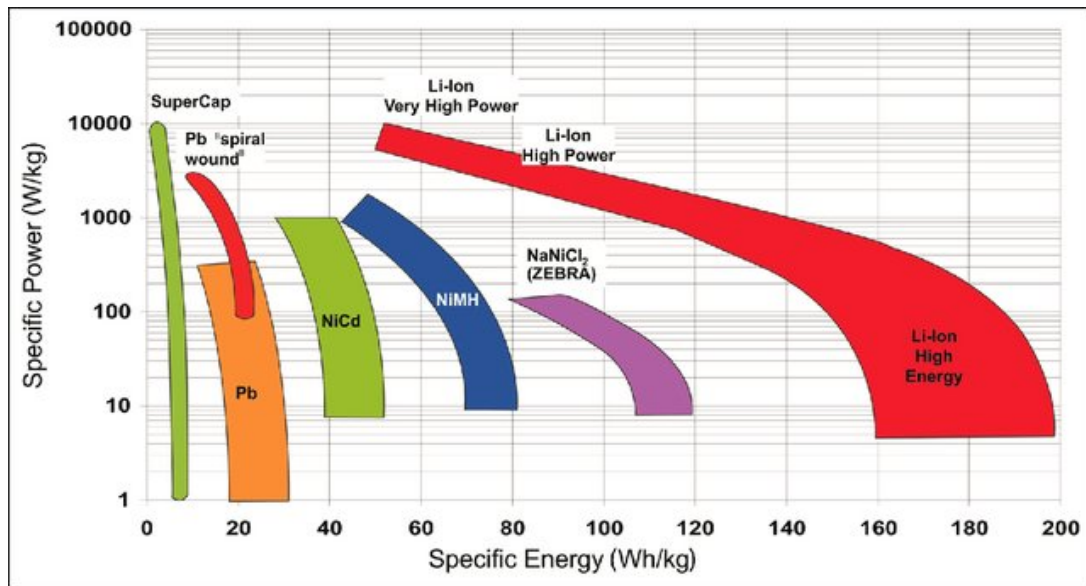


Figure 3.4: A Ragone Plot of commonly used battery chemistries, showing the significant advantage of Li-ion cells for high specific energy, from [50].

---

[2]The Lithium-Ion family encompasses a large subset of Lithium-based battery chemistries including Lithium-Polymer (LiPo), a popular variant that can be packaged in a wider variety of form-factors.
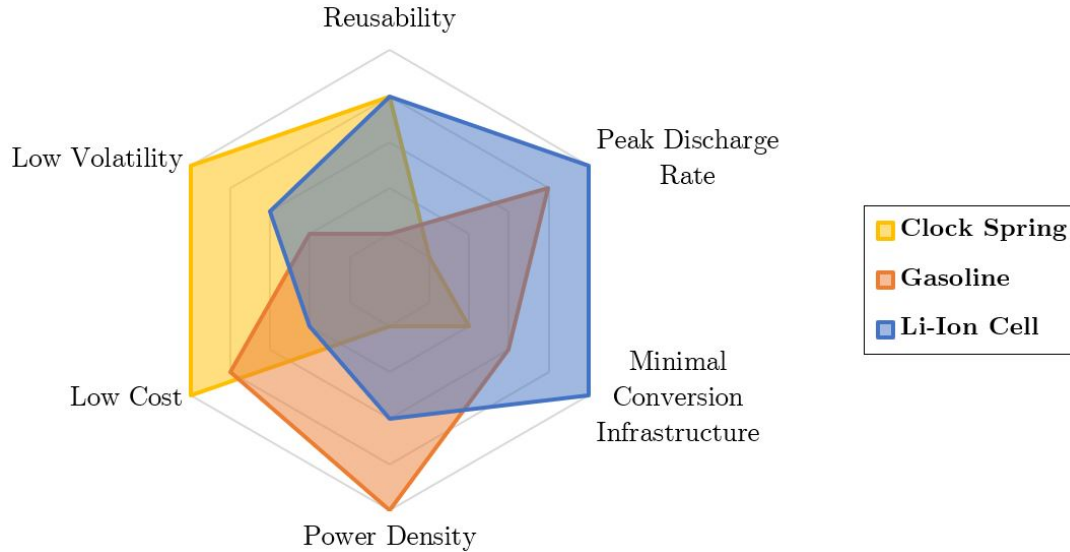
Figure 3.5: A comparison of some representative energy storage architectures where all values are relative and the ideal system spans the perimeter of the radar.

## 2. Motors

Since it is impractical to store kinetic energy in its raw form with high specific energy mechanisms, an actuator needs a motor to convert the stored energy to mechanical work. This component is the heart of an actuator, the actual interface between control signals and physical effects. Motors can convert any type of energy to mechanical energy, but the most common is the electric motor, which pushes electric current through coils of wire to induce magnetic fields and generate a torque about a shaft. While engines and motors that convert other forms of energy are interesting, this section will focus exclusively on electric DC motors, which are the most relevant to the Titan 6 project.

In general, the torque of a DC motor is determined by the current drawn through the coils and the speed is determined by the voltage. All motors can be modelled with a speed-torque curve that indicates the viable operating conditions for a certain motor design subject to the applied voltage, as shown in Figure 3.6. While these curves provide a good idea of the expected outputs with the recommended motor inputs, they are usually based on the rated power and inherent heat dissipation of the motor itself. Using a standard motor model in Eqs. 3.1 and 3.2, it is clear that the

performance of a motor in terms of speed and torque can be improved by increasing applied voltage and applied current beyond the nominally stated values. However, to do so safely it is critical to avoid overheating the motor with the additional input power, which is why custom heat dissipation in an actuator is critical to improve performance.
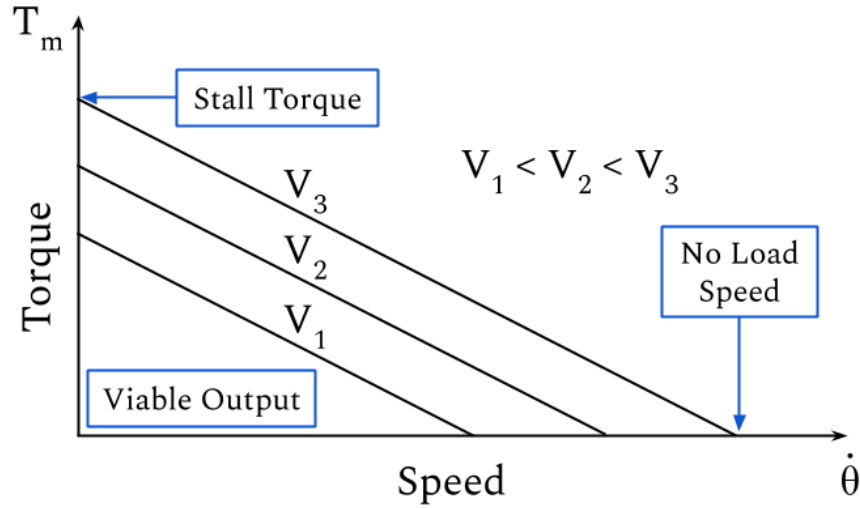


Figure 3.6: An idealized speed-torque curve for a motor showing multiple curves for varying voltages.

Table 3.2: Motor Model Parameters

| Name | Symbol |
|------|--------|
| Applied Voltage | $V_t(t)$ |
| Applied Current | $i(t)$ |
| Internal Resistance | $R_a$ |
| Winding Leakage Inductance | $L_a$ |
| Speed | $\dot{\theta}(t)$ |
| Torque | $\tau_m(t)$ |
| Speed Constant | $k_s$ |
| Torque Constant | $k_t$ |

$$V_t(t) = L_a \frac{\partial i(t)}{\partial t} + R_a i(t) + k_s \dot{\theta}(t) \qquad (3.1)$$

$$\tau_m(t) = k_t i(t) \qquad (3.2)$$

27

These models and parameters are crucial for selecting the best motor for a given task, but there are critical characteristics of different motor designs that can seriously affect the performance of an actuator. Though multiple motors may meet speed and torque requirements, it is important to consider the importance of position, velocity, and torque control resolution for the application as well as form factor, mass, efficiency, and motor lifetime. For this reason, the first step in motor selection is to determine the type of motor and winding style to be used.

## Types of Motors

All types of DC motors have the same main components. The **stator** is the portion that remains fixed to the base, usually with electrical connections to the **motor driver**, an electrical device that regulates input voltage and current to turn the rotor. The **rotor** or armature is concentric with the stator and rotates when voltage is applied, turning the **shaft**, the mechanical coupling used to attach a transmission. Most motors keep their rotors and stators constrained with bushings or bearings set into the casing, which usually includes mount points to the stator; the shaft support and housing together are known as the **frame**.

**Brushless:** These motors, also known as interior permanent magnet DC motors, are commonly used in robotic applications for their smooth output. As shown in Figure 3.7, the rotor consists of a ring of permanent magnets aligned with radial poles alternating N-S outward orientation. The stator consists of a series of coiled wires, which produce a localized magnetic field when powered. Each time a subset of coils, or phase, is powered, the magnets on the rotor will turn the shaft to align the magnetic fields. By sending current through the coils in the appropriate order at the proper frequency, the motor driver can create smooth rotational speed trajectories [51]. This controller is often aided by an encoder or hall-effect sensor to indicate the position or speed of the shaft.

Brushless motors can produce high speeds and high torques with tuned magnetic forces from the coils, but require complex and sometimes costly motor controllers. These motor controllers can draw lots of power and require separate cooling systems, which can be a major drawback of using brushless DC motors. However, they offer long lifetimes, fantastic controllability, and are readily available from many manufacturers

with huge variety in form factor and speed-torque capabilities. Rotational friction is minimized because there are no electrical connections between rotor and stator, and the coils are located in the stator, shortening the path of residual heat out of the motor into the surroundings. Some brushless DC motor models are frameless; doing away with the shaft, bearings, and casing to save weight. A motor cannot operate without a frame, so the components must be built into the actuator to constrain the stator and rotor, but this can reduce weight in highly optimized systems.
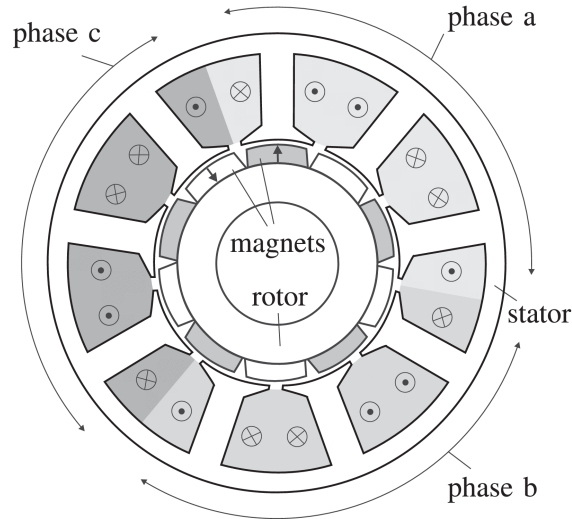


Figure 3.7: Down-shaft view of a three-phase brushless DC motor, with radial permanent magnets arrayed on the rotor and coils arrayed on the stator, from [52].

**Brushed:** Brushed motors are able to do away with the complicated motor control circuitry by using a **commutator** on the shaft and **brushes** on the stator that mechanically switch the current path to provide the alternating magnetic fields from the coils to drive the motor. By placing the permanent magnets in the stator and the windings in the rotor, as shown in Figure 3.8, the angular position of the rotor ensures the current is flowing in the proper direction to generate the desired torque. Because frequency of the coil switching is not coupled to logic circuitry as it would be with a motor controller, brushed motors are very good at hitting high speeds with minimal control effort. However, the brushes must maintain sliding contact with the commutator, and friction can degrade the electrical connection over time, shortening the lifetime of the motor [53]. This style of brushed DC motor is often the least expensive motor option.

Brushed motors can be wound in several different ways to produce different behavior characteristics. The permanent magnets in the stator can be replaced by additional wire coils to generate a magnetic field that is variable with the current applied. In **shunt-wound** motors, the stator coils are connected in parallel to the rotor coils, significantly improving speed control, but can reduce the torque applied. **Series-wound** motors connect these two sets of coils in series, which can improve the torque output because the current through both sets of coils can be increased together, causing higher driving magnetic field torques. The field coils can be split between series and parallel wirings to improve the high-speed control while maintaining high torques, as is the case in **compound-wound** motors [54].
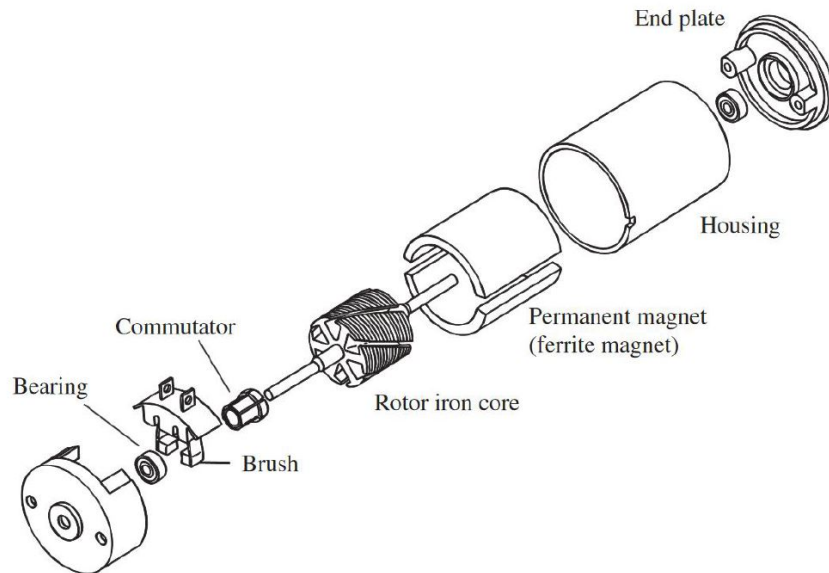


Figure 3.8: Exploded view of an external permanent magnet brushed DC motor, from [55].

**Stepper:** A stepper motor is a specialized type of brushless DC motor that is designed in such a way that the rotor always moves in discrete **steps** to specific positions. This is achieved with a "toothed" permanent magnet encoder that has 50 to 100 alternating N-S poles and similar "toothed" coils in the stator. The result is a system with some large number of discrete equilibrium positions for the rotor that can be effectively stepped through by activating the stator coils in sequence, as shown in Figure 3.9. Some stepper motors add toothed permanent magnets to the

stator as well, allowing them to hold the current step without power. This makes stepper motors very useful for precise, open-loop position control, because the shaft is guaranteed to be in exactly the commanded position. However, a stepper motor can skip steps if the rated torque is exceeded, which can accumulate error very quickly and potentially shorten the motor's lifetime [56].
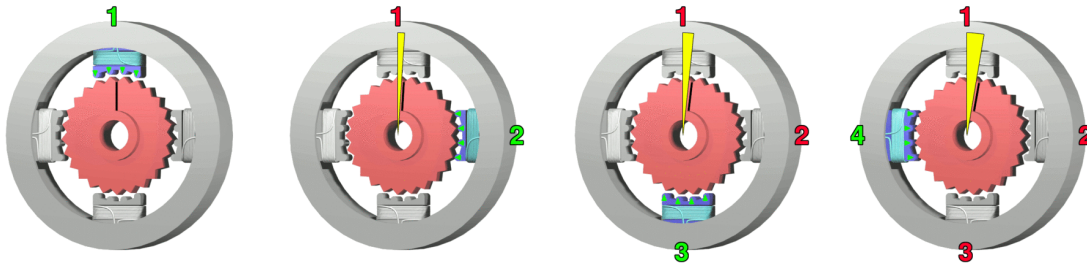


Figure 3.9: A simplified four phase stepper executing three steps by powering each of four coils in order, with the wedge indicating change in angle, adapted from [57].

Stepper motors can be unipolar or bipolar, which corresponds to the ability to pass current in different directions through the coils to reverse the magnetic field in the stator. While unipolar motors are less expensive and have simpler control circuitry, bipolar stepper motors have significantly better torque ratings. Some stepper controllers support microstepping, which allows for up to sixteen substeps between full steps, which can increase positional resolution and reduce resonance problems but significantly lowers holding torque [58].

Stepper motors are the only option when considering open-loop position control for systems that run for a long time with high precision requirements, such as the joints of a leg. They can be made to handle extremely high torques by stacking rotor magnets and stator coils axially, and well tuned controllers have impressive speed ranges. Additionally, holding position without added brake or clutch components can be highly advantageous for legged robots that need to stand for extended periods of time, which would normally draw nearly as much power as walking. However, stepper motors require massive frames to house components in exact relative locations and the magnetic stator alone can have mass on the order of comparable non-stepper motors. They also react poorly to dynamic or shock loading experienced by leg joints, since these can skip steps without any sensor to acknowledge the error.

## Scaling Effects and Limitations

Motor torque generally scales linearly with mass, which is usually advantageous for industrial uses and wheeled systems [59]. Unfortunately, this is an unfavorable trend for legged robots, which are extremely mass conscious and torque limited. Scaling up motors to provide additional power is infeasible for a legged robot such as Titan 6, especially because that additional power must be drawn from similarly scaling energy storage. Titan 6 must optimize its actuators for torque-density rather than power-density, and the motor selection process is key to pushing performance limits.

While motors get better every year, there are fundamental limitations on DC motor torque density. Solving the Maxwell-Ampere Equation (Eq. 3.3) for a coil of wire like those found in a DC motor shows that coils of wire emit magnetic fields with strength proportional to the number of wraps and the current running through them (Eq. 3.4). This presents a problem as thicker wire is needed to carry more current, but fewer thick wire coils can fit in a given volume. Currently, motor performance is limited by the state of material science; as wires are able to carry more current with less internal resistance and as magnets become stronger motors will improve. Given current motor technology that focuses on power-density, we must optimize actuator torque-density through transmission design instead.

Table 3.3: Magnetic Field Equation Parameters

| Name | Symbol |
|------|--------|
| Magnetic Field | $\boldsymbol{B}$ |
| Core Permeability | $\mu$ |
| Current Density | $J$ |
| Core Permittivity | $\varepsilon$ |
| Electric Field | $\boldsymbol{E}$ |
| Number of Coils | $N_c$ |
| Current | $I$ |

$$\nabla \times \boldsymbol{B} = \mu J + \mu \varepsilon \frac{\partial \boldsymbol{E}}{\partial t} \tag{3.3}$$

$$\boldsymbol{B} = \mu N_c I \tag{3.4}$$

# 3.   Transmissions

While the energy storage and energy conversion methods have huge implications on the power and mass of an actuator, transmission selection can give an actuator unique properties specific to its use case. Transmissions are principally used to convert high-speed, low-torque motion from a motor or engine output to more useful speed-torque ranges or to transfer mechanical energy from where it is generated to where it is used. The output can take the form of rotational or linear motion, and often incurs efficiency losses in the transition. Some transmissions are variable, such as those in automobiles which can vary the direction and speed of the output shaft, but these are out of the scope of this section, since variable transmissions are usually too large or complex for individual small actuators. The transmissions discussed here are all fixed-ratio and designed to be paired with an electric motor unless otherwise noted. The chief attributes of the ideal transmission are defined and compared below.

Table 3.4: Transmission Equation Parameters

| Name | Symbol |
|------|--------|
| Efficiency | $\eta$ |
| Transmission Ratio | $N$ |
| Backlash | $\theta_b$ |
| Power | $P$ |
| Inertia | $J$ |
| Torque/Force | $\tau$ / $F$ |
| Rotational/Linear Position | $\theta$ / $x$ |

## Transmission Concepts

**Efficiency:** The efficiency of a transmission, $\eta$, is simply the ratio of power at the input to the power at the output, shown in Eq. 3.5. These values can be simply calculated as the product of torque and speed for the bare motor shaft and for the output transmission, and are often predefined for each transfer component in a transmission. Typically, involving more energy transfers lowers the overall efficiency since each adds opportunities for friction or heat loses. Efficiency is usually dependent on input speed, load torque, temperature, and lubrication but does not consider transient spin-up loads or inertia of the transmission.

$$\eta = \frac{P_O}{P_I} = \begin{cases} \frac{\tau_o \dot{\theta}_o}{\tau_i \dot{\theta}_i} & \text{for rotational output} \\ \frac{F_o \dot{x}_o}{\tau_i \dot{\theta}_i} & \text{for linear output} \end{cases} \tag{3.5}$$

**Ratio:** The transmission ratio, $N$, describes the relationship between input and output speeds, shown in Eq. 3.6. It is unitless in rotational output cases and usually described in length per revolution for linear outputs. A ratio of $N < 1$ has an output faster than the input and is known as geared up; the opposite is known as geared down. Actuators for use in robotic joints are almost always geared down to reduce motor speeds from raw values in the thousands of revolutions per minute (rpm) to more useful speeds. The ratio is also used to describe the output torque of a transmission, but Eq. 3.7 (derived from Eq. 3.5 and 3.6) also takes the efficiency into account since some torque is lost to internal friction.

$$N = \frac{\dot{\theta}_i}{\dot{\theta}_o} \tag{3.6}$$

$$\tau_o = \eta N \tau_i \tag{3.7}$$

**Backlash:** Every instance of two mechanical components moving past each other requires some gap in between to allow unimpeded motion. Narrowing this gap increases friction loses, prevents lubrication from entering, and can cause a transmission to seize or bind. This inevitable gap is the source of backlash, $\theta_b$, the small amount of play in the output shaft present when the input is held still. Typically backlash is small, measured in fractions of degrees or millimeters, but each moving transmission component adds a small amount of system backlash, shown in Eq. 3.8.[3] This idealized equation only models the kinematic component of backlash, though there are significant negative effects of backlash on the dynamics of a robot limb [60]. This motion is completely uncontrollable from the input, so it adds uncertainty to output position that can only be measured with an output encoder. Backlash can be mediated with consistent torque in a chosen direction on the output, since the components will always be forced to the same side of the gap. This can be achieved by selecting trajectories that avoid direction changes or with a mechanical preload

---

[3]$N_{k+1}$ indicates the transmission ratio starting from the $k$th component to the output shaft in a transmission with $n$ components.

to bias the backlash in one direction. However, these trajectories are rarely viable in legged robots and preload springs add friction that reduces efficiency. Systems with high backlash often see noisy motor signals and generate vibrations when output direction changes as the system slips briefly as the backlash bias flips. Many groups have tried to mitigate or model backlash using a variety of methods with some success, though many incur significant mechanical [61] or programmatic complexity [62].

$$\theta_b = \sum_{k=1}^{n-1} \theta_{bk} N_{k+1} \tag{3.8}$$

**Backdrivability:** The rotor of a non-stepper motor can be easily turned in the absence of powered holding torque. This is known as backdriving, which essentially turns the motor into an electric generator by forcing current through the coils via the turning armature. Some transmissions are similarly backdrivable, allowing an unpowered actuator to be rotated manually. This implies that a legged robot using backdrivable actuators must constantly expend power to stay standing, even when not moving, whereas a nonbackdrivable actuator would be able to stand unpowered. However, a fully backdrivable system is much more robust to mechanical failures due to impacts. When a legged robot collides with an obstacle, a nonbackdrivable system has the worst possible load path, starting in the leg link and going through the entire structure and every component in the transmission system, which is rigidly fixed by the nonbackdrivable component. This can shear off gear teeth, strip lead screws, or break bearings, whereas a fully backdrivable actuator would simply resist the motion until the motor torque was overcome, keeping the loads on the power train low. Backdrivability is largely a binary feature based on the most resistant component, but some transmission designs are marginally backdrivable.

**Transparency:** A transmission's transparency quantifies the ease of energy flow between the motor and the output shaft and is typically tied to its backdrivability. Whereas backdrivability indicates the steady-state torque on the output shaft required to turn the motor shaft, transparency is related to the transient spin up torque. Systems with high transmission ratios have low transparency as a result of the reflected inertia of the actuator, calculated in Eq. 3.9. In these systems every turn of the output shaft corresponds to $N$ turns of the rotor, which can take significant energy to spin up to speed. High transparency actuators have gear ratios near $N = 1$,

and have benefits such as viable torque sensing via measuring motor current draw and high bandwidth control [63].

$$J_o = N^2 J_i \tag{3.9}$$

## Rotational Output Transmissions

**Direct Drive:** The trivial transmission, or direct drive, has many intruiging properties and advantages over high ratio actuators, and has been effectively used in limbed robots for over thirty years. The original CMU Direct Drive Arms [64, 65] proved that specially designed motors without transmissions are able to match performance of similar size conventional actuators for precise position control in a robotic limb. Parallel-mechanism legs such as those on the Minitaur [31] or GOAT leg (see Figure 3.10) [32] have proven the advantages of current-sensing proprioception. These systems have the benefit of perfectly efficient transmissions with no backlash and very high backdrivability and transparency. The actuators can be made space-efficient without bulky gear trains and the resulting system is extremely fast.

However, these actuators are extremely power hungry, drawing significant current to hold relatively small torques without the aid of a high transmission ratio, and can move faster than would be safe on a long-legged robot, wasting the upper bandwidth of motor control. Motors are most efficient when operating in high-speed, low-torque regimes, which is only reachable using large transmission ratios. As as result, the thermal cost can prohibit desired trajectories or behaviors which may burn out the motor more quickly than a motor operating in a higher efficiency regime. Cogging, in which the permanent magnets in the rotor prefer to sit in discrete stable equilibria when interacting with the ferrous core of the stator, can be a pervasive issue in direct drive control as well.

Quasi-direct drive can shift an actuator's working regime to higher speed and lower torque and alleviate many of the problems posed by pure direct drive. In these systems a low ratio ($1 < N < 10$) planetary gearbox is combined with a motor designed for direct drive applications to retain the high-transparency, low backlash benefits but give the motor a torque boost. Unfortunately, as the ratio increases so does the proprioceptive noise, and even with a torque increase of 10x, a quasi-direct

drive actuator would need a prohibitively large radius to meet Titan 6's specifications (the torque required by a Titan 6 joint is similar to that of the CMU Direct Drive Arm's fourth joint, which had a transmissionless motor with a 0.238 meter diameter and 19.6 kg mass [64]).



Figure 3.10: A Tiger Motor designed for direct drive applications, from [66] (left), and the GOAT leg which used three direct drive actuators to power a parallel leg mechanism for dynamic movement with proprioception, from [32] (right).

**Parallel Shaft Gear Trains:** The most common transmission for electric motors in robotic applications makes use of parallel shaft gear trains, in which a pinion gear on the motor shaft drives a larger gear to decrease speed and increase torque. Chaining compound gears together can provide any desired ratio, though these are typically in the range of $10 < N < 1000$. They also have the benefit of being extremely simple to design and cheap to produce, having been the industry standard for decades. However, as the number of gears in the train increases, the actuator efficiency decreases, backlash increases, and transparency decreases. Stiction, or startup friction, can also become a problem in gearboxes, requiring messy lubrication or expensive bearings to reconcile. Parallel axis gear trains are convenient for modular packaging as they are compact and able to adjust the placement of the output shaft relative to the motor, as demonstrated by the USnake [9] and SEA Snake Modules [67] in Figure 3.11.
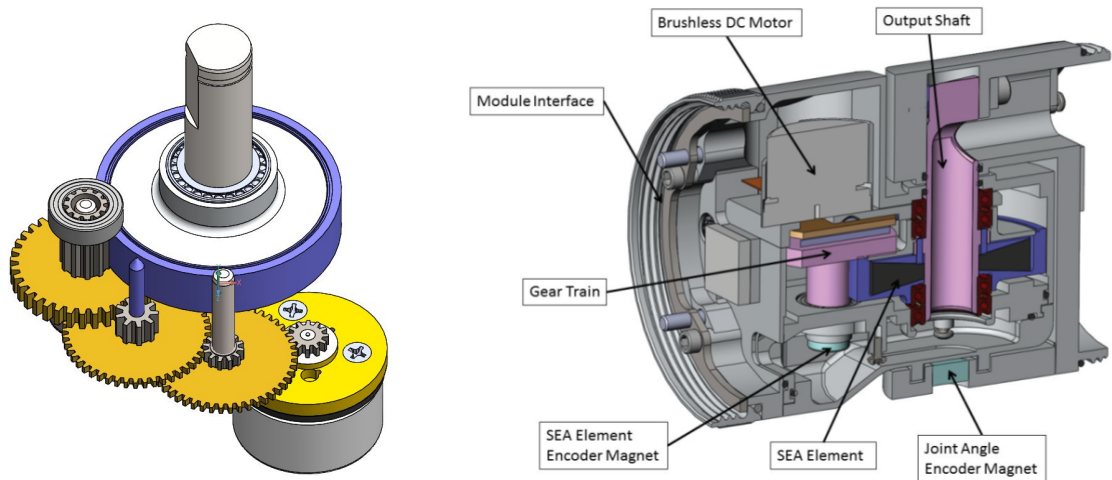
Figure 3.11: The gear train used in the SEA Snake Module spread out (left) and in context in the compact modular packaging, from [67] (right).

**Skew or Perpendicular Shaft Gear Trains:** Worm gears, bevel gears, and screw gears are all useful for transferring motor torque to output shafts at odd angles. This is useful for legged robots that can pack the motor into the leg links and still achieve rotation about an orthogonal joint. It is important to note the tight shaft alignment tolerances with these gears, making highly customizable gearboxes expensive to manufacture. Worm gears can provide much higher single-stage gear ratios than standard gears, but worms are completely nonbackdrivable. These have been used effecively in compact modular systems such as Sambot [68] and the Biorobotics Lab's Tread Module, as shown in Figure 3.12.

**Belt and Chain Drives:** Timing belts and drive chains can act as replacements for parallel shaft gears in larger actuators. The main benefits of these transmission are their extreme flexibility in output shaft location, ability to withstand some misalignment, and resilience to particulates that can cause grinding in gears. Backlash is particularly poor in actuators that use belts that are not prestretched or chains without tensioners, with loosening causing problems over time as the materials age. These drives can be designed with some inherent compliance from the stretching of the belt of chain tensioner, but this correlates to poor positional accuracy under load. Overall, these transmissions can be useful for simple, low cost systems, but are not particularly well suited for compact actuators.
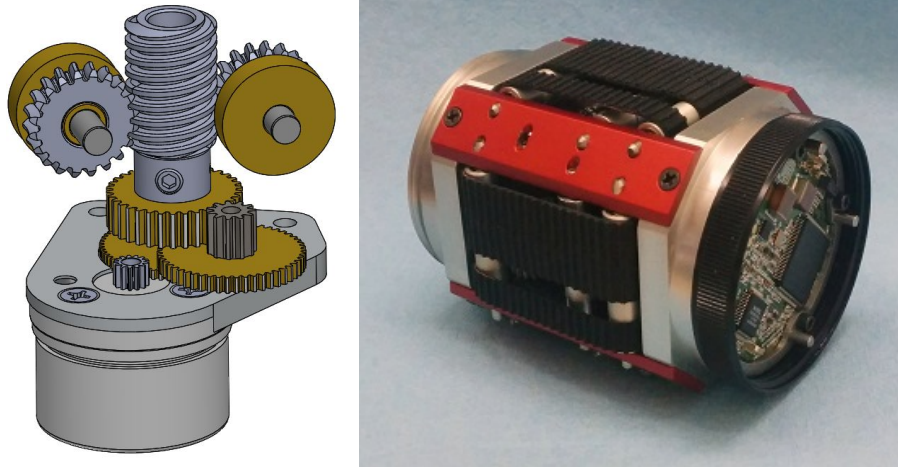
Figure 3.12: The worm gear used in the Tread Module (left) and the full Tread Module with four orthogonal outputs driven by one motor and a combination transmission of parallel axis gears, skew axis gears, and belt drives (right).

**Axial Compound Drives:** Planetary gears, can achieve high single-stage gear ratios in small packages that stack axially along the motor shaft. They generally have lower backlash and higher efficiency than traditional spur gears, which makes them a fantastic candidate for modular actuators [69]. However, these are achieved by balancing gear separation forces with multiple planet gears driven by the sun or ring gear, which compounds the reflected inertia of the transmission and complicates the nonlinear dynamic actuator model [70]. Planetary gears can be mounted in one of three ways: planet carrier fixed, ring fixed, or sun fixed. The mounting strategy affects the transmission ratio as shown in Eq. 3.10.[4] This presents an interesting opportunity for a variable-transmission compact actuator, but this is out of the scope of the Titan 6 project.

Cycloidal drives are extremely compact transmissions that can generate high ratios for torque dense actuators. They are theoretically backlash free and usually operate near $\eta = 0.93$. However, unlike planetary gears that are inherently balanced, the eccentric bearing and cycloidal disc can generate vibrations and wear on the system. A multistage cycloidal drive can help to balance vibrations, but exacerbates problems with the outer casing flexing [71]. This flexing is often difficult to account

---

[4]Planetary gears must be designed such that $T_{ring} = T_{sun} + 2T_{planet}$.

for as it is directly correlated with the desired output torque of the actuator. Even made of hardened steel, casings may need to be thick enough to offset the compact and lightweight benefits of cycloidal drives. If not properly supported, this flexing will introduce backlash into the drive. Initial testing with custom low-pressure angle 3D printed cycloidal drives for Titan 6, shown in Figure 3.13, yielded positive results, but shoring up casing designs to account for high internal loads eventually showed that these would be too large and heavy for legged robot use.

Harmonic drives work on the same principle as cycloidal drives, rotating an inner shape to match a toothed circular spline. However, harmonic drives are able to accomplish this with an elliptical wave generator and toothed flex spline rather than sliding cycloidal discs, which lowers the inertia of the transmission and is vibrationally balanced. The main drawbacks are design complexity and hyper-tight tolerances, which leads to high costs, long lead times, and inability to customize drive form factor for specific uses because manufacture is limited to a handful of companies that are often saturated with orders. However, the transmission ratio of both cycloidal and harmonic drives is solely dependent on the number of teeth on the splines (Eq. 3.10), so they are highly customizable within a given form factor. These have become the gold standard transmission for limbed robotic actuators that require high repeatability with high torque density. Harmonic drives are compared to each other form of rotary transmission in Figure 3.14, illustrating why they are promising for Titan 6.
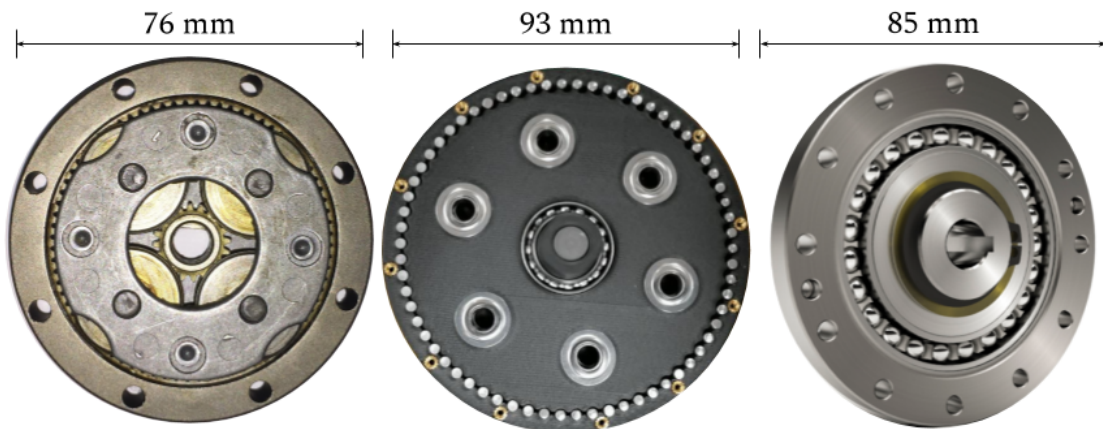


Figure 3.13: A 4:1 planetary gear stage (left), 65:1 cycloidal drive (center), and 100:1 harmonic drive, from [72] (right), considered for Titan 6 use.

Table 3.5: Transmission Ratio Equation Parameters

| Name | Symbol |
|---|---|
| Transmission Ratio | $N$ |
| Number of Gear Teeth | $T$ |
| Radius | $r$ |
| Number of Pins | $P$ |
| Number of Lobes | $L$ |

$$N = \frac{\dot{\theta}_i}{\dot{\theta}_o} = \begin{cases} 1 & \text{for direct drive} \\[2mm] \frac{-T_2}{T_1} & \text{for spur, bevel, screw, and worm gears} \\[2mm] \frac{r_2}{r_1} & \text{for belt and chain drives} \\[2mm] \frac{-T_{ring}}{T_{sun}} & \text{for planetary gears with fixed carrier} \\[2mm] 1 + \frac{T_{ring}}{T_{sun}} & \text{for planetary gears with fixed ring} \\[2mm] 1 + \frac{T_{sun}}{T_{ring}} & \text{for planetary gears with fixed sun} \\[2mm] \frac{P-L}{L} & \text{for cycloidal drives} \\[2mm] \frac{T_{flex}-T_{spline}}{T_{flex}} & \text{for harmonic drives} \end{cases} \tag{3.10}$$
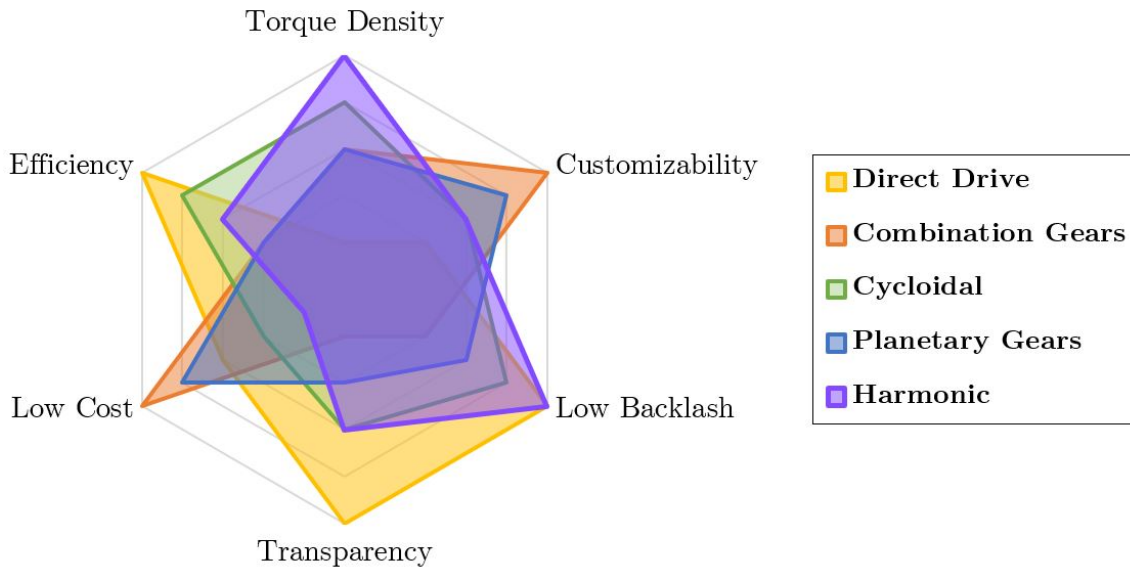


Figure 3.14: A comparison of the available rotational output transmissions where all values are relative and the ideal system spans the perimeter of the radar.

## Linear Output Transmissions

**Lead Screws:** Crankshafts, rack/pinions, cams, linkages, and many other transmission designs have been effectively used to operate linear actuators, but lead screws remain the most common mechanism to convert rotational motion to controlled linear output. While the actuator structure stays consistent, lead screws are highly customizeable in radius, length, thread pitch, number of starts, and material and can be optimized for a desired actuator strength and speed. The lead determines the transmission ratio and efficiency according to Eqs. 3.11 and 3.12, and the force output is determined by the geometric and material properties in Eq. 3.13. Low pitch lead screws are particularly inefficient, but are completely nonbackdrivable and excellent for positional accuracy with high resolution. High pitch screws are more efficient and backdrivable in some cases, but do not have the high force output usually required of a linear actuator. Ball screws are an improved form of lead screw that use ball bearings to mitigate friction with the screw, increasing efficiency and minimizing backlash but increasing cost and weight.

Lead screw linear actuators are often used in statically stable robots bearing high loads, such as MAX [18]. These systems make use of precise positioning and nonbackdrivability to move rotary joints with basic linkages and avoid using energy unless moving. Walking with joints that lock in place in stance and need to exert very little force to move in swing is extremely energy efficient. Though lead screws tend to require more structure and mass in rails, linear bearings, the screw itself, and associated joint linkages than rotary actuators, they are able to use lighter motors and power storage options due to this efficiency.

$$l = \frac{\dot{x}}{\dot{\theta}} \tag{3.11}$$

$$\nu = \frac{\tan(h)}{\tan(h + \arctan(\mu))} \tag{3.12}$$

$$\tau = \begin{cases} \frac{Fd_m}{2} \frac{l + \pi \mu d_m \sec(\alpha)}{\pi d_m - \mu l \sec(\alpha)} & \text{when force coincides with motion} \\ \frac{Fd_m}{2} \frac{\pi \mu d_m \sec(\alpha) - l}{\pi d_m + \mu l \sec(\alpha)} & \text{when force is opposite motion} \end{cases} \tag{3.13}$$

Table 3.6: Lead Screw Equation Parameters

| Name | Symbol |
|---|---|
| Driving Torque | $\tau$ |
| Output Force | $F$ |
| Input Speed | $\dot{\theta}$ |
| Output Speed | $\dot{x}$ |
| Coefficient of Friction | $\mu$ |
| Lead | $l$ |
| Minor Diameter | $d_m$ |
| Thread Angle | $\alpha$ |
| Helix Angle | $h$ |

**Tendon Drive:** There are several types of tendon driven actuator, the most common being a tendon-pulley combination to generate mechanical advantage in linear motion. The main advantage of tendon-driven legs is the opportunity to consolidate the majority of actuator mass in the body, with only the cable and a few pulleys making up the distal mass. While this is typically more useful in small systems such as robot hands, legged robots follow similar principles and can even be considered as world-manipulating hands [73]. Tendons can be routed nearly anywhere in a robotic system, especially in ways that mimic biological flexors/extensors, such as in the LIMS system [74], shown in Figure 3.15. This tendon drive system is torque dense, highly transparent, low mass, efficient, and well suited for limbed robots.

Another intriguing style tendon drive system is the twisted wire actuator [75]. These rely on the tension resultant from twisting two parallel cables about each other, which can yield large transmission ratios and apply large forces with little actuator mass. These actuators also benefit from long, straight sections along which to run the tendons, of which Titan 6 has plenty inside the femur and tibia links.

Though initially considered for Titan 6 hip and knee actuators, these tendon drive systems were eliminated due to their inability to be modular in a legged robot architecture. When cables are routed through multiple joints, the system becomes hopelessly coupled, preventing single actuators from being swapped out in-situ without long repair times. Additionally, stretching over long lengths of tendons can contribute to actuator backlash and unwanted compliance [76].

43
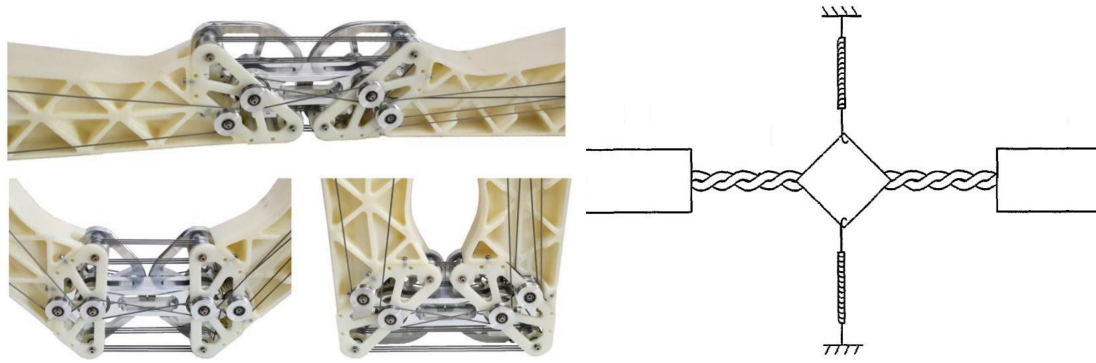
Figure 3.15: Two tendon drive actuators; a joint on LIMS, from [74] (left), and a twisted wire actuator, from [75] (right).

## Hydraulics

Hydraulics may often be treated like an entirely separate regime of actuation,[5] but in reality it is simply a form of transmission with an extra energy conversion stage in the motor-driven pump. Though hydraulics are typically used in industry for large scale actuation such as construction equipment and active vehicle suspensions, smaller scale high-fidelity hydraulic systems have been used effectively in many of the Boston Dynamics legged robots such as BigDog with a gas motor for power generation and Atlas with an electric power train. As shown in Figure 3.16, this style of hydraulic actuation is inherently centralized, relying on one large motor-pump for energy conversion and a series of manifolds, valves, and lines acting as the transmission to drive cylinders located at the joints. This centralization allows it to be high force and high speed simultaneously with great efficiency (depending on flow path and pump selection), with one extremely energetic flow available wherever it is needed. The downside of this centralization is that every joint is now coupled, and driving all eighteen of Titan 6's joints simultaneously would degrade performance in each. Of course, traditional centralized hydraulics can hardly be modular; even with hydraulic quick-connects allowing cylinders and valves to be swapped out, damage to the motor or pump would cripple the entire robot [77].

---

[5]Pneumatics are in the same branch of centralized actuation with fluid transmission, but are not considered for Titan 6 due to the compressability of air. Unlike incompressible hydraulic fluid, air-based actuation is unavoidably compliant and a stalled leg can lead to dangerous energy storage that could be released by kicking operators up to two meters away.
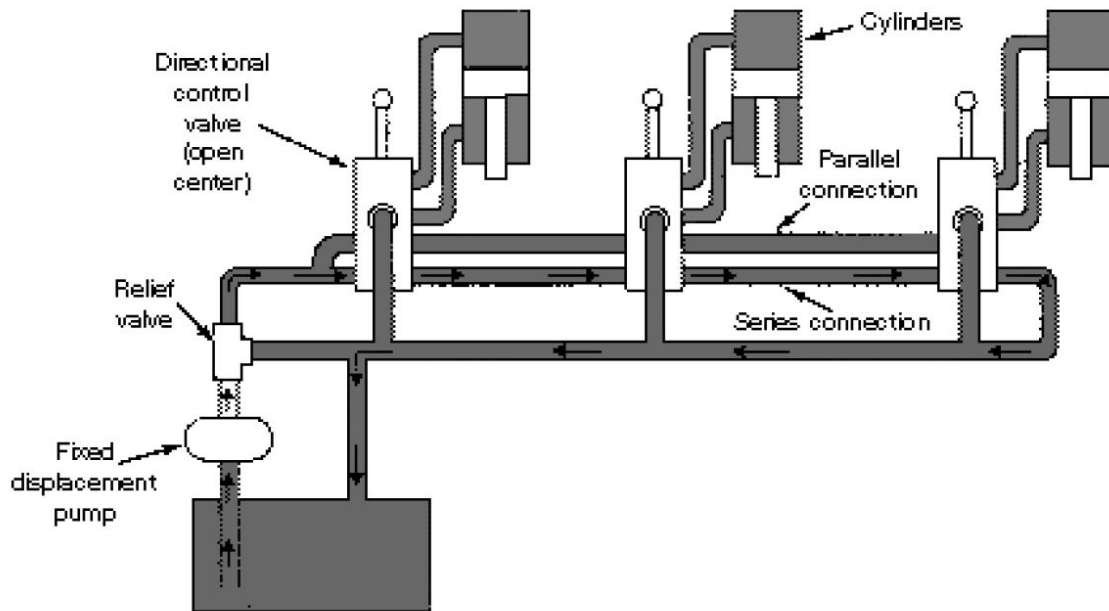
Figure 3.16: A centralized hydraulic system with three double-acting cylinders combined in a relatively standard but low efficiency flow path, from [77].

However, recent advances in micro-hydraulic technology have made distributed modular hydraulics more realistic [78]. Rather than a traditional system that uses valves, which can weight several kilograms each, to direct flow to the correct joint, it is possible to have a battery-motor-pump-reservoir combination hooked up to each cylinder directly [79]. This design would be exorbitantly expensive for an 18-DoF system, but it would be torque-dense, robust, backlash free, and fully modular.

While some pumps can be backdriven as hydraulic motors, the transparency would be poor, ultimately limiting proprioception resolution [80]. Inline pressure sensing is simple and noninvasive, and would provide a highly accurate measurement of the force on the cylinder rod, which could be used as a stand-in for proprioception [81]. Controlling the pressure in the line rather than position of the output shaft would allow for force control of the joint, affording most of the benefits of highly transparent systems without the need expend energy to hold position. It is important to note that this approach to hydraulics is limited by the spin-up speed of the motor-pump, requiring detailed motor models to design controllers that use viable trajectories.

45

# 4.   Brakes and Clutches

Backdrivable actuators are both a blessing and a curse. Under dynamic loading they can save gear teeth and allow the motor to dissipate the shock energy as heat in the coils, but under static loading it can force the motor to expend energy in a zero-efficiency configuration ($\dot{\theta}_o = 0 \implies \eta = 0$ by Eq. 3.5). Components such as brakes and clutches allow actuators to be **selectively backdrivable**, either by locking the output shaft in place or by disengaging a nonbackdrivable transmission. This concept has been used for mechanical force control in grippers [82] and selective compliance in early iterations of self-tapping anchors [83].

It is important to note that electromagnetic brakes and clutches can draw significant amounts of current to maintain either their locked or unlocked state. Though the design of the locking interface is much more efficient at holding position than a motor coil, the energy economics of the added weight of the component, nominal locking current draw, and benefit to performance must be considered carefully for every legged robot. An excellent review of robotic joint locking technology for selective backdrivability can be found in [84], with a summary in Figure 3.17.



| Locking Principle | | |
| --- | --- | --- |
| **Mechanical** | **Friction** | **Singularity** |
| Latches<br>Ratchets<br>Dog Clutches<br>Hydraulic Locks | Electromagnetic (EM)<br>Overrunning<br>Self-Amplifying<br>Capstans<br>Piezoelectric<br>Bistable<br>Statically Balanced<br>Thermic | Four-Bar<br>Linkages |
| Latches<br>Ratchets<br>Cam Based | Overrunning<br>Nonbackdrivable | Nonlinear<br>Transfer Ratio |

Figure 3.17: A categorized list of joint locking mechanisms from [84].

# 5.  Heat Dissipation

The performance of an actuator's power train is fundamentally limited by its ability to dissipate generated heat away from sensitive components. Every watt of power that is lost between the storage and end-effector ends up as heat (shown by Eq. 3.14 and Figure 3.1), with certain components such as motor coils, motor controllers, computers, and high-friction points in transmissions especially vulnerable to burning themselves out. Some actuators have the luxury of temperature sensors to ensure safety and others have to rely on provably safe, worst-case thermal models, but either way heat dissipation elements must be incorporated to achieve optimal performance.[6]

$$\dot{Q} = P_i(1 - \eta_m\eta_t) + P_e \tag{3.14}$$

Passive elements such as fin-array heat sinks are common in robotic actuators that can spare the room; otherwise anodized aluminum casings can do a good job of radiating heat away from internals [85]. In systems with more extreme thermal issues, active dissipation such as fans or liquid cooling may be employed. These are usually power hungry systems in and of themselves, so are not a good match for legged robots. However, it is possible to use the already high-speed motor shaft to drive a cooling fan at minimal cost to actuator efficiency. By piggybacking on existing rotation to drive a fan, a separate fan actuator is avoided, saving weight and providing thermal transfer coefficients several orders of magnitude larger than free convection or radiation. The idea of a rotor fan with open casing was explored in early designs of modular Titan 6 actuators, shown in Figure 3.18. In a nonbackdrivable actuator that can hold stance without heating up, this idea is viable, but in a system that will generate most heat when standing still, coupling the fan to the actuator motion means that the cooling does not operate when it is most needed. Adding a "breathing" behavior, in which the robot gently oscillates vertically in stance, is an easy software fix in theory, but the thermal model has not been created to verify that this added motion will reduce heat build up.

---

[6]Remember from Section 3.2. that an electric motor can always output more torque or speed based on its $k_t$ and $k_s$ values as long as that extra heat can be dissipated.
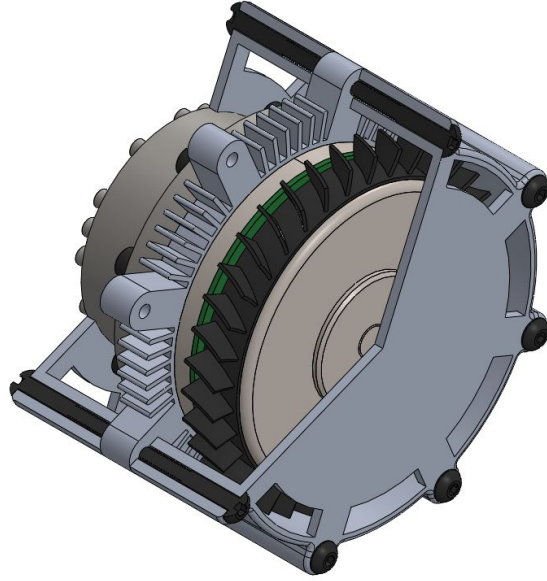
Figure 3.18: Cutaway of an early design of a modular Titan 6 actuator with rotor fan providing forced convection over a heat sink to allow the motor to operate above its rated current limit.

# 6.   Computation, Communication, and Control

Onboard computers take on a supporting role in modular actuators, handling low-level motor commands and feedback control from position and torque sensors. Often their job is to handle reflex commands quickly that would take too long to send to the main computer and wait for a return signal. This could include capping motor current as windings heat up, handling selective backdrivability for actuator safety, or even adjusting the leg motion for uneven terrain. However, Titan 6 does not have a central computer, so its modular processing responsibilities must balloon to handle both low-level and mid-level control parameters, such as basic gait cycles. High-level control such as path planning or operator interaction can be handled by a communication module with a single centralized computer or by designating one module as the leader, allowing it to delegate out parallel processes to other modules.

Intermodule communications require choosing between information packet, signal, and wiring/wireless standards. It can be tempting to try to craft custom bus and wire harness designs to fit a robot's exact needs, but often selecting from an existing

protocol, such as Ethernet, CAN bus, or I$^2$C is sufficient. Titan 6 has large distances between modules, making USB communication unreliable and non-paired signals noisy even with proper shielding. Running long signal lines through leg segments can end up acting as antennae, picking up noise from wireless networks or even other components in the robot. The size of Titan 6 is just at the edge of justifying wireless intermodule communication such as Wifi 802.11 or Bluetooth Low Energy (BLE). Though these methods have significantly lower data transfer rates and are subject to busy signal bandwidths from nearby networks, they can prevent using over twelve meters of cable that would weight almost a kilogram, and would increase the modularity of the system.

# 7.   Sensing

For legged robots, joint sensing is almost as important as the module power train for effective locomotion. Position sensing is vital to closing the loop on control, but the addition of torque sensing can improve an actuator's ability to cope with unpredictable environments in the same way a biological system can adjust its gait based on proprioceptive feedback. Additionally, many modern sensors have been shrunk down to integrated circuits (ICs) or printed circuit boards (PCBs), allowing modular actuators to incorporate fairly extensive sensor payloads with negligible mass or power draw. By distributing many of these sensors across the robot's joints, patterns may emerge that can be interpreted by convolutional neural networks (CNNs).

   Listed below are a handful of sensors that are easily integrated into actuator electronics packages along with their uses on a legged system. Inertial measurement units (IMUs) can provide orientation data for pose adjustment on uneven ground and sense accelerations from leg impacts. Ambient or component-embedded temperature sensors can inform thermal models for expected heat dissipation and define safe limits of continuous operation. Current and voltage sensing at various places throughout the power train can inform the computer of battery charge levels, electrical malfunctions, and motor power input. Environmental sensors can keep the robot informed of dust and moisture ingress before it becomes problematic. These examples are only a few of the sensor possibilities and say nothing of their capabilities for measurement in

actual field deployments, where the entire goal could be to collect data from a certain set of built-in sensors.

## Position Sensing

Position sensing is typically accomplished with an encoder, which can be incremental or absolute. Incremental encoders are simpler, cheaper, and usually smaller, but can only measure a change in position, so every time the system is power cycled it must be recalibrated to account for movement while turned off. These work well in tight spaces, especially for nonbackdrivable systems with onboard memory, preventing the need for calibration on every startup. Alternatively, absolute encoders are able to individually encode some number of joint positions with distinct markers so they are always able to determine the absolute position with respect to the original calibration. These are usually more expensive and often include a small processor to read and interpret the sensor value.

The placement of an encoder in the power train is critical to its performance; measuring the output of the motor and multiplying by the transmission ratio does not take backlash into account like directly measuring the joint angle would. Magnetic encoders rely on precisely calibrated magnet rings, disks, or strips, which can be demagnetized by nearby hot components or give noisy readings if too close to the motor coils. Hall effect sensors are sometimes included on motor casings for measuring the position and velocity of the rotor, but nearby permanent magnets from other encoders may corrupt their readings.

## Force/Torque Sensing

**Current Sensing:** Motor torque output can be calculated as a function of the input current (Eq. 3.2), and the output force/torque of a transmission is a direct function of the motor torque and transmission ratio (Eq. 3.7). Thus, in an ideal world measuring the current draw of the motor should inform the torque experienced at the joint. Unfortunately, efficiencies are time varying, backlash corrupts measurements, and these models are not perfect, making it difficult to rely on current-based torque sensing in systems with high transmission ratios. Systems that use direct drive can ignore the efficiency term and don't experience backlash, and have demonstrated

highly capable current-based proprioception [86]. While early uses on legged robots were only to determine the instance of ground contact, more recent results have shown the ability to sense force with enough fidelity to measure ground force reactions for gait control [87] or for terrain identification [88]. While current sensing is possible for systems with large transmission ratios, it is only suitable for determining moment of impact and direction of torque about the joint. It is worth noting that this is the only form of force sensing that does not require additional mechanical components in the power train that add complexity and points of failure.

**Series Elasticity:** By incorporating a flexible element into a transmission and providing measurements of its deflection during actuator operation, series elasticity essentially turns the force sensing problem into a position sensing problem, which robotic actuators are already adept at solving [89]. It is possible to get accurate, high resolution torque feedback from a series elastic actuator using Hooke's law to determine the torque on a spring attached to the output shaft of a transmission. This method of force control works especially well in geared transmissions, as evidenced by Figure 3.19, where the elastic element can be hidden inside one of the gears [67, 90] as shown in Figure 3.11. It is also useful for force sensing in linear transmissions such as lead screw or hydraulic cylinder driven joints [91].

This method of torque sensing does come with a trade-off between sensing resolution and additional actuator compliance. A lower spring stiffness corresponds to higher deflections under the same load, which widens the sensing window of an
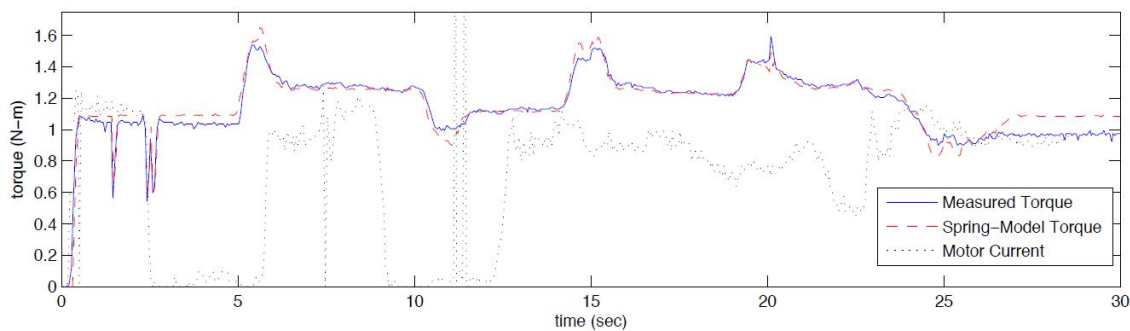


Figure 3.19: A torque plot for a highly-geared series elastic actuator, showing the torque sensed by the spring-model closely tracking ground truth torque and unusable levels of noise corrupting the current sensing-based torque measurement, from [90].

encoder of fixed resolution. This added compliance can be beneficial for legged loco-motion [92]; reducing shock loads on the power train, making the robot safer around operators, and preventing uneven ground from toppling the system. However, for Titan 6 to use series elastic actuators with its long links and not incorporate massive amounts of uncertainty in foot position, the spring would need to be extremely high stiffness, which would be too low resolution to be useful.

**Strain Gauge:** Strain gauges are thin resistive loops designed to measure strain in deflecting surface to which they are attached. They have been used effectively to sense minute deflections in actuator components in the load path to determine force/torque output. However, strain gauges only report a single value for strain measurement, and this aggregates strain from tension, compression, torsion, and bending that may be affecting the measured area. It follows that this sensing method would be prone to noise from deflection resulting from out of plane torques or forces. Multiple sensors attached to a custom component designed for outsize deflection from torque about the appropriate axis, as shown in Figure 3.20, can solve this problem, but add significant complexity to the actuator design [93]. Some work has been done to use the flex spline part of a harmonic drive as such a component, since it is flexible and well supported against loads other than torsion [94]. Sensor wiring presents a logistical issue for these designs, as the gauges are on a rotating component, limiting continuous rotation of the actuator.
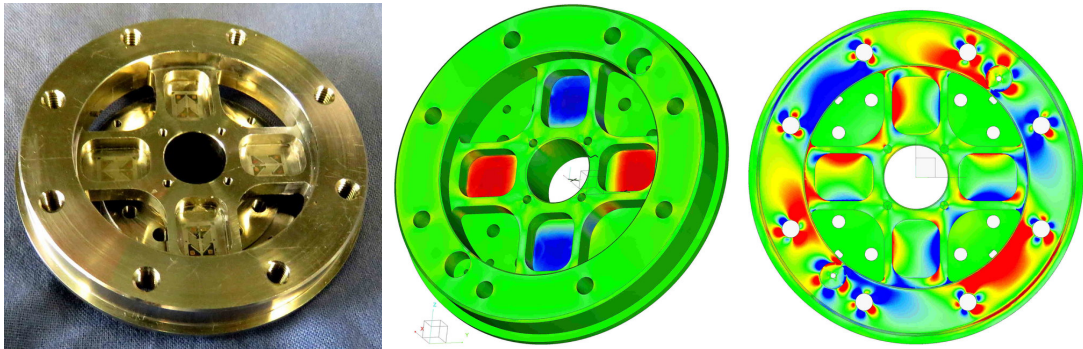


Figure 3.20: An actuator component designed to measure output torque using four strain gauges (left), Finite Element Analysis (FEA) results showing the component under torsional load with concentrated strain on four surfaces where the gauges are mounted (center), and FEA results showing the component under a shear force load with minimal strain near the gauges, adapted from [93].

# 8.  Discussion

At the conclusion of the literature and technology review for designing Titan 6's modular leg actuators, it is clear that the target actuator should prioritize torque density. The power storage should have high specific energy and allow for highly efficient power conversion with an electric motor. The power conversion should be a brushless DC motor that is frameless to cut down on redundant casing mass. The transmission should have low backlash and be resilient to high impact loading, and it would be optimal if the legs were selectively backdrivable. High resolution position sensing on the output shaft without repeated calibration is necessary, high-fidelity force sensing at the joints is desired but a rough estimate may be sufficient.

With these expectations laid out, two models of Titan 6 joints were designed in parallel to explore the actuator design space and determine the performance on a full-size legged robot. These designs are described in Chapter IV.

# Chapter IV

# System Design

In the process of designing Titan 6, four models were produced, as summarized in Table 4.1. Each version of Titan 6 is meant to explore a different aspect of the system. This approach ensured that the development of localization algorithms, controllers, and actuator designs could proceed in parallel. Teams working on each robot were able to share discoveries throughout the process, giving valuable feedback that factored into later iterations. Mat-6, the scale model, was built quickly to provide a legged robot upon which to develop the top-level control: global planners and SLAM algorithms. Hebi-6 soon followed as an early prototype used to characterize the dynamics of such a long-legged robot and develop appropriate gaits and controllers, and was redesigned multiple times to improve performance. The capabilities of these systems, along with the Hexapod Actuation Calculator (see Chapter II) and actuator technology survey (see Chapter III) enabled the informed design of the final Titan 6 modules and system architecture. The two leading transmission designs from early analysis were pursued through the Harmonic-6 and Hydraulic-6 systems, with the goal of completing the designs of both modular actuators and building a test leg from each. The results from this test leg characterization then would determine which design would move forward to build the final Titan 6 robot and if any advantageous design aspects from the losing model could be subsumed by the winner. This chapter describes the design process and goals of developing each system along with an examination of key mechanical design intricacies.

Table 4.1: Geometric Descriptions of All Titan 6 Prototypes

| Name | Leg Length (m) | Mass (kg) | Development Focus |
|---|---|---|---|
| Mat-6 | 0.62 | 21.6 | High Level Planning |
| Hebi-6 | 2.0 | 23.0 | Controller & Gait Design |
| Harmonic-6 | 1.98 | 70* | Harmonic Actuator Testing |
| Hydraulic-6 | 2.0 | 135* | Hydraulic Actuator Testing |

\* These values are estimated from CAD models and prototype module masses.

# 1.  Mat-6 Scale Model

The Mat-6 design, shown in Figure 4.1, uses modular actuators that were commercially available from Hebi Robotics, a spin-off from the Biorobotics Lab, to accelerate the design process. These modules, known as X8-16s, are repackaged versions of the series elastic actuation technology from the SEA Snake [67] (see Figure 3.11) in a more general-purpose form factor. Each has a computer that handles joint-level control using encoders and series elastic elements to sense position, velocity, and force. While they require an external power source, the X8-16 actuators are otherwise self-contained, using a brushless DC motor with a parallel axis gear train to drive an output shaft 15 rpm at 16 Nm (38 Nm peak). Additional sensors provide temperature, orientation, acceleration, and power draw feedback, which can be read over Ethernet connections [95]. These modules formed a baseline for the future Titan 6 modular actuator development, and served well in the Mat-6 and Hebi-6 designs before the Titan 6 modules were fully developed.

Mat-6 is an approximately 1 : 3 scale model of the specified size for Titan 6; a leg length to joint torque ratio that is well studied and easily supported by the X8-16 actuators. This is key for allowing Mat-6 to use static stability assumptions (see Chapter I) to simplify control. The leg kinematics and static assumptions of this system are exactly the conditions simulated by the Hexapod Actuation Calculator App, and Mat-6 was used during tool development to verify outputs with measured speeds and torques on the real system. It also served as a platform to test sensor payloads and footstep planners in unstructured terrain. Because mapping and footstep placement are a fully geometric problems, they scale up well, but the scale model was not a useful dynamic analog for gait and controller development.
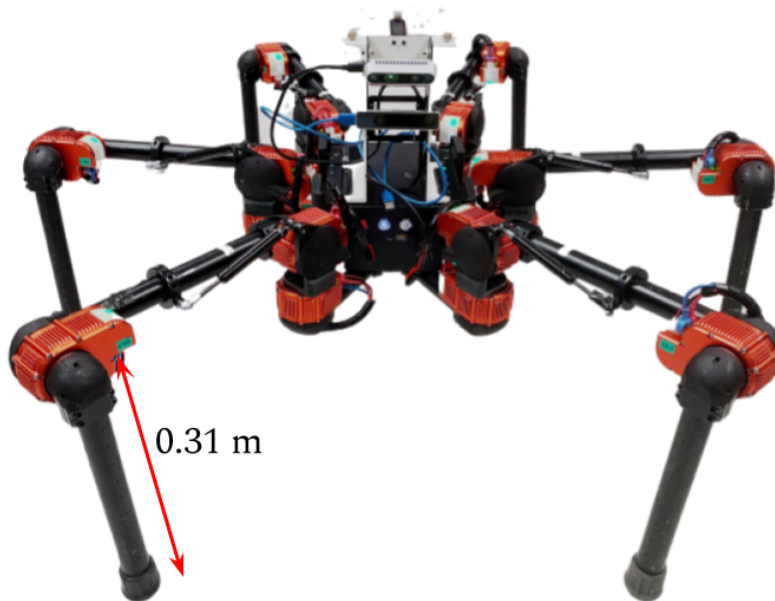
Figure 4.1: The Mat-6 scale model robot with an early perception payload for high level autonomy development.

## 2.   Hebi-6 Model

Titan 6 is an interesting platform because legged robot control enters a new regime when the resonant frequency of the system drops into the controllable bandwidth (see Chapter V for details). Mat-6 is easy to control, but nonlinear scaling in joint torques and resonant frequencies made Mat-6 an especially poor model for full-size long-limbed controller development, so Hebi-6, shown in Figure 4.2, was built to study to dynamics of sprawled-posture, thin-limbed, under-powered walking. This system was built in the early discovery phase of the project when the team was still gathering data to define the specifications of the Titan 6 joint modules, so Hebi X8-16 actuators were again used as a stand-in for the custom joints. These actuators, with low transparency, some backlash, and unwanted dynamic effects from the series elastic elements were not ideal for developing this system, but helped to illustrate the worst-case dynamics for an eventual finalized Titan 6 model. With the legs scaled up to the full size of 1.0 meter femur and tibia links, the module torque was severely insufficient to lift the body even with six legs, so the hip joint torque was doubled by

adding a second actuator acting in parallel. This solution increased the weight of the hip joint, drew significantly more power in stance, and was generally a brute-force solution to increasing the hip torque. While Hebi-6 was able to stand and shuffle along slowly, the added mass crippled the system's mobility and required a tether to off-board power to reduce weight and operate for useful amounts of time.



Figure 4.2: A render of the original Hebi-6 design with doubled hip modules and no onboard electronics shown.

## Differential Hip

Results from the actuation calculator showed early on that each joint in a Titan 6 leg requires completely different speeds and torques to execute a given gait. With the chosen kinematic leg configuration, the base joint has very low torque requirements, but its speed is the limiting factor for the walking speed of the robot. Also, as Figure 4.3 shows, the hip joint requires much more torque than the knee joint. Actuation requirement disparity between joints makes the system a poor candidate for modularity using a common actuator system-wide. The speed-torque curve of a universal module must meet the requirements of all joints, and an actuator with the desired speed of the base and the torque of the hip would be too heavy.
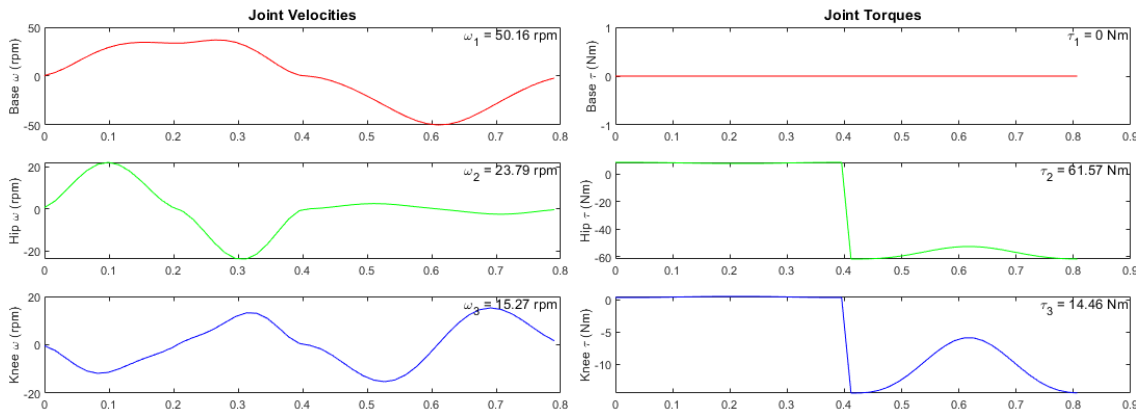
Figure 4.3: Calculator output using Hebi-6 geometry showing the requirement dispar- ity between each joint while executing one step of an alternating tripod gait.

Even optimizing the gait pattern and leg stance positions to bring the torque and speed requirements into similar operating zones was insufficient, so the differential hip joint was developed as a mechanical solution. This joint allows two modules to do the work of three by coupling two hip modules through a differential with its pinion fixed to the body of the robot. Per Eqs. 4.1, 4.2, and 4.3, by turning the actuators in opposite directions the differential does not rotate and the mechanism acts as a lifting hip joint with their combined torques, and by turning the actuators in the same direction the leg will rotate about the pinion gear, acting as a swinging base joint with speed increased by the ratio of teeth in the bevel gears to teeth in the pinion gear. These examples are extreme cases, but combination motions are possible: moving both the virtual hip and virtual base joints simultaneously at reduced torque as shown in Figure 4.4. This mechanism decreases the requirement disparity between Hebi-6's joints, focusing on torque about one axis and speed about the other by using two actuators in tandem that could not meet either of these requirement sets alone.

$$N_d = \frac{T_{bevel}}{T_{pinion}} \tag{4.1}$$

$$\theta_{base} = N_d(\theta_1 + \theta_2) \quad \text{and} \quad \theta_{hip} = \theta_1 - \theta_2 \tag{4.2}$$

$$\tau_{base} = \frac{\tau_1 + \tau_2}{N_d} \quad \text{and} \quad \tau_{hip} = \tau_1 - \tau_2 \tag{4.3}$$

59

Figure 4.4 illustrates the advantage of the differential base-hip design over a decoupled design. The blue line is the convex hull summarizing the base-hip torque requirements for Hebi-6. These values represent a full torque requirement set derived from the Hexapod Actuation Calculator App. When the original design for the base-hip as decoupled modules in series is considered, the base module is well within its operating range, but the hip module is unable to reach the blue-outlined required torques. In the differential hip design both modules operate within saturation limits, and a larger portion of the blue-outlined area lies in low-torque regions, indicating reduced power draw of the system.
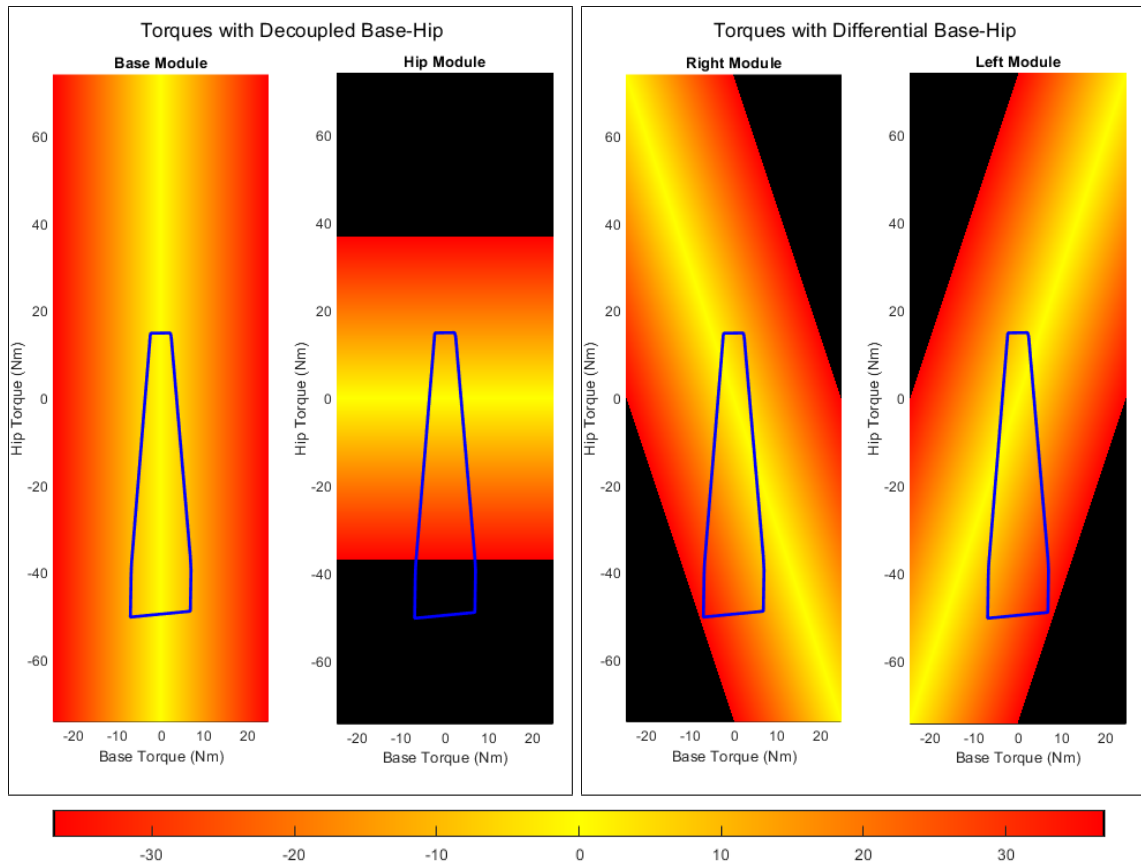


Figure 4.4: Two sets of torque maps for the decoupled base-hip (left) and the differential base-hip (right). The blue line, which is identical across all four plots, indicates required torque output of the two modules. The gradient in each of the four plots from left to right is specific to the decoupled base module, the decoupled hip module, the right differential module, or the left differential hip module. Yellow areas indicate low torque requirements, red areas indicate high torque requirements, and black areas indicate unreachable torques based on the strength of an X8-16 actuator.

Repeated iterations of this design have reduced the mass of the differential and associated structure to less than the weight of one actuator, so by implementing the differential hip Hebi-6 improves performance of two joints, reduces mass, reduces nominal power draw by one module per leg, and cuts cost of each leg significantly. However, while the differential hip makes Hebi-6 better adapted for a universal module solution, it requires adding several moving components to the robot design outside of the modular actuator, which can make the system more difficult to repair in the field. To ensure that the repairability of the modular architecture would not be undercut by the differential hip, it's Factor of Safety (FoS) in static, shock, and fatigue loading is significantly larger than other components. Additionally, a sacrificial part in the form of a clip-on retaining ring was added to the last iteration of the mechanism. This component is designed to fail before the rest of the differential, thus protecting the rest of the more expensive and essential components by decoupling the leg from the body under extreme load. The sacrificial retaining ring costs only $0.22 and can be replaced quickly [96]. During testing of Hebi-6, the differential hip has been a point of failure twice thusfar; in both instances the retaining ring failed as intended to decouple the leg and protected the more valuable leg components including the differential shafts and modular actuators. The main iterations of Hebi-6's base/hip assemblies are shown in Figure 4.5.
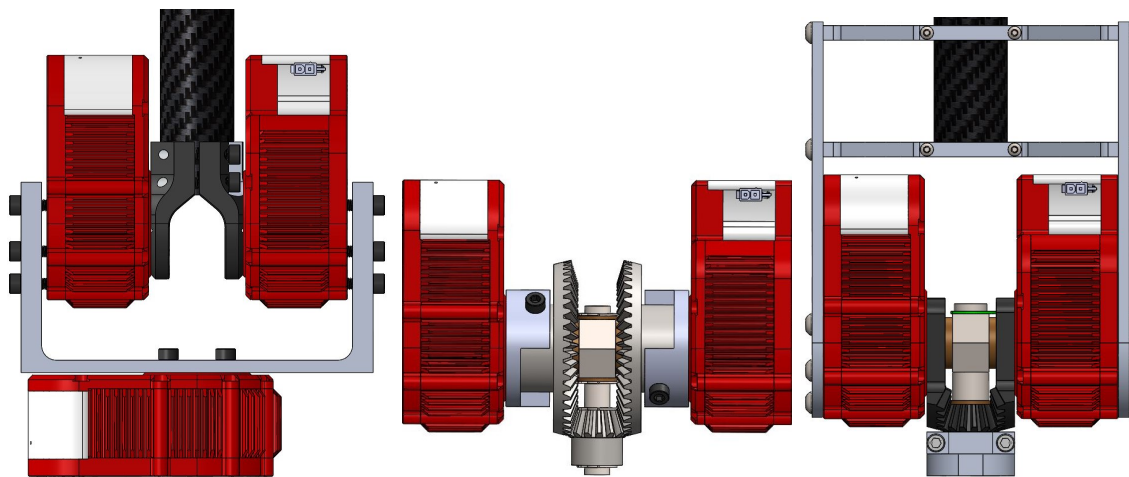


Figure 4.5: The evolution of the Hebi-6 hip from two rigidly coupled modules (left) to the differential hip (center) to the mass-optimized differential hip with sacrificial retaining ring shown in green (right).

# 3.   Harmonic-6 Model

The Harmonic-6 modular actuator (shown in Figure 4.6) is the culmination of the actuator technology research explored in Chapter III. It uses a custom LiPo battery pack for energy storage, a frameless brushless DC motor for energy conversion, and a harmonic drive transmission to increase the torque output. The module is designed specifically to meet the system requirements described in Chapter I and set by the Hexapod Actuation Calculator App, and exists as a joint-link combination module for the legs of Titan 6. Design specifications and achieved results can be found in Table 4.2. As of the publication of this thesis, the Harmonic 6 module design has been finalized and a single prototype module has been fully assembled and tested. Alongside two more modules currently in production, this will form the test leg that will be evaluated against the Hydraulic-6 modules before the full production run of eighteen for the full Titan 6 robot.
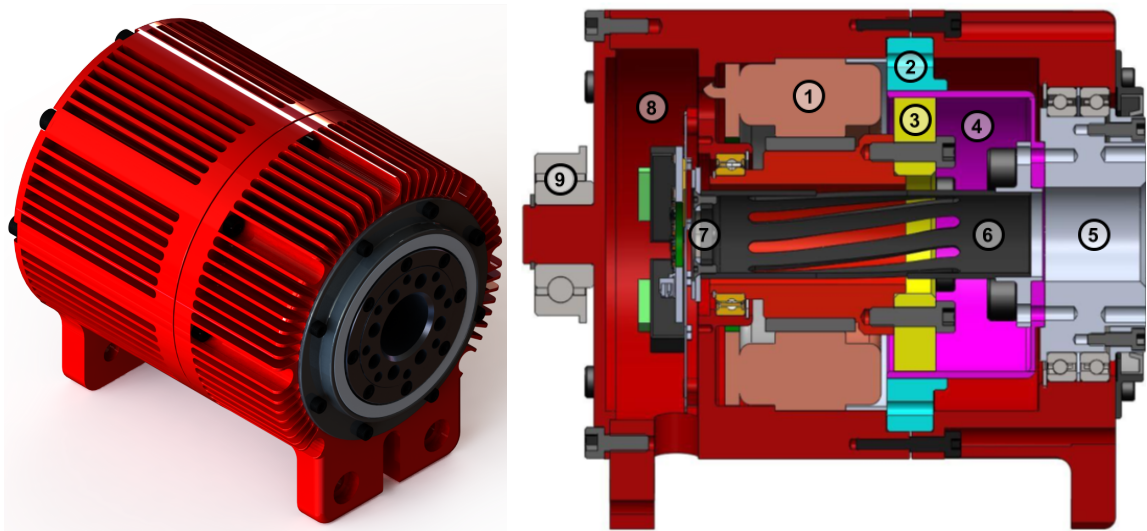


Figure 4.6: An isometric render of the Harmonic-6 joint module (leg link with battery not visible) showing red anodized aluminum heat sink casing (left) and drive train cross section with labeled components: 1) motor stator, 2) harmonic circular spline, 3) harmonic wave generator, 4) harmonic flex spline, 5) bearing-supported output hub, 6) internal fan/encoder mount, 7) output encoder, 8) electronics bay, and 9) output double support bearing.

Table 4.2: Harmonic-6 Actuator Design Specifications and Results

| Property | Specified | Actual |
|---|---|---|
| Joint Mass (kg) | 2.0 | 1.8 |
| Nominal Torque (Nm) | 80 | 77 |
| Peak Torque (Nm) | 100 | 243 |
| Output Speed (rpm) | 34 | 39 |
| Battery Mass (kg) | 0.5 | 0.88 |
| Estimated Runtime (min) | 30 | 40 |

## Motor and Harmonic Selection

This actuator was designed to minimize mass while meeting the above joint requirements, which starts with choosing a highly power-dense motor. The analysis in Chapter III showed that torque-density is key for the actuator, but a key feature of a harmonic drive is the ability to provide a huge range of transmission ratios in the same packaging size by modifying the number of teeth on the flex-spline and circular spline [97]. This decouples the transmission ratio from the transmission size, thus allowing us to focus motor selection on power density with the assumption that the appropriate ratio is available to convert that power to a useful speed-torque range. By surveying existing robotic actuators and a selection of motors from several potential suppliers, summarized in Figure 4.7, it became clear that frameless motors were highly power dense and fell within reasonable size and mass constraints. The selected motor is the Kollmorgen TMB(S)-7615-A, which has a nominal output of 0.964 Nm stall and 3930 rpm free.

 With the motor selected and a desired output range given, the required transmission ratio was determined to be in the range of 103:1 to 116:1 to meet or exceed actuator outputs. The Nidec-Shimpo WPC-63-100-CN-11K harmonic drive was selected because it is rated for the expected actuator loads and has a similar radius to the motor to simplify module packaging. This 100:1 transmission with an estimated efficiency of $\eta = 0.8$ [97] produces an actuator output of up to 77 Nm and 39 rpm. While this output is slightly less nominal torque than desired, the gap can be accounted for by overdriving the motor slightly. The lead time of components was a significant concern, leading to the selection of a standard 100:1 harmonic that is readily available but requires slightly more heat dissipation over a custom 110:1 harmonic that would take months for special ordering.
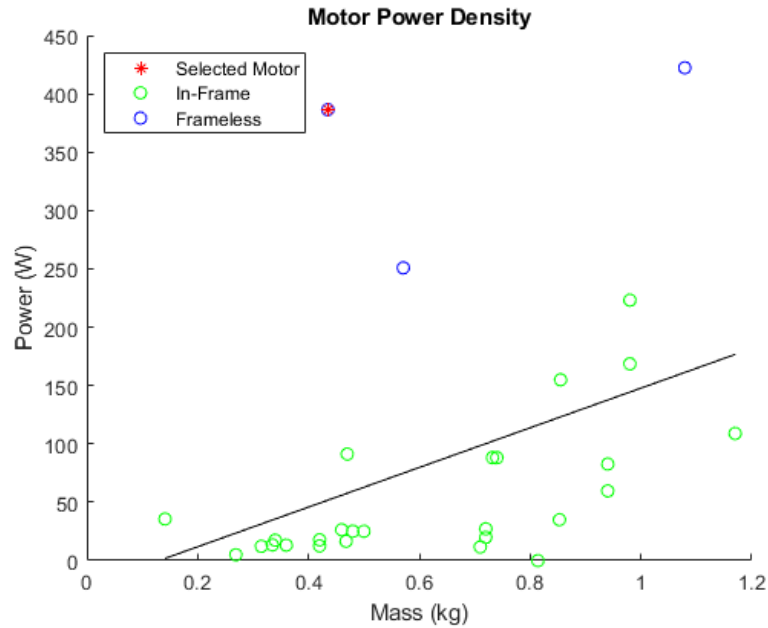
Figure 4.7: A comparison of considered motors for the Harmonic-6 actuator, with the more power-dense options above the fit line.

## Thermal Design

The Harmonic-6 motor can draw over 400 W nominally and up to 1250 W at peak current, of which 20% to 100% is converted to heat depending on the active speed of the actuator. This necessitates a robust heat dissipation system that can draw heat away from sensitive components like electronics, motor windings, or the flex-spline. Conveniently, the long-limbed architecture of Titan 6 thermally isolates the joints, allowing the thermal analysis to be performed on a single module at a time with the assumption that the surrounding air is the ambient temperature and unaffected by other heated components.

Using a one-eighth symmetry model of a Harmonic-6 module shown in Figure 4.8, two load cases were considered in designing the casing heat sink: steady state holding the torque needed by the hip joint to maintain a standing position and transient analysis of running a simple walking gait for five minutes. These cases describe the thermal loads expected in normal use and provided a baseline temperature for testing peak draw loading. With an ambient temperature of 25°C these loads were applied

as heat flow through the the main heat-generating components: the stator and the harmonic drive. The heat generated in the harmonic drive was split equally between the flex spline and circular spline and applied at the interfacing surface. Though these components touch at two points, this interface was approximated as adiabatic.
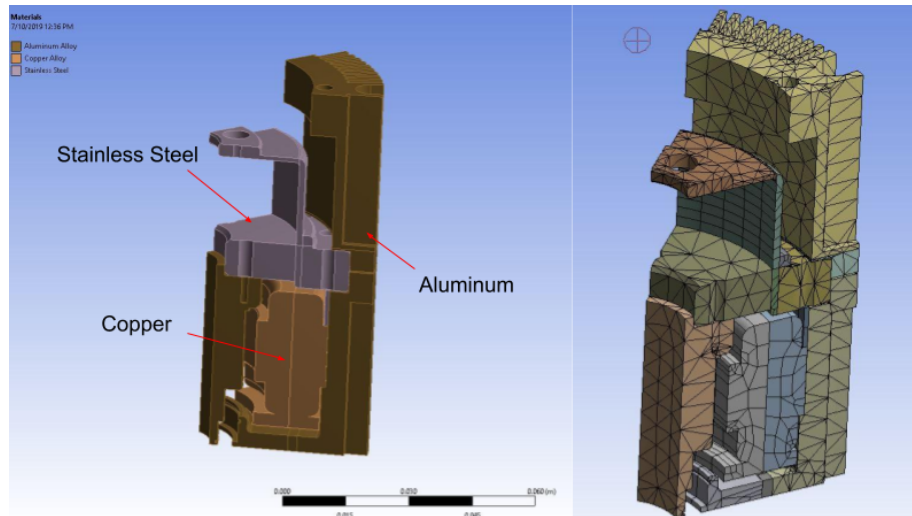


Figure 4.8: The simplified thermal model used to analyze the Harmonic-6 module with material assignments (left) and the generated mesh for finite element analysis (right).

Early results showed that proximity to the casing heat sink kept the motor, circular spline, and electronics well within a margin of safety under the baseline and peak draw loads, but the flex spline of the harmonic drive was building up heat quickly without a consistent path for heat to flow to the environment. However, early tests indicated that even a slight amount of forced convection through the hollow shaft of the module would sufficiently dissipate internal heat. This inspired an iteration of the encoder mount that included slits cut down the length to allow some air flow inside the flex spline and rotor mount. Unlike a true fan blade that spins to push air one way or the other, these slits were designed to direct the revolving air generated by the rotor spinning at one hundred times the speed of the encoder mount up into the cup of the flex spline. Using a "breathing" motion at discussed in Chapter III, a robot using the Harmonic-6 modules can keep the components safe and the casing below operating temperatures specified in Chapter I, as demonstrated by the results in Figure 4.9.
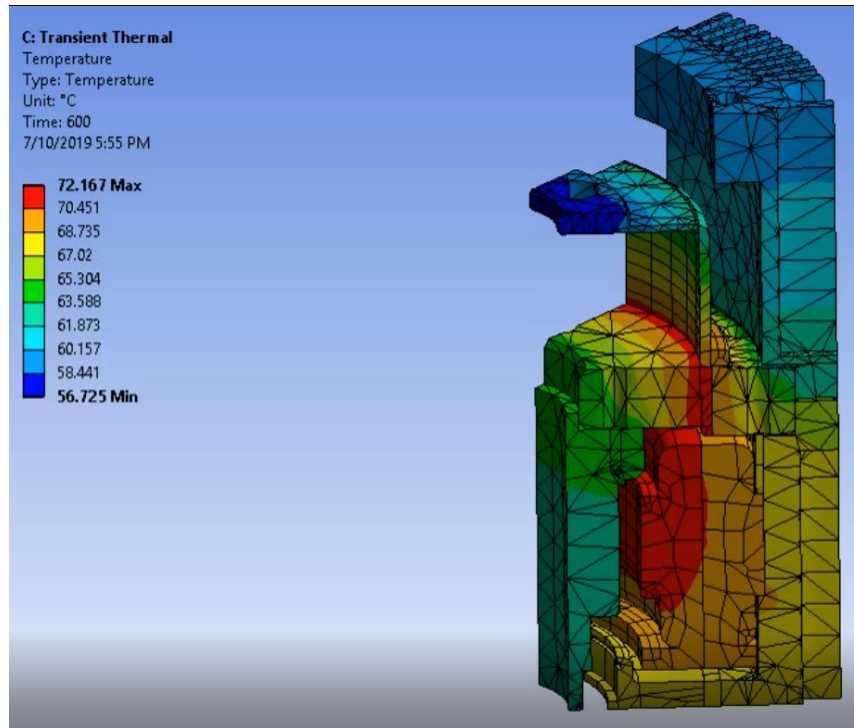
Figure 4.9: Results of the thermal analysis with a simplified model showing the components remain well within safe operating ranges in a normal operating case.

## Power System Design

Each joint actuator is accompanied by a LiPo battery pack to provide distributed power throughout the system. These packs are stored within the carbon fiber tubes that make up Harmonic-6's legs alongside each joint as shown in Figure 4.10. The packs were designed with discharge rates that match the expected draw of the Kollmorgen motor: 480 W continuous and up to 720 W peak draw for less than 10 seconds. Under normal operating conditions the packs will last approximately 40 minutes, but this is highly dependent on the duty cycle of the motor and the actual tasks performed by the robot. The battery management system regulates the output current to balance the cells and ensure that appropriate current is drawn as the cells discharge from a full 50.4 V to an empty 36.0 V. This voltage range is safe for the Harmonic-6 electronics, but additional testing is needed to determine the degree to which actuator performance degrades as the voltage falls over the span of a discharge.
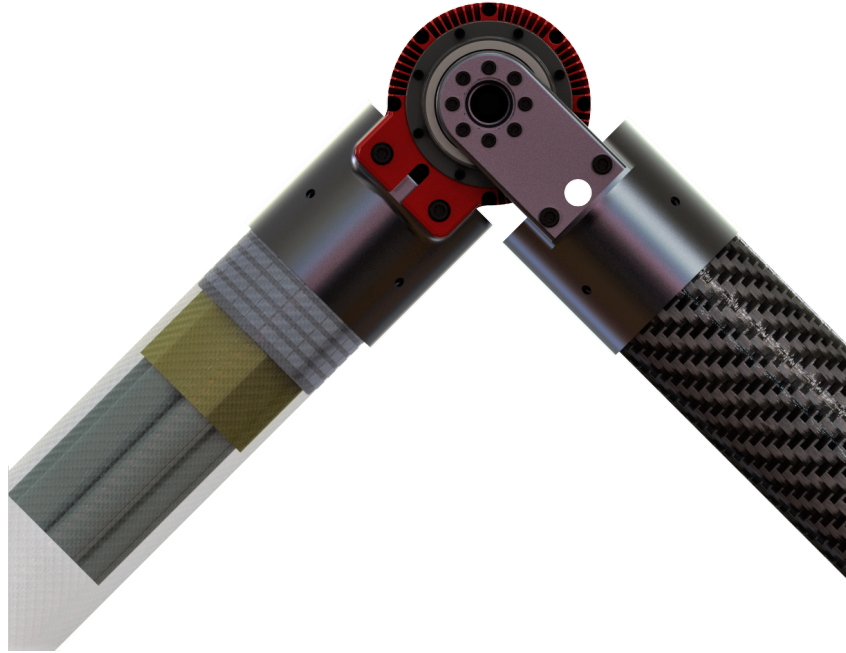
Figure 4.10: A complete Harmonic-6 module used as the knee joint of a leg. The carbon fiber link is transparent to show the custom battery pack.

# 4.  Hydraulic-6 Model

Hydraulic transmissions are often ideal for lifting large loads, and can be designed to be selectively backdrivable using inline pressure sensors without the complexity of locking mechanisms. They were of particular interest in designing Titan 6 as a system that can hold stance without drawing additional power. Furthermore, with a hydraulic module that uses a linear output, we can design linkages to drive joints at varying speed-torque ratios determined by their location in the system, which is ideal for a legged robot that needs torque in stance, speed in swing, and must use a common actuator.

## Centralized Hydraulics

Like other legged hydraulic robots, [98], this system was prototyped using centralized hydraulics powered by an off-board hydraulic power unit, shown in Figure 4.11. The leg was designed to be pseudo-modular; using quick-disconnect hose fittings to

fabricate joints that could be interchanged in under one minute without tools while sharing a centralized pump/motor for maximum efficiency. While extremely powerful and capable of both high speeds and torques, testing revealed several major issues with control of hydraulic joints. Air in the lines was a constant problem, allowing the hydraulic fluid to foam and damage the pump via cavitation and dry-running. The air also compressed under pressure, which slowed the system response time and added unwanted compliance. These issues caused by air in hydraulic lines are well studied [99], but these pervasive problems in the prototype leg demonstrated that a centralized hydraulic system would not be reasonable for Titan 6. Each time the joints were swapped, a small amount of air was introduced into the lines, making the pseudo-modular approach unsustainable. It was immediately clear that a hydraulic model of Titan 6 would need a sealed hydraulic circuit to avoid the presence of free or entrained air.

Even with a fully air-bled system, the compliance problem persisted; backpressure from the cylinder was able to flex long umbilical hoses routed back to the power unit
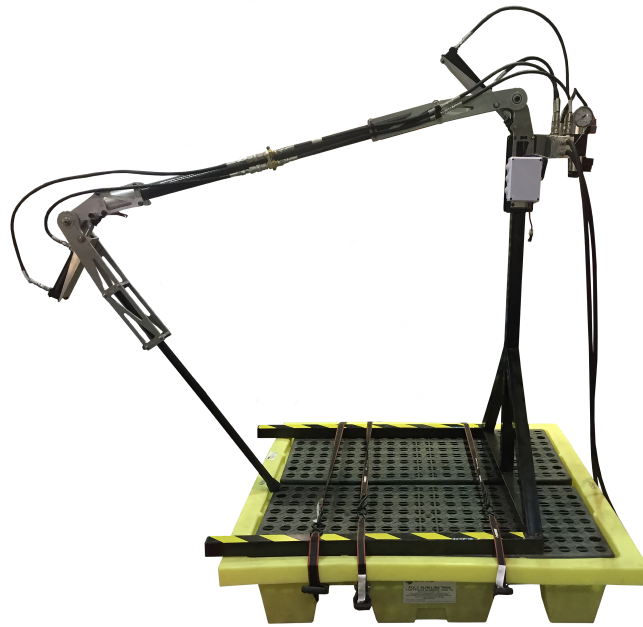


Figure 4.11: The two-joint centralized hydraulic test leg used to characterize hydraulic performance. Later this setup was repurposed to stress and impact-test leg link materials.

and move the output position of the joint up to 15 degrees under expected stance loading. These compliance issues were inherently exaggerated in the low-precision design of the prototype, but illustrated issues that could affect a full size Titan 6 robot, which would have at least 8 meters of hoses that would add unavoidable compliance and air ingress points to the system.

Finally, the prototype leg used double-action on-off valves to direct flow to and from the cylinder ports, which were ineffective for precision control. These valves forced the joints to act in one of three states: stationary, full-power extension, or full-power retraction. A bang-bang controller using an output encoder on the joint for feedback managed an approximation of position control, but often overshot the target position, plotted in Figure 4.12. This on-off control caused massive inertial accelerations, which flipped and eventually snapped the test stand in early testing. This illustrates how difficult these forces would be to counteract in a free-standing robotic system. Servo-proportional valves endow a hydraulic actuator with much better controllability, but are both too expensive and too heavy for use in Titan 6.
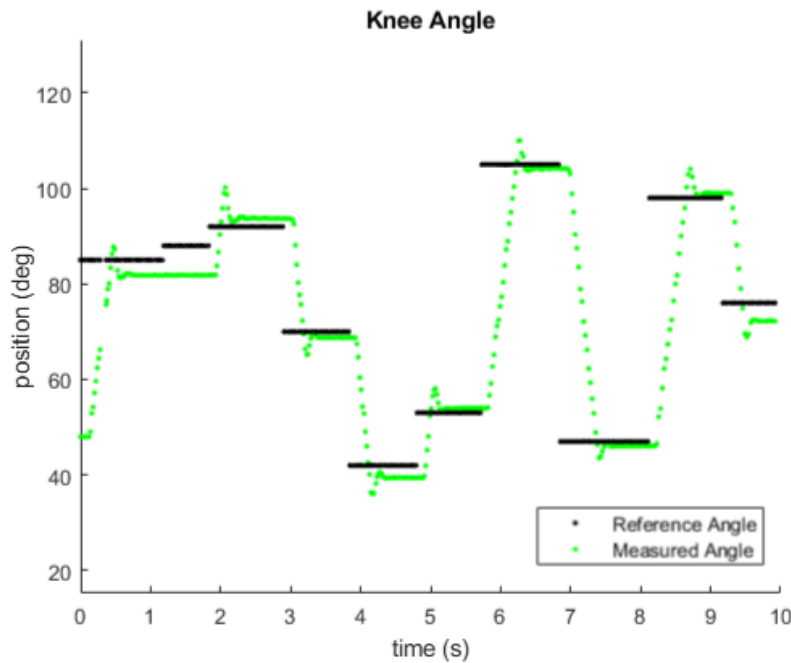


Figure 4.12: A plot showing the tuned bang-bang knee controller attempting to track a reference position (black) using joint encoder feedback (green). The poor rise time and overshoot is partially due to air in the lines.

## Modular Hydraulic Architecture

Despite the efficiency and weight-saving characteristics of centralized hydraulic transmissions, there is simply no way to make the system as modular as Titan 6 strives to be. Instead, we turned to microhydraulic transmissions that bypass the need for flow-directing valves by fitting each cylinder with a separate hydraulic circuit. This distributed approach draws significant benefits from the use of conventional motor control to drive a joint as a Single Input Single Output (SISO) system, decoupling the outputs of discrete joints. Additionally, this approach reduces the amount of hydraulic hard-line or hose routed through the legs and the need for a large central fluid reservoir to fill these lines, drastically reducing system weight. Figure 4.13 shows a basic overview of the electro-hydraulic circuit in the Hydraulic-6 modules, including the valveless hydraulic circuit, mechanical joint, and electric motor control using position feedback.
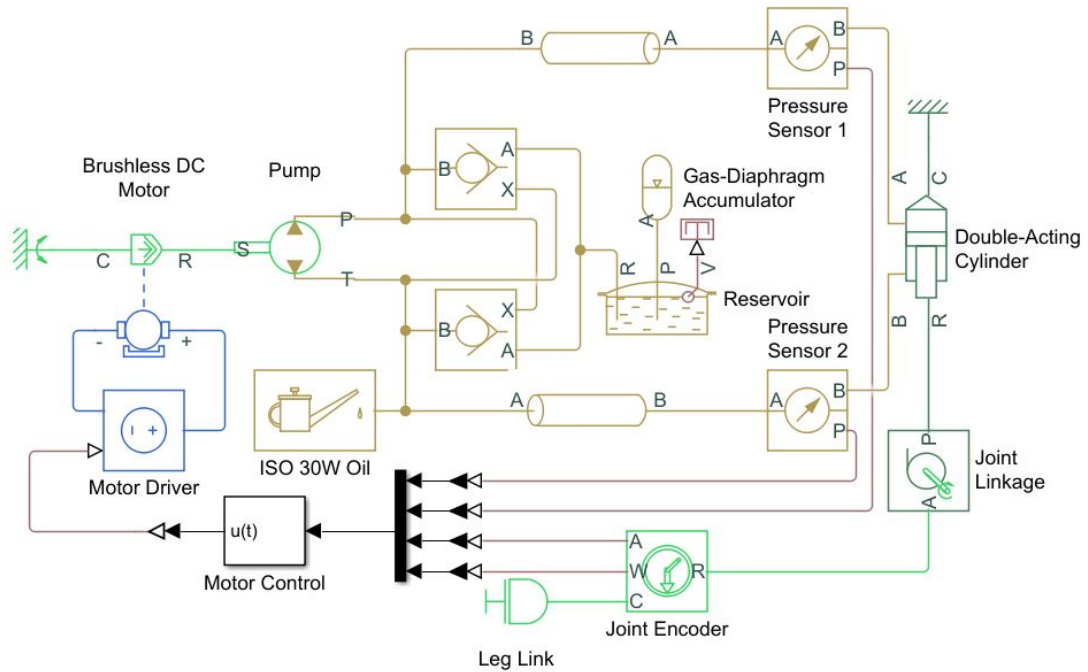


Figure 4.13: A Simulink diagram of the Harmonic-6 module showing the interaction of hydraulic lines (yellow), mechanical connections (green), electrical power wires (blue), electrical signal wires (maroon), and computer control (black). Note that the intake pilot valves are integrated into the pump in the physical system.

The design of these modules (see Figure 4.14) started by selecting a microhydraulic pump with the desired power output to match the Hexapod Actuation Calculator output for the Hydraulic-6 weight budget. Because the pump only determines a power output and the cross sectional area of the cylinder actually determines the output speed and force, we chose the Hydro-Leduc G_N002715 to maximize output. This selection also will benefit from the next iteration of this micro pump, which will triple flow capacity (and joint speed) as a drop in replacement in the future. This is driven by a Maxon 305015 brushless DC motor and is coupled to a custom $3.42 \times 10^{-3}$ m$^2$ bore cylinder to achieve the properties listed in Table 4.3. The same battery pack is shared between the Harmonic-6 and Hydraulic-6 modules, but we expect much longer runtimes from the Hydraulic-6 if static standing time is factored in as this only requires the nominal electronics power, $P_e$, to hold position.

Table 4.3: Hydraulic-6 Actuator Design Specifications and Results

| Property | Specified | Actual |
|---|---|---|
| Joint/Link Mass (kg) | 3.0 | 6.5 |
| Joint Torque (Nm) | 404 | 578* |
| Joint Speed (rpm) | 34 | 2.1* |
| Battery Mass (kg) | 0.5 | 0.88 |
| Estimated Runtime (min) | 30 | 100+ |

* These values are estimated using a baseline joint linkage.
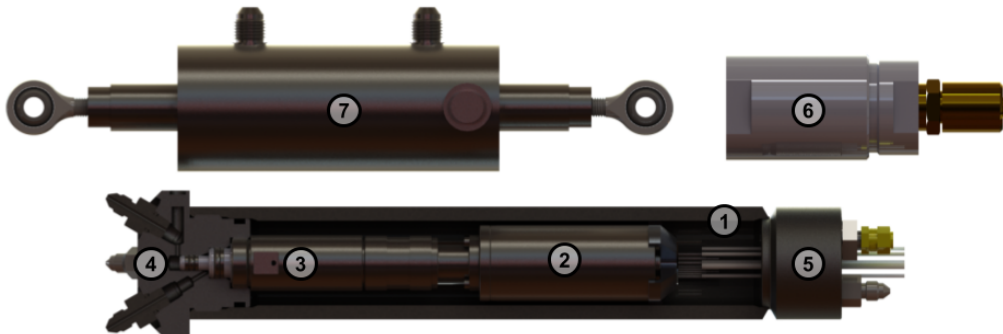


Figure 4.14: Partial cutaway of the major components of the Hydraulic 6 module laid out next to each other with no hydraulic lines shown. In the assembly they would be aligned end-to-end inside the carbon fiber leg tube. Parts are numbered as follows: 1) reservoir, 2) motor, 3) micro pump, 4) manifold block, 5) electrical passthrough, 6) gas-diaphragm accumulator, and 7) cylinder.

At a total mass of 135 kg, Hydraulic-6 would be significantly lighter than most existing robots of this scale, especially the centralized hydraulic prototype that was never fully built. While the Hydraulic-6 modules have plenty of torque and can support the body without expending power, this module mass is prohibitive for Titan 6. Interestingly, the core actuator power train components (i.e. the batteries, motor, pump, oil, and pressure sensors together) have a mass of only 1.75 kg per module. However, the thick-walled steel infrastructure needed to support high-pressure hydraulics (i.e. the reservoir, manifold, accumulator, and cylinder) added an unmanageable amount of mass per joint. Testing and characterization of the Hydraulic-6 modules will continue despite the mass and speed problems; redesigning the infrastructure to reduce mass, using the upgraded micro pump, and optimizing the joint linkage for speed may shift this system closer to viability in the future.

In the end each model of Titan 6 was able to produce interesting results or inspire novel designs. The Harmonic-6 modules are moving forward to leg-level testing and soon after a full build of Titan 6. However, this will require the integration of high-level planning from Mat-6 and gait design from Hebi-6, the development of which will be discussed in Chapter V.

# Chapter V

# Robot Control and Experiments

Even when the electromechanical systems of a walking robot are fully capable, the performance is highly dependent on the robot's control scheme. Traditionally, controller design and testing takes place either on the final system or in a simulation. The compressed project timeline of Titan 6 necessitated parallel development of modular actuators and the robot controllers, so it was impossible to wait for Harmonic-6 and Hydraulic-6 to be viable before starting controller exploration. Despite huge advances in the capacity of simulation technology, it is often difficult to model unique properties of novel mechanical designs and their affect on the control architecture. Even with well-characterized components, factors such as sensor/communication noise [100], actuator backlash [60], foot slip [101], and mechanical hysteresis [102] are extremely difficult to model accurately in conjunction with the robot dynamics and each other. For each factor that affects the controllability and observability of the system, there are inherent assumptions baked into the model, and the interactions between these factors can be inadvertently ignored in even the most complete simulations [103]. Simulations are doomed to succeed [104] - given full control over the environment, physics, and system model, making adjustments to make a simulation successful can end up hurting validity. Simulated testing may result in optimizing a controller for the conditions of the simulation rather than the real world, which has spawned research in sim-to-real control [105]. However, sim-to-real transference and even the design of the simulator itself still requires intricate knowledge of the governing forces and key factors that most complicate the system controllability, even if it allows for

some uncertainty in the actual values. Titan 6 stands apart from existing robotic walkers, operating in its own quasi-dynamic regime with extremely low-frequency resonant modes and other uncommon factors to consider during controller design, which were unknown at the start of testing. For these reasons we eschewed simulation for full robot controller design, instead opting for an iterative design approach that enabled real-world controller tests on prototype robots that were subject to the same environmental conditions as the final Titan 6. Hebi-6 was built as one such testbed upon which we could derive and evaluate controllers. This chapter will detail the process of designing Hebi-6's balancing and walking controller and the lessons learned that will undoubtedly transfer to the final iteration of Titan 6.

# 1. Hebi-6 Control Structure

Titan 6 uses a hierarchical control structure to ensure that the system is fully modular and incrementally testable. This includes three levels of control: joint-level to account for 1-DoF position and force control, leg-level to manage leg kinematics and trajectories through the workspace, and body-level to handle balance and gaits, shown in Figure 5.1. This decouples the body and leg-level controllers from the
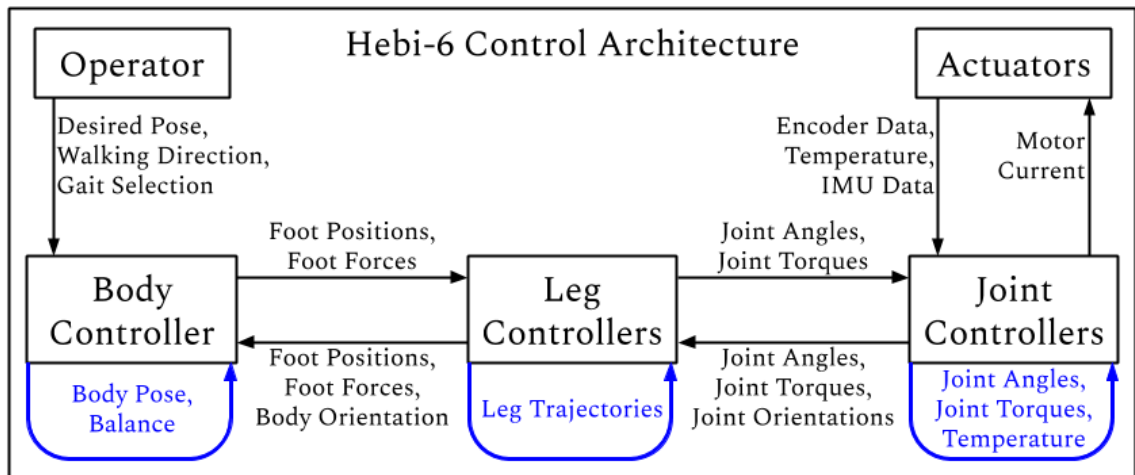


Figure 5.1: Visualization of the responsibilities of each controller (blue) and the communications between the controllers, system, and operator. Upstream communications indicate measurements and downstream communications indicate commands.

physical actuators, making the work done on Hebi-6 mostly transferable to Titan 6 with gain tuning adjustments for altered dynamics. The completed Hebi-6 is driven by a human operator to handle higher level planning for footstep placement and terrain navigation separately from balancing and gait control.

## Joint Control

Each Hebi X8-16 module contains an onboard computer that handles joint control independently of the rest of the system. This controller uses preprogrammed strategies to translate position, velocity, and torque commands into electrical current levels to send to the brushless DC motor driver. Encoders and series elastic elements provide position and force feedback, and the computer performs closed loop PID control. The computer and controller are preprogrammed as shown in Figure 5.2, but the PID gains for position and torque control have been custom tuned based on the module's location in the system. The $k_p$ and $k_d$ gains were tuned to eliminate high-frequency leg oscillations in swing, with the $k_i$ and punch gains set to remove steady state error while supporting large loads in stance. The differential hip modules share one set of gains, and the knee modules share another set.
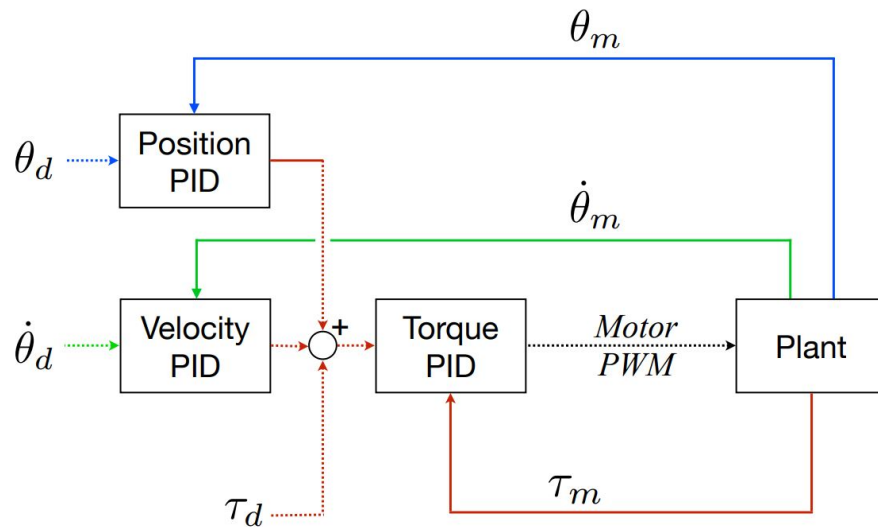


Figure 5.2: Block diagram showing the joint-level controllers running onboard the Hebi modules, from [106].

Thermocouples placed near the motor measure the winding temperature, which is used to limit the maximum current command when the module is above a preset safe temperature threshold. Additionally, each module contains an IMU, which an onboard pose filter uses to estimate module orientation. While the full orientation quaternion is reported, integrating accelerometer noise results in drift over time, making the module's yaw (orientation about the world frame z-axis) reporting unreliable. The joint controller reduces the module pose estimation to a gravity vector in the module's reference frame, which it sends to higher-level controllers for robot pose estimation.

## Leg Control

The leg-level control is an intermediate step in the control process, handling all of the kinematics and dynamics of leg motion. This mainly involves translating between joint angles and foot positions via the kinematic map (see Appendix A) and between foot forces and joint torques via the Jacobian (see Chapter II). Unlike other levels of control, there is no explicitly feedback-controlled parameter but rather a feedforward trajectory generation. Early testing with an isolated leg indicated that an intelligently chosen trajectory through the workspace with the joint-level controllers handling disturbance rejection on a lower level outperformed (with respect to minimizing leg oscillations) an explicit leg-level control loop on the foot position with dynamically suboptimal trajectories.

**Minimum Jerk Trajectories:** It has been noted that humans and other biological systems tend to move their limbs in such a manner to minimize the derivative of acceleration, or jerk, of the joints [107]. Given a set of waypoints with specified positions ($\theta_i$), velocities ($\dot{\theta}_i$), accelerations($\ddot{\theta}_i$), and timestamps ($t_i$), it is possible to find a unique function that minimizes the jerk of the motion using Eqs. 5.1 and 5.2.[1] Selecting waypoints in the joint space is most effective for minimizing the inertial effects of the motion on the system, but produces meandering end-effector positions in the workspace, which is unacceptable when the foot is in contact with the ground. For this reason we use minimum jerk trajectories in the joint space while the leg is in swing and minimum jerk trajectories in the foot workspace when in stance.

---

[1]The derivations for these equations can be found in [35].

$$
\begin{aligned}
T &= t_1 - t_0 \\
a_0 &= \theta_0 \\
a_1 &= \dot{\theta}_0 \\
a_2 &= 0.5 * \ddot{\theta}_0 \\
a_3 &= \frac{1}{2T^3}\left(20(\theta_1 - \theta_0) - (8\dot{\theta}_1 + 12\dot{\theta}_0)T - (3\ddot{\theta}_1 - \ddot{\theta}_0)T^2\right) \\
a_4 &= \frac{1}{2T^4}\left(-30(\theta_1 - \theta_0) + (14\dot{\theta}_1 + 16\dot{\theta}_0)T + (3\ddot{\theta}_1 - 2\ddot{\theta}_0)T^2\right) \\
a_5 &= \frac{1}{2T^5}\left(12(\theta_1 - \theta_0) - 6(\dot{\theta}_1 + \dot{\theta}_0)T - (\ddot{\theta}_1 - \ddot{\theta}_0)T^2\right)
\end{aligned}
\tag{5.1}
$$

$$
\theta(t) = a_5 t^5 + a_4 t^4 + a_3 t^3 + a_2 t^2 + a_1 t + a_0
\tag{5.2}
$$

## Body Control

The body-level control is responsible for balancing the robot as a whole, preventing falls and rejecting disturbances from foot slip, collisions, or inertial reactions of swing legs. At its core, this controller estimates the pose of the body and evaluates the correct action to take in response. It uses the positions and applied forces of the feet to adjust the robot's pose and walk as directed by the operator.

**Pose Estimation:** One unique benefit of the distributed modular approach to Hebi-6's design is allowing the twelve hip modules to combine measurements to filter IMU noise and generate a stable estimation of the body orientation. However, these modules are only rigidly coupled in pairs, none of which are directly attached to the body. Thus, the leg controller must transform the estimated gravity vector from the two modules that make up a hip to the body frame, introducing some noise based on the motion of the joint and backlash in the differential.

The body pose can also be calculated kinematically by Eqs. 5.3 and 5.4, since it is fully defined by knowledge of at least three foot contact points in the body frame. However, these equations require knowledge of the actual terrain slope angle, which must be estimated by the inertial sensing capabilities or a prior terrain map. Together, the leg kinematics (with ground contact detection) and inertial measurements provide suitably accurate estimation of the body pose in the world frame for control [108].

Table 5.1: Kinematic Pose Estimation Symbols

| Name | Symbol |
|---|---|
| Foot Position Vector | $[f_i]_r$ |
| Foot Position Matrix | $F_r$ |
| Foot Position Centroid | $\bar{F}_r$ |
| Singular Value Decomposition | $U\Sigma V^*$ |
| Foot Plane Normal Vector | $\hat{n}$ |
| Ground Normal Vector | $\hat{z}$ |
| Rotation Matrix From World to Body | $R_w^r$ |
| Pose Homogeneous Transform | $H_w^r$ |

$$F_r = \begin{bmatrix} [f_1]_r & \cdots & [f_n]_r \end{bmatrix}$$

$$F_r - \bar{F}_r = U\Sigma V^* \tag{5.3}$$

$$\hat{n} = U_{*,3}$$

$$c = \hat{z} \cdot \hat{n}$$

$$v = \hat{z} \times \hat{n}$$

$$[v]_\times = \begin{bmatrix} 0 & -v_3 & v_2 \\ v_3 & 0 & -v_1 \\ -v_2 & v_1 & 0 \end{bmatrix} \tag{5.4}$$

$$R_w^r = I + [v]_\times + [v]_\times^2 \frac{1}{1+c}$$

$$H_w^r = \begin{bmatrix} R_w^r & \bar{F}_r \\ \vec{0} & 1 \end{bmatrix}$$

**Body Stabilization:** The flexibility of Hebi-6's series elastic actuators and long links combined with the near-saturation loads experienced by the joints and the high center of gravity make balancing a precarious act, even with a wide support polygon. Early tests without pose estimation revealed that a small disturbance in the form of a push on the body would send the robot into low-frequency ($\sim$1 Hz) oscillations as the eighteen joint controllers simultaneously tried to compensate for a body-level pose offset, as shown in Figure 5.3. Additionally, whenever a subset of the legs were raised as if in swing, the body would slowly roll/pitch and translate in the direction of a removed support leg, eventually tipping the entire system.

The implementation of a 4-DoF[2] body stabilization controller solved these problems by adding coordinated pose offsets based on feedback from the pose estimation. With separate PID controllers on the roll-pitch and x-y components of the body pose, Hebi-6 is robust to large forces ($\sim$100 N) on the body in the transverse plane, multiple legs in the air, and minor stance foot slippage. The roll-pitch controller focuses on large $k_p$ and $k_i$ gains to prevent falls by halting tipping before it approaches the limits where the base joints of each leg saturate. Resonance was never observed about any rotational axis, so the $k_d$ gain was kept small in these controllers. By contrast, the most important function of the x-y controller is to prevent oscillation in the transverse plane. These controllers had relatively small $k_p$ and large $k_d$ gains to discourage oscillation in favor of some compliance along these axes. The $k_i$ and punch gains were omitted here, with steady state error alleviated by taking a step in the direction of the pose displacement. This helps prevent the robot from pushing off of walls or obstacles it may be inadvertently in contact with; instead stepping away safely.
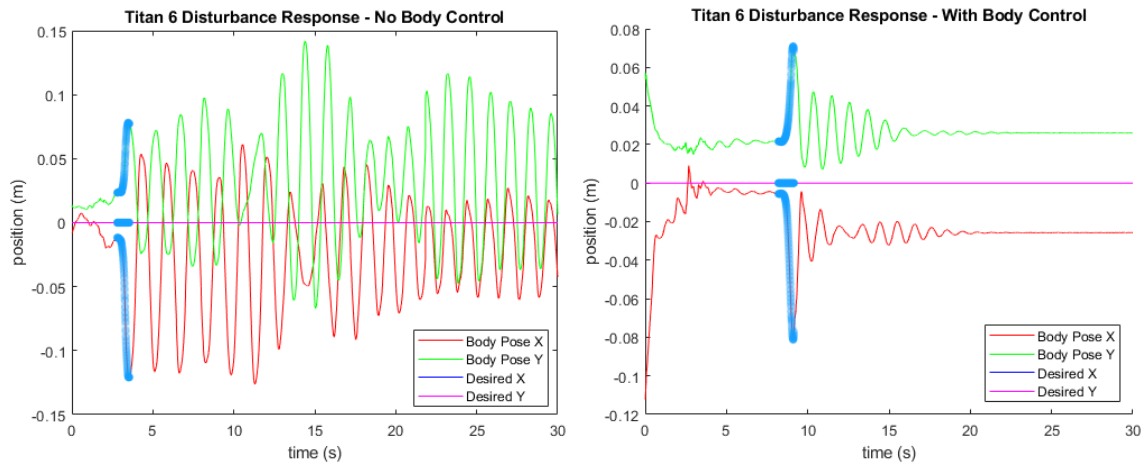


Figure 5.3: The pose estimation of Hebi-6's body after a small impulse is applied without a body-level feedback controller (left) and with the tuned balancing controller (right). The blue highlighted data indicates the time that the impulse was applied.

---

[2]Control of yaw was omitted due to inability to accurately estimate its value. Feedback control of z-translation was deemed unnecessary after implementing gravity compensation feedforward control.

**Gravity Compensation:** The above pose estimation with respect to the foot positions enables use of the Grasp Map described in Chapter II to calculate the expected stance foot forces required to balance the body. These forces are then fed back through the leg controllers to the joints as feedforward torque terms. Though the robot can balance and walk without this gravity compensation, as shown in Figure 5.4, its performance benefits from a prediction of the joint torques needed rather than expecting the low-level controllers to compensate for the robot's weight retroactively. This is only an estimate of the static load applied by the lumped mass of the robot, and may benefit from future expansion to include leg masses or an estimation of dynamic loads.
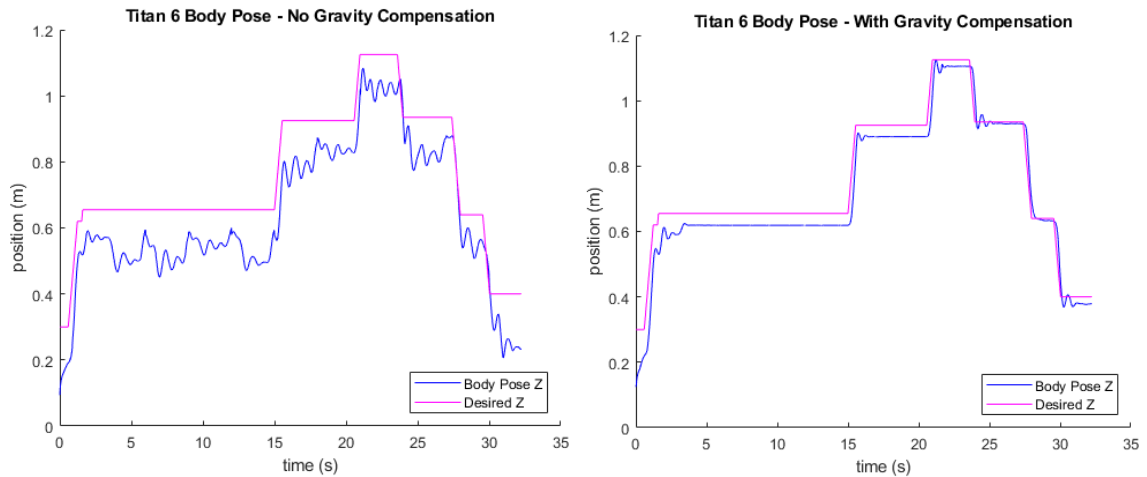


Figure 5.4: The measured height of Hebi-6's body while following a scripted pose trajectory using only feedback control (left) and with added feedforward gravity compensation (right). Clearly the gravity compensation aids in reference tracking and improves stability in stance. The remaining steady state error might be fixed with a feedback controller, but it falls within an acceptable error margin.

## 2.   Gait Design

With a robust body-level controller handling quasi-static balancing of Hebi-6 and trajectory generation built into the leg controllers, extending from balancing to walking is simple. The body stabilization automatically tries to restore the body pose to be in the center of the feet, but when it senses the combined xy-translation error

is above a certain threshold, a step is triggered. A step consists of $1 \leq N_l \leq 3$ legs lifting off of the ground and following minimum jerk trajectories to new positions centered on the current body pose. If possible, the controller will select the $N_l$ most "uncomfortable" legs to move, or those that are furthest from the current body pose. This ensures that the robot will follow a normal wave gait cycle automatically if the body is pushed far enough in one direction that multiple steps are required to recover posture. Step sizes naturally adjust to the speed and motion of the body until the body pose is within the stance threshold again.

With this balancing infrastructure in place, it follows that we can induce walking simply by commanding a pose shift in the desired direction and forcing the legs to catch up, as shown in Figure 5.5. As long as the pose command is outside of the step threshold, the robot will continue to walk in that direction while adjusting for disturbances. It is important that the body pose remain within the stable pose limit to stay viable, so the walk-inducing pose shift is limited to within a radius of the current foot center to ensure that the legs can always keep up with the body. Walking
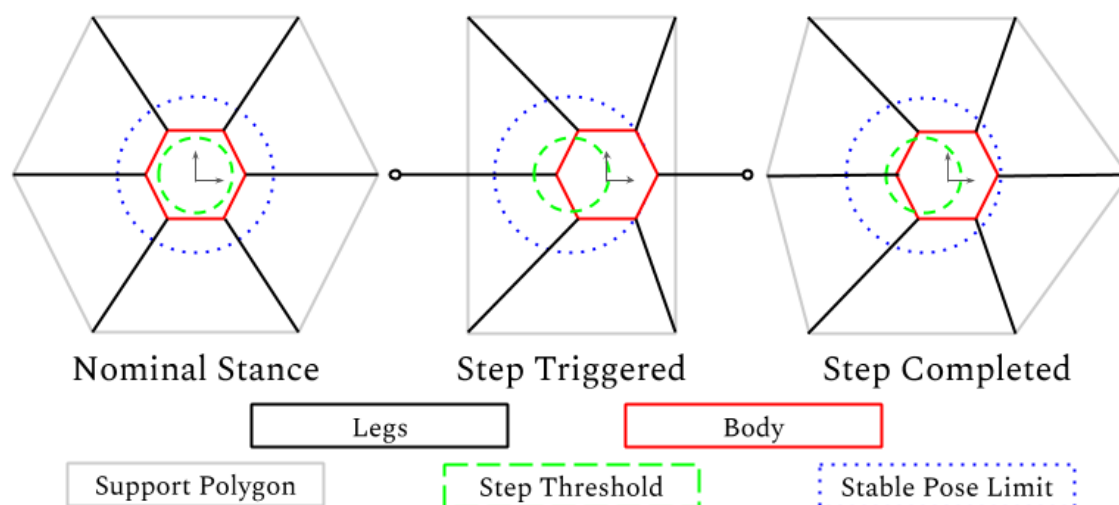


Figure 5.5: A representation of one cycle of the stepping pattern in which the robot is standing with its desired polygon of support (left), the robot is perturbed past the step threshold so it lifts two legs to take a step (center), and the step is completed so the body is back within the step threshold (left). Note that even if there are no further perturbations, the other two sets of legs will take steps to reset the polygon of support.

is sped up by the robot naturally falling in the direction of least support, which always coincides with the body lean direction. By adjusting the pose of the robot in the desired direction of motion, we can direct the falling motion while the legs are in swing, provided that those legs return to stance in appropriate positions to catch the body.

With this basic stepping control to maintain balance in place, the only explicitly designed gait parameters are the step threshold radius and the number of swing legs. It is important to note that certain sets of legs always move together as a "virtual leg," though the step order of the virtual legs is nondeterministic. When $N_l = 2$, legs opposite each other move together (i.e. Legs 1/6, 2/5, or 3/4), and when $N_l = 3$, the virtual legs are alternating tripods (i.e. 1/4/6 or 2/3/5). The step threshold depends on $N_l$, because the radius of poses with viable support shrinks with fewer stance legs to support the suspended mass.

## 3. Results and Discussion

In a controlled testing environment, Hebi-6 has demonstrated stable walking that is robust to applied impulses and some obstacle collisions. As of the publication of this thesis, the maximum recorded speed is 0.1 m/s, far less than required for the final Titan 6 robot. Even though the actuation calculator indicates that the robot should be able to reach speeds of 1.0 m/s with the differential hip, it is hindered by its unfavorable dynamics. The geometric gait parameters affect walking speed, but the true limiting factor is step time, $t_s$, or the duration of one full step cycle. Assuming the robot always takes the largest possible step, the overall speed is inversely proportional to $t_s$. However, aggressive swing leg speeds are likely to produce destabilizing inertial effects through the base joint's reaction torque on the body. Minimum jerk trajectories are not well behaved for rushed motions of limbs, where the spline produced between $\theta_0$ and $\theta_1$ with $\dot{\theta}_0 = \dot{\theta}_1 = 0$ always has a large velocity spike at the center of the trajectory. As the joint controllers lag behind the requested velocity, error can build up though there is no opposing force other than the large inertia of the leg about the hip, leading to overshooting the desired foot position or setting off leg oscillations. Instead, we may consider a ramp-up/ramp-down trajectory that quickly accelerates to the module's maximum speed then back down. Attempts to reduce leg

inertia by pulling the leg closer to the body during the fast swing instead introduced inertial effects about the hip joint, which is effectively more destabilizing because this disturbance is along the shortest chord of the support polygon.

Interest in decreasing step time is not only to speed up system locomotion, but rather to improve stability by allowing for more rapid support polygon adjustment. Truly dynamic systems like like ATRIAS and Atlas are well known for their ability to take punishing shoves [19] and cross-checking [109] then backpedal quickly to regain footing. Right now, Hebi-6 (see Figure 5.6) is limited to more static pushing forces because step time is too large, but this may just be inherent to the system topology. Sprawled posture systems rely on their wide base of support, and Hebi-6 can simply lower its body when it experiences large forces. In a low stance, all external impulses are simply damped out by the body-level controller without needing to take a step unless the force is large and sustained.

However, while sprawled posture may outperform upright stance robots in push tests, it is evident from early test results that foot slip will be a pervasive problem throughout the Titan 6 models. Not only is the load distributed across six legs, reducing normal force at any one contact, but the leg shape also relies heavily on



Figure 5.6: The final iteration of the Hebi-6 robot standing in the testing area.

friction to maintain stance. If the angle between the tibia link and the ground normal vector is greater than approximately 20°, the leg is likely to slip out from under the robot. With the grasp map explicitly depending on the vertical force provided by that leg to support the body at that contact point, it can be difficult to recover from a slip if neighbor legs are in swing. Extending the step adjustment bandwidth would allow Hebi-6 to take smaller steps to keep the tibia link as upright as possible or even help the robot catch itself during a slip. This lesson has spurred the pursuit of better foot designs for future Titan 6 models. New feet are being manufactured to reduce slip in three ways: higher coefficients of friction from material selection and surface features, ability to sense normal force at the contact to more accurately model friction cones so the system stays away from limits, and shear force sensing to detect slip as early as possible to maximize time for the balance controller to adjust the stance.

Future work on the controllers may push Titan 6 further into the dynamic gait space. Energy based control [110] is particularly intriguing in the context of Hebi-6, which has very low-frequency resonant modes which are well within the control bandwidth of the joints. This control architecture focuses on the energy stored in an underactuated system, particularly kinetic energy such as that in a resonating structure, and can execute otherwise impossible maneuvers by incrementally adding energy to the system. While typically considered in the context of pendulums [111], energy based control has been applied to pseudo-passive legged systems with some success [112]. I believe that energy based control may be the key to control of large, flexible robots with actuators that operate near saturation, like Hebi-6. This approach may produce interesting dynamic behaviors such as running with landing and push-off forces timed to add energy to and draw energy from the swaying of the body. Early testing with the series elastic actuators on Hebi-6 indicated that they were inefficient at storing potential energy in the statically loaded spring element, but the system could maintain resonant swaying with little input power. With much faster step times and a body-level control overhaul, it could be possible to dynamically swing the body, opportunistically taking a step with the furthest leg from the current body pose in a motion not unlike that of a rotary engine.

# Chapter VI

# Conclusions

In this thesis I have demonstrated design and control of large, modular hexapods, with exciting prospects for the future culmination of work set forth here. This is accomplished using a methodology specialized for a long-legged system such as Titan 6. It begins with the determination of stability criterion, which dictates the control regime and much of the robot's topology and posture. Then we choose the leg and body kinematics of the system which allows us to estimate of joint-level requirements for speed and torque. Here this is accomplished using the Hexapod Actuation Calculator App, which has been customized for the Titan 6 sprawled posture system, but is extensible to other statically stable arrangements of legs. Next, the key to a successful robot is meeting these requirements with the appropriate actuator technology, especially in the main power train of a module; characteristic properties of each element must be considered carefully along with how they can be leveraged to benefit the system as a whole. Using the selected core technology, actuators can then be designed to meet requirements based on early estimations of desired robot behaviors from simulations and system prototypes. Several iterations of these designs are necessary to optimize performance and ensure the final system is fully capable of meeting expectations. Competing actuator models can be especially useful in forcing parallel evolution of a design that avoids the pitfalls of fixating in on a single path by keeping the team focused on the larger goal and open to the unique benefits afforded by differing actuation systems. Finally, hierarchical testing of the joint, leg, and system works well alongside hierarchical controller development to create

a coherent modular system that retains local functionality even when leg geometry changes or when broken down into constituent actuators. This methodology provides plenty of room for building on existing ideas or combining intrinsic component aspects to form a unique whole that is greater than the sum of its parts. The associated tools, research, analysis, and design philosophy have guided the impending creation of Titan 6, the world's largest modular walking robot.

# 1.  Contributions

The practice described above is largely accepted for building legged robots, but here it is specifically adapted for modular systems which must utilize one common universal actuator design across all joints and for projects with relatively short lifetimes. The issue of sharing the load and speed requirements evenly across all modules is solved using the differential hip. Though this mechanism is similar to those used in robot wrists [113], it is designed specifically to bear the load of a large robot safely. Also, the idea that it exists as an extramodular transmission to act as two virtual joints with varying speed and torque requirements is relatively new. Additionally, the background research and literature review in Chapter III provides rationale for component selections and consolidates my research and design experience into a stand-alone guide to robot joint design for future students and engineers. Finally, I present Harmonic-6 and Hydraulic-6: two styles of modular systems in which each joint is fully self-sufficient while remaining deployable and capable as a coherent system using a control architecture prototyped in Chapter V. A more detailed breakdown of contributions within the team can be found in Appendix B. Titan 6 builds upon many legged robots that come before it, and while its components are all well-proven in the field of robotics, it will demonstrate modularity and mobility unlike any prior system.

# 2.  Future Work

The Titan 6 project still has significant development ahead before a final modular architecture can be implemented and deployed. Further characterization of the

performance of the Harmonic-6 and Hydraulic-6 actuators on a single-leg test stand is needed before the chosen system can be iterated upon and built. Even when the combined planning from Mat-6, controls from Hebi-6, and actuators from Harmonic-6/Hydraulic-6 are fused into the final Titan 6, there will still be significant development time spent on improving robustness of control over uneven terrain, especially low-level autonomy for foot placement and waypoint following so that search and rescue operators can focus on operation goals rather than explicitly driving the system.

However, an avenue of research that is similarly interesting is the exploration of the design space for robots made using a combination of multiple types of actuator unified under the same modular architecture. The project goals of Titan 6 focused on creating a single joint that could handle the task of any in the system, but the possibilities for building both mobile and fixed-base robots from a combination of modules developed during this project are endless. The prospect of quickly assembling or reconfiguring robots in the field to adapt to live requirement updates for any deployment scenario is truly exciting research. The success of the nascent Titan 6 modularity research presented here could spark a new chapter in adaptable field robotics.

# Appendix A

# Robot Kinematic Description

A kinematic chain of $n$ joints can be described by $4 \times n$ parameters, known as the Denavit-Hartenberg Parameterization, $[a, d, \alpha, \theta]$, called out on the leg model in Figure A.1. These parameters can be used to algorithmically generate the forward kinematic map (from $\vec{\theta}$ to $\vec{x}$) with Eq. A.1 and A.2[1]. Tables A.1, A.2, and A.3 describe the kinematics of the various models of Titan 6.
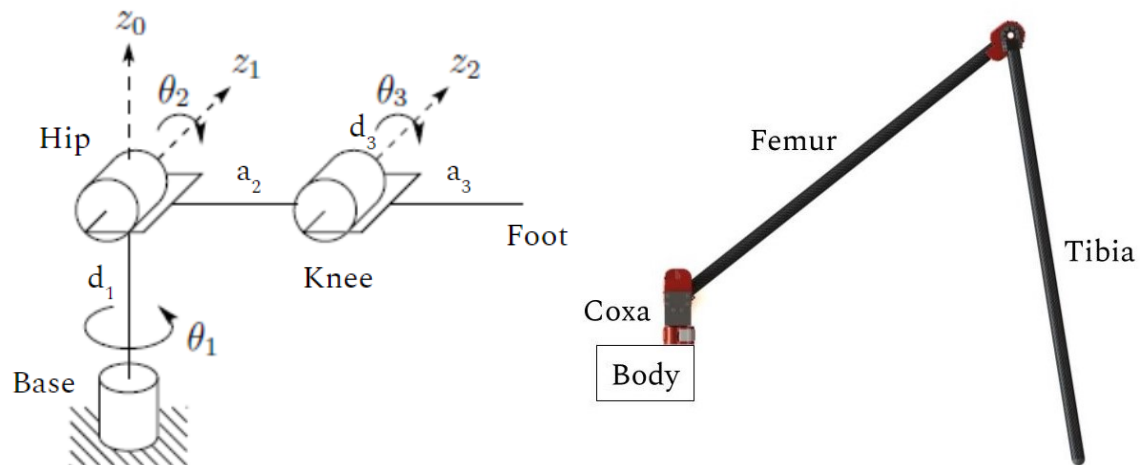


Figure A.1: Generalized kinematic model of the Titan 6 legs with joint names and parameters called out, adapted from [33] (left) and an early CAD model of a Titan 6 leg with link names called out (right) [replicated from Chapter II].

---

[1] $s(\theta)$ and $c(\theta)$ are shorthand for $\sin(\theta)$ and $\cos(\theta)$ respectively.

$$
H_{i-1}^i = \begin{bmatrix} c(\theta_i) & -s(\theta_i)c(\alpha_i) & s(\theta_i)s(\alpha_i) & a_i c(\theta_i) \\ s(\theta_i) & c(\theta_i)c(\alpha_i) & -c(\theta_i)s(\alpha_i) & a_i s(\theta_i) \\ 0 & s(\alpha_i) & c(\alpha_i) & d_i \\ 0 & 0 & 0 & 1 \end{bmatrix}
\tag{A.1}
$$

$$
H_0^n = H_0^1 \dots H_{n-1}^n
\tag{A.2}
$$

Table A.1: Hebi-6 Denavit-Hartenberg Parameters

| $i$ | 1 | 2 | 3 |
|---|---|---|---|
| $a_i$ | 0 | 1.0 | 1.0 |
| $d_i$ | 0.096 | 0 | $-0.085$ |
| $\alpha_i$ | 1.571 | 0 | 0 |
| $\theta_i$ | $\theta_1^*$ | $\theta_2^*$ | $\theta_3^*$ |

* These values are variable; driven by the actuator at that joint.

Table A.2: Harmonic-6 Denavit-Hartenberg Parameters

| $i$ | 1 | 2 | 3 |
|---|---|---|---|
| $a_i$ | 0 | 0.711 | 1.264 |
| $d_i$ | 0.060 | 0 | 0 |
| $\alpha_i$ | 1.571 | 0 | 0 |
| $\theta_i$ | $\theta_1^*$ | $\theta_2^*$ | $\theta_3^*$ |

* These values are variable; driven by the actuator at that joint.

Table A.3: Hydraulic-6 Denavit-Hartenberg Parameters

| $i$ | 1 | 2 | 3 |
|---|---|---|---|
| $a_i$ | 0 | 1.0 | 11.0 |
| $d_i$ | 0.057 | 0 | 0 |
| $\alpha_i$ | 1.571 | 0 | 0 |
| $\theta_i$ | $\theta_1^*$ | $\theta_2^*$ | $\theta_3^*$ |

* These values are variable; driven by the actuator at that joint.

The inverse kinematic map converts from end-effector positions, $\vec{x}$, to joint angles, $\vec{\theta}$, allowing for trajectory generation through the workspace. Because all models of Titan 6 use the same general joint configuration, Eq. A.3, A.4, and A.5 are applicable to Hebi-6, Harmonic-6, and Hydraulic-6 with the appropriate parameters substituted in.

$$l = \sqrt{x^2 + y^2 - d_3^2} \qquad\qquad r = \sqrt{l^2 + (z - d_1)^2}$$

$$\theta_1 = tan^{-1}\left(\frac{y}{x}\right) + tan^{-1}\left(\frac{d_3}{l}\right) \tag{A.3}$$

$$\theta_2 = tan^{-1}\left(\frac{z - d_1}{l}\right) - cos^{-1}\left(\frac{a_3^2 - r^2 - a_2^2}{-2a_2 r}\right) \tag{A.4}$$

$$\theta_3 = cos^{-1}\left(\frac{r^2 - a_2^2 - a_3^2}{-2a_2 a_3}\right) - \pi \tag{A.5}$$

The above kinematic mappings transform from the leg frame to the foot frame. Each leg has a static transform to the robot's body frame, found in Eq. A.6 as a rotation about the z-axis and a translation along the x-axis. The radii of leg attachment points, $r_{leg}$, for Hebi-6, Harmonic-6, and Hydraulic-6 are 0.165 m, 0.207 m, and 0.279 m respectively. The angles of rotation for legs $l_i = [1, 2, 3, 4, 5, 6]$ are $\phi_i = [30°, 330°, 90°, 270°, 150°, 210°]$ respectively.

$$H_r^l = \begin{bmatrix} c(\phi_i) & -s(\phi_i) & 0 & r_{leg}c(\phi_i) \\ s(\phi_i) & c(\phi_i) & 0 & r_{leg}s(\phi_i) \\ 0 & 0 & 1 & 0 \\ 0 & 0 & 0 & 1 \end{bmatrix} \tag{A.6}$$

# Appendix B

# Distribution of Contributions

The Titan 6 project was performed by a large team in the Carnegie Mellon Biorobotics Laboratory. This document closely follows my contributions in particular, mostly omitting separate tracks of research to be published separately. However, my contributions are deeply intertwined with the work of certain staff members. In particular, the actuator technology review was conducted together with Lu Li, the Harmonic-6 module design was led by Yizhu Gu, and the Hydraulic-6 module design was led by Ralph Boirum. A summary of personnel and contributions is provided in Table B.1.

Table B.1: Titan 6 Personnel and Roles

| Name | Role | Main Contribution |
| --- | --- | --- |
| Howie Choset | Robotics Professor | Principal Investigator |
| Matt Travers | Systems Scientist | Principal Investigator |
| H. Benjamin Brown | Project Scientist | Harmonic-6 Mechanical |
| Ralph Boirum | Project Staff | Hydraulic-6 Mechanical |
| Yizhu Gu | Project Staff | Harmonic-6 Mechanical |
| Charles Hart | Project Staff | Harmonic-6 Electrical/Firmware |
| Lu Li | Project Staff | Harmonic-6 Electrical/Firmware |
| Jim Picard | Project Staff | General Mechanical/Fabrication |
| Mike Schwerin | Project Staff | Harmonic-6 Electrical/Firmware |
| Nathan Shoemaker-Trejo | Project Staff | General Mechanical |
| Peng Yin | Project Staff | Perception/SLAM |
| Tim Angert | Shop Manager | General Mechanical/Fabrication |
| Zhaoyuan Gu | Graduate Student | Mat-6/Hebi-6 Controls |
| Evan Harber | Graduate Student | Force Sensing Feet |
| Ruixin Liu | Graduate Student | Hebi-6 Controls |
| Sara Misra | Graduate Student | Force Sensing Feet |
| Justin Mitchell | Graduate Student | Harmonic-6 Mechanical |
| Evan Schindewolf | Graduate Student | Force Sensing Feet |
| Shuo Yang | Graduate Student | Mat-6/Hebi-6 Controls |
| Peter Bi | Student Intern | Hebi-6 Electrical |
| Victoria Britcher | Student Intern | Test Equipment |
| Annie Chen | Student Intern | General Mechanical/Fabrication |
| Michael Fernandez | Student Intern | Mat-6 Controls |
| Mitrhil Hugunin | Student Intern | Hebi-6/Harmonic-6 Mechanical |
| Nalini Jain | Student Intern | Hebi-6 Mechanical |
| Jay Maier | Student Intern | Centralized Hydraulics |
| Grayson Moyer | Student Intern | General Electrical |
| Victoria Ortega | Student Intern | General Fabrication |
| Xinyu Wang | Student Intern | Force Sensing Feet |
| James Wong | Student Intern | General Mechanical/Fabrication |
| Joey Wood | Student Intern | Custom Cycloidal Drive |

# Bibliography

[1] D. W. Anthony, *The Horse the Wheel and Language: How Bronze-Age Riders from the Eurasian Steppes Shaped the Modern World.* Princeton University Press, 2007. 1

[2] T. T. Vong, G. A. Haas, and C. L. Henry, "NATO reference mobility model (NRMM) modeling of the DEMO III experimental unmanned ground vehicle (XUV)," *Army Research Laboratory*, Apr 1999. 1

[3] M. H. Raibert, *Legged Robots That Balance.* The MIT Press, 1986. 1

[4] R. Altendorfer, E. Moore, H. Komsuoglu, M. Buehler, H. Brown, D. McMordie, U. Saranli, F. RJ, and D. Koditschek, "RHex: A biologically inspired hexapod runner," *Autonomous Robots*, vol. 11, pp. 207–213, 11 2001. 2, 3

[5] M. Raibert, K. Blankespoor, G. Nelson, and R. Playter, "BigDog, the rough-terrain quadruped robot," *IFAC Proceedings Volumes*, vol. 41, no. 2, pp. 10822–10825, 2008. 2, 6, 24

[6] J. Bares, M. Hebert, T. Kanade, E. Krotkov, T. Mitchell, R. Simmons, and W. Whittaker, "Ambler: An autonomous rover for planetary exploration," *Computer*, vol. 22, no. 6, pp. 18–26, 1989. 2, 5

[7] B. H. Wilcox, "ATHLETE: A cargo and habitat transporter for the moon," *2009 IEEE Aerospace Conference*, 2009. 2, 5

[8] A. Ferworn, C. Wright, J. Tran, C. Li, and H. Choset, "Dog and snake marsupial cooperation for urban search and rescue deployment," *2012 IEEE International Symposium on Safety, Security, and Rescue Robotics (SSRR)*, 2012. 2

[9] C. Wright, A. Buchan, B. Brown, J. Geist, M. Schwerin, D. Rollinson, M. Tesch, and H. Choset, "Design and architecture of the unified modular snake robot," *2012 IEEE International Conference on Robotics and Automation*, 2012. 2, 37

[10] P. Hebert, M. Bajracharya, J. Ma, N. Hudson, A. Aydemir, J. Reid, C. Bergh, J. Borders, M. Frost, M. Hagman, and et al., "Mobile manipulation and mobility as manipulation-design and algorithms of RoboSimian," *Journal of Field Robotics*, vol. 32, no. 2, pp. 255–274, 2015. 2, 8, 12

[11] S. Aharon, B. A. Huber, and E. Gavish-Regev, "Daddy-long-leg giants: revision of the spider genus artema walckenaer, 1837 (araneae, pholcidae)," *European Journal of Taxonomy*, Aug 2017. 3

[12] C. M. Hubicki, *From Running Birds to Walking Robots: Optimization as a Unifying Framework for Dynamic Bipedal Locomotion.* PhD thesis, Oregon State University, 2015. 3

[13] S. Kalouche, N. Wiltsie, H. J. Su, and A. Parness, "Inchworm style gecko adhesive climbing robot," *2014 IEEE/RSJ International Conference on Intelligent Robots and Systems*, 2014. 3

[14] S. Seok, A. Wang, M. Y. Chuah, D. J. Hyun, J. Lee, D. M. Otten, J. H. Lang, and S. Kim, "Design principles for energy-efficient legged locomotion and implementation on the MIT Cheetah robot," *IEEE/ASME Transactions on Mechatronics*, vol. 20, no. 3, pp. 1117–1129, 2015. 3, 6

[15] S. Hirose, Y. Fukuda, K. Yoneda, A. Nagakubo, H. Tsukagoshi, K. Arikawa, G. Endo, T. Doi, and R. Hodoshima, "Quadruped walking robots at Tokyo Institute of Technology," *IEEE Robotics & Automation Magazine*, vol. 16, no. 2, pp. 104–114, 2009. 5

[16] J. E. Bares and D. S. Wettergreen, "Dante II: Technical description, results, and lessons learned," *The International Journal of Robotics Research*, vol. 18, no. 7, pp. 621–649, 1999. 5, 12

[17] S. Kalouche, D. Rollinson, and H. Choset, "Modularity for maximum mobility and manipulation: Control of a reconfigurable legged robot with series-elastic actuators," *2015 IEEE International Symposium on Safety, Security, and Rescue Robotics (SSRR)*, 2015. 5, 8

[18] A. Elfes, R. Steindl, F. Talbot, F. Kendoul, P. Sikka, T. Lowe, N. Kottege, M. Bjelonic, R. Dungavell, T. Bandyopadhyay, and et al., "The Multilegged Autonomous eXplorer (MAX)," *2017 IEEE International Conference on Robotics and Automation (ICRA)*, 2017. 5, 42

[19] C. Hubicki, J. Grimes, M. Jones, D. Renjewski, A. Sprwitz, A. Abate, and J. Hurst, "ATRIAS: Design and validation of a tether-free 3D-capable spring-mass bipedal robot," *The International Journal of Robotics Research*, vol. 35, pp. 1497–1521, Nov 2016. 5, 6, 83

[20] M. H. Raibert, H. B. Brown, M. Chepponis, J. Koechling, J. K. Hodgins, D. Dustman, W. K. Brennan, D. S. Barrett, C. M. Thompson, J. D. Hebert, W. Lee, and L. Borvansky, "Dynamically stable legged locomotion," *Technical report 1179 LL-6*, Jan 1989. 6

[21] M. Hutter, C. Gehring, M. Bloesch, M. A. Hoepflinger, C. D. Remy, and R. Siegwart, "StarlETH: A compliant quadrupedal robot for fast, efficient, and

versatile locomotion," *Adaptive Mobile Robotics*, pp. 483–490, 2012. 6

[22] S. Kuindersma, R. Deits, M. Fallon, A. Valenzuela, H. Dai, F. Permenter, T. Koolen, P. Marion, and R. Tedrake, "Optimization-based locomotion planning, estimation, and control design for the ATLAS humanoid robot," *Autonomous Robots*, vol. 40, no. 3, pp. 429–455, 2015. 6

[23] E. Guizzo, "Boston Dynamics' Spot robot dog goes on sale," *IEEE Spectrum: Technology, Engineering, and Science News*, Sep 2019. 6

[24] U. Saranli, M. Buehler, and D. E. Koditschek, "RHex: A simple and highly mobile hexapod robot," *The International Journal of Robotics Research*, vol. 20, no. 7, pp. 616–631, 2001. 6

[25] R. Altendorfer, D. E. Koditschek, and P. Holmes, "Stability analysis of a clock-driven rigid-body SLIP model for RHex," *The International Journal of Robotics Research*, vol. 23, no. 10-11, pp. 1001–1012, 2004. 6

[26] A. M. Johnson, M. T. Hale, G. C. Haynes, and D. E. Koditschek, "Autonomous legged hill and stairwell ascent," *2011 IEEE International Symposium on Safety, Security, and Rescue Robotics*, 2011. 6

[27] H. Choset and M. Travers, "Titan-6: Large-scale modular hexapod robot," *ONR Project Proposal*, 2018. 7

[28] M. Yim, D. G. Duff, and K. D. Roufas, "PolyBot: A modular reconfigurable robot," in *ICRA*, pp. 514–520, 2000. 8

[29] P. Hebert, J. Ma, J. Borders, A. Aydemir, M. Bajracharya, N. Hudson, K. Shankar, S. Karumanchi, B. Douillard, J. Burdick, and et al., "Supervised remote robot with guided autonomy and teleoperation (SURROGATE): A framework for whole-body manipulation," *2015 IEEE International Conference on Robotics and Automation (ICRA)*, 2015. 8

[30] A. G. Curtis, J. Nash, S. Higa, J. J. Hoschchild, and A. Parness, "IceWorm: Ice climbing robots for glaciology and beyond," *AGU Fall Meeting Abstracts*, Dec 2018. 8

[31] G. Kenneally, A. De, and D. E. Koditschek, "Design principles for a family of direct-drive legged robots," *IEEE Robotics and Automation Letters*, vol. 1, no. 2, pp. 900–907, 2016. 11, 36

[32] S. Kalouche, "GOAT: A legged robot with 3D agility and virtual compliance," *2017 IEEE/RSJ International Conference on Intelligent Robots and Systems (IROS)*, 2017. xiv, 11, 36, 37

[33] M. W. Spong, S. Hutchinson, and M. Vidyasagar, *Robot Modeling and Control*. Wiley, 2006. xiii, 12, 89

[34] F. Tedeschi and G. Carbone, "Design issues for hexapod walking robots,"

*Robotics*, vol. 3, pp. 181–206, Oct 2014. 14

[35] K. Kyriakopoulos and G. Saridis, "Minimum jerk path generation," *Proceedings. 1988 IEEE International Conference on Robotics and Automation*, 1988. 15, 76

[36] L. Han, J. Trinkle, and Z. Li, "Grasp analysis as linear matrix inequality problems," *Proceedings 1999 IEEE International Conference on Robotics and Automation (Cat. No.99CH36288C)*, 1999. 15

[37] L. Dong and B. Nelson, "Tutorial - robotics in the small part II: Nanorobotics," *IEEE Robotics & Automation Magazine*, vol. 14, no. 3, pp. 111–121, 2007. 19

[38] "Wartsila Sulzer RTA96-C / Engine." Available: `www.emma-maersk.com/engine/Wartsila_Sulzer_RTA96-C.htm`, 2007. 19

[39] J. Whitman, N. Zevallos, M. Travers, and H. Choset, "Snake robot urban search after the 2017 Mexico City earthquake," *2018 IEEE International Symposium on Safety, Security, and Rescue Robotics (SSRR)*, 2018. 19

[40] R. S. Pierre and S. Bergbreiter, "Gait exploration of sub-2 g robots using magnetic actuation," *IEEE Robotics and Automation Letters*, vol. 2, no. 1, pp. 34–40, 2017. 20

[41] F. Larsson, P. Andersson, P. Blomqvist, and B.-E. Mellander, "Toxic fluoride gas emissions from lithium-ion battery fires," *Scientific Reports*, vol. 8, no. 1, 2018. 21

[42] S. Scoles, "Samsung isn't the only one with lithium ion battery problems. just ask NASA." Available: `media.wired.com/photos/5926a837cfe0d93c47430f84/master/w_582,c_limit/robot-explosion.gif`, Jun 2017. xiii, 22

[43] B. D. McCloskey, "Expanding the Ragone Plot: Pushing the limits of energy storage," *The Journal of Physical Chemistry Letters*, vol. 6, no. 18, pp. 3592–3593, 2015. 22

[44] L. Hall, "Automaton rover for extreme environments (AREE)." Available: `www.nasa.gov/directorates/spacetech/niac/2017_Phase_I_Phase_II/Automaton_Rover_Extreme_Environments/`, Apr 2017. 23

[45] "Mainspring." Available: `en.wikipedia.org/wiki/Mainspring`, Aug 2019. xiii, 23

[46] D. F. B. Haeufle, M. D. Taylor, S. Schmitt, and H. Geyer, "A clutched parallel elastic actuator concept: Towards energy efficient powered legs in prosthetics and robotics," *2012 4th IEEE RAS & EMBS International Conference on Biomedical Robotics and Biomechatronics (BioRob)*, 2012. xiii, 23

[47] J. C. Conklin and J. P. Szybist, "A highly efficient six-stroke internal combustion engine cycle with water injection for in-cylinder exhaust heat recovery," *Energy*, vol. 35, no. 4, pp. 1658–1664, 2010. 23

[48] J. Townsend, J. Biesiadecki, and C. Collins, "ATHLETE mobility performance with active terrain compliance," *2010 IEEE Aerospace Conference*, 2010. 24

[49] "Energy density." Available: `en.wikipedia.org/wiki/Energy_density`, Oct 2019. xviii, 24

[50] H. Budde-Meiwes, J. Drillkens, B. Lunz, J. Muennix, S. Rothgang, J. Kowal, and D. U. Sauer, "A review of current automotive battery technology and future prospects," *Proceedings of the Institution of Mechanical Engineers, Part D: Journal of Automobile Engineering*, vol. 227, no. 5, pp. 761–776, 2013. xiii, 24, 25

[51] T. M. Jahns, G. B. Kliman, and T. W. Neumann, "Interior permanent-magnet synchronous motors for adjustable-speed drives," *IEEE Transactions on Industry Applications*, vol. IA-22, no. 4, pp. 738–747, 1986. 28

[52] D. Faustner, W. Kemmetmuller, and A. Kugi, "Field weakening in flatness-based torque control of saturated surface-mounted permanent magnet synchronous machines," *2015 IEEE Conference on Control Applications (CCA)*, 2015. xiv, 29

[53] K. Hameyer and R. Belmans, "Permanent magnet excited brushed DC motors," *IEEE Transactions on Industrial Electronics*, vol. 43, no. 2, pp. 247–255, 1996. 29

[54] R. Condit, "Brushed DC motor fundamentals," *Microchip Technology Inc.*, vol. AN905, 2004. 30

[55] S. Cetinkunt, *Mechatronics with Experiments*. Wiley, 2015. xiv, 30

[56] K. Balakrishnan, B. Umamaheswari, and K. Latha, "Estimation of rotor position and speed for hybrid stepper motor under various phase excitation schemes and compensated resonance," *2011 International Conference on Power Engineering, Energy and Electrical Drives*, 2011. 31

[57] "Stepper motor." Available: `en.wikipedia.org/wiki/Stepper_motor`, Sep 2019. xiv, 31

[58] M. Bodson, J. Chiasson, R. Novotnak, and R. Rekowski, "High performance nonlinear feedback control of a permanent magnet stepper motor," *The First IEEE Conference on Control Applications*, 1993. 31

[59] K. Dermitzakis, J. P. Carbajal, and J. H. Marden, "Scaling laws in robotics," *Procedia Computer Science*, vol. 7, pp. 250–252, 2011. 32

[60] L. Márton and B. Lantos, "Friction and backlash measurement and identification method for robotic arms," *2009 International Conference on Advanced Robotics*, pp. 1–6, 2009. 34, 73

[61] J. Brauer, "Transmission error in anti-backlash conical involute gear transmis-

sions: A global-local FE approach," *Finite Elements in Analysis and Design*, vol. 41, no. 5, pp. 431–457, 2005. 35

[62] C. He, Y. Zhang, and M. Meng, "Backlash compensation by neural-network online learning," *Proceedings 2001 IEEE International Symposium on Computational Intelligence in Robotics and Automation (Cat. No.01EX515)*, 2001. 35

[63] A. Bhatia, A. M. Johnson, and M. T. Mason, "Direct drive hands: Force-motion transparency in gripper design," *Robotics: Science and Systems*, 2019. 36

[64] H. Asada and T. Kanade, "Design of direct-drive mechanical arms," *Journal of Vibration and Acoustics*, vol. 105, pp. 312–316, Jan 1983. 36, 37

[65] T. Kanade and D. Schmitz, "Development of CMU Direct-Drive Arm II," *American Control Conference*, 1985. 36

[66] "Tiger Motor U8-10 170kv U-power professional motor." Available: `www.getfpv.com/tiger-motor-u8-10-170kv-u-power-professional-motor.html`. xiv, 37

[67] D. Rollinson, Y. Bilgen, B. Brown, F. Enner, S. Ford, C. Layton, J. Rembisz, M. Schwerin, A. Willig, P. Velagapudi, and et al., "Design and architecture of a series elastic snake robot," *2014 IEEE/RSJ International Conference on Intelligent Robots and Systems*, 2014. xiv, 37, 38, 51, 56

[68] H. Wei, Y. Cai, H. Li, D. Li, and T. Wang, "Sambot: A self-assembly modular robot for swarm robot," *2010 IEEE International Conference on Robotics and Automation*, 2010. 38

[69] E. Gouda, S. Mezani, L. Baghli, and A. Rezzoug, "Comparative study between mechanical and magnetic planetary gears," *IEEE Transactions on Magnetics*, vol. 47, no. 2, pp. 439–450, 2011. 39

[70] Y. Guo and R. G. Parker, "Purely rotational model and vibration modes of compound planetary gears," *Mechanism and Machine Theory*, vol. 45, no. 3, pp. 365–377, 2010. 39

[71] W. S. Lin, Y. P. Shih, and J. J. Lee, "Design of a two-stage cycloidal gear reducer with tooth modifications," *Mechanism and Machine Theory*, vol. 79, pp. 184–197, 2014. 39

[72] "CSF-11-30-2A-R." Available: `www.electromate.com/csf-11-30-2a-r/`. xiv, 40

[73] M. Mason, D. Pai, D. Rus, L. Taylor, and M. Erdmann, "A mobile manipulator," *Proceedings 1999 IEEE International Conference on Robotics and Automation (Cat. No.99CH36288C)*, 1999. 43

[74] Y.-J. Kim, "Design of low inertia manipulator with high stiffness and strength

using tension amplifying mechanisms," *2015 IEEE/RSJ International Conference on Intelligent Robots and Systems (IROS)*, 2015. xiv, 43, 44

[75] M. Shoham, "Twisting wire actuator," *Journal of Mechanical Design*, vol. 127, pp. 441–445, Jul 2004. xiv, 43, 44

[76] Y. Lu and D. Fan, "Transmission backlash of precise cable drive system," *Proceedings of the Institution of Mechanical Engineers, Part C: Journal of Mechanical Engineering Science*, vol. 227, pp. 2256–2267, Oct 2013. 43

[77] E. K. Shinseki, *Hydraulics*, vol. FM 5-499. Department of the Army Headquarters, C1 ed., 2001. xiv, 44, 45

[78] S. Alfayad, F. B. Ouezdou, F. Namoun, and G. Gheng, "High performance integrated electro-hydraulic actuator for robotics part I: Principle, prototype design and first experiments," *Sensors and Actuators A: Physical*, vol. 169, no. 1, pp. 115–123, 2011. 45

[79] S. Lee, J. Oh, Y. K. Lee, and J. Choi, "Development of micro hydraulic actuator for force assistive wearable robot," *IEEE ISR 2013*, 2013. 45

[80] H. Kaminaga, T. Yamamoto, J. Ono, and Y. Nakamura, "Backdrivable miniature hydrostatic transmission for actuation of anthropomorphic robot hands," *2007 7th IEEE-RAS International Conference on Humanoid Robots*, 2007. 45

[81] H. Kaminaga, J. Ono, Y. Nakashima, and Y. Nakamura, "Development of backdrivable hydraulic joint mechanism for knee joint of humanoid robots," *2009 IEEE International Conference on Robotics and Automation*, 2009. 45

[82] T. Morita and S. Sugano, "Design and development of a new robot joint using a mechanical impedance adjuster," *Proceedings of 1995 IEEE International Conference on Robotics and Automation*, 1995. 46

[83] A. Curtis, M. Martone, and A. Parness, "Roving on ice: Field testing an ice screw end effector and sample collection tool," *2018 IEEE Aerospace Conference*, 2018. 46

[84] M. Plooij, G. Mathijssen, P. Cherelle, D. Lefeber, and B. Vanderborght, "Lock your robot: A review of locking devices in robotics," *IEEE Robotics & Automation Magazine*, vol. 22, no. 1, pp. 106–117, 2015. xiv, 46

[85] J. L. Golden, "Anodized aluminum on LDEF," *Boeing Defense & Space Group*, 1993. 47

[86] H. Komsuoglu, D. McMordie, U. Saranli, N. Moore, M. Buehler, and D. Koditschek, "Proprioception based behavioral advances in a hexapod robot," *Proceedings 2001 ICRA. IEEE International Conference on Robotics and Automation (Cat. No.01CH37164)*, 2001. 51

[87] D. J. Hyun, S. Seok, J. Lee, and S. Kim, "High speed trot-running: Implemen-

tation of a hierarchical controller using proprioceptive impedance control on the MIT Cheetah," *The International Journal of Robotics Research*, vol. 33, no. 11, pp. 1417–1445, 2014. 51

[88] C. Ordonez, J. Shill, A. Johnson, J. Clark, and E. Collins, "Terrain identification for RHex-type robots," *Unmanned Systems Technology XV*, 2013. 51

[89] G. Pratt and M. Williamson, "Series elastic actuators," *Proceedings 1995 IEEE/RSJ International Conference on Intelligent Robots and Systems. Human Robot Interaction and Cooperative Robots*, 1995. 51

[90] D. Rollinson, S. Ford, B. Brown, and H. Choset, "Design and modeling of a series elastic element for snake robots," *ASME 2013 Dynamic Systems and Control Conference*, Oct 2013. xiv, 51

[91] J. Pratt, B. Krupp, and C. Morse, "Series elastic actuators for high fidelity force control," *Industrial Robot: An International Journal*, vol. 29, no. 3, pp. 234–241, 2002. 51

[92] J. W. Hurst, *The Role and Implementation of Compliance in Legged Locomotion.* PhD thesis, Carnegie Mellon University, 2008. 52

[93] N. Kashiri, J. Malzahn, and N. G. Tsagarakis, "On the sensor design of torque controlled actuators: A comparison study of strain gauge and encoder-based principles," *IEEE Robotics and Automation Letters*, vol. 2, no. 2, pp. 1186–1194, 2017. xv, 52

[94] M. Hashimoto, Y. Kiyosawa, and R. Paul, "A torque sensing technique for robots with harmonic drives," *IEEE Transactions on Robotics and Automation*, vol. 9, pp. 108–116, Feb 1993. 52

[95] "X-series actuator - technical specifications." Available: `docs.hebi.us/resources/datasheets/X-SeriesDatasheet.pdf`, 2018. 56

[96] "Retaining rings." Available: `www.mcmaster.com/retaining-rings`, 2019. 61

[97] K. Ueura and R. Slatter, "Development of the harmonic drive gear for space applications," *European Space Agency Publications*, vol. 438, pp. 259–264, 11 1999. 63

[98] C. Semini, N. G. Tsagarakis, E. Guglielmino, M. Focchi, F. Cannella, and D. G. Caldwell, "Design of HyQ  a hydraulically and electrically actuated quadruped robot," *Proceedings of the Institution of Mechanical Engineers, Part I: Journal of Systems and Control Engineering*, vol. 225, no. 6, pp. 831–849, 2011. 67

[99] V. G. Magorien, "Effects of air on hydraulic systems," *Hydraulics & Pneumatics*, 1967. 68

[100] N. Jakobi, P. Husbands, and I. Harvey, "Noise and the reality gap: The use of simulation in evolutionary robotics," *Advances in Artificial Life Lecture Notes*

*in Computer Science*, pp. 704–720, 1995. 73

[101] D. Marhefka and D. Orin, "A compliant contact model with nonlinear damping for simulation of robotic systems," *IEEE Transactions on Systems, Man, and Cybernetics - Part A: Systems and Humans*, vol. 29, no. 6, pp. 566–572, 1999. 73

[102] M. Ruderman, F. Hoffmann, and T. Bertram, "Modeling and identification of elastic robot joints with hysteresis and backlash," *IEEE Transactions on Industrial Electronics*, vol. 56, no. 10, pp. 3840–3847, 2009. 73

[103] M. Mckenna and D. Zeltzer, "Dynamic simulation of autonomous legged locomotion," *Proceedings of the 17th Annual Conference on Computer Graphics and Interactive Techniques - SIGGRAPH 90*, 1990. 73

[104] R. A. Brooks and M. J. Mataric, "Real robots, real learning problems," in *Robot Learning* (J. H. Connell and S. Mahadevan, eds.), vol. 233 of *The Springer International Series in Engineering and Computer Science (Knowledge Representation, Learning and Expert Systems)*, ch. 8, Springer, 1993. 73

[105] X. B. Peng, M. Andrychowicz, W. Zaremba, and P. Abbeel, "Sim-to-real transfer of robotic control with dynamics randomization," *2018 IEEE International Conference on Robotics and Automation (ICRA)*, 2018. 73

[106] D. Rollinson, *Control and Design of Snake Robots*. PhD thesis, Carnegie Mellon University, 2014. xvi, 75

[107] A. Piazzi and A. Visioli, "Global minimum-jerk trajectory planning of robot manipulators," *IEEE Transactions on Industrial Electronics*, vol. 47, no. 1, pp. 140–149, 2000. 76

[108] M. Bloesch, M. Hutter, M. Hoepflinger, S. Leutenegger, C. Gehring, C. D. Remy, and R. Siegwart, "State estimation for legged robots - consistent fusion of leg kinematics and IMU," *Robotics: Science and Systems VIII*, Sep 2012. 77

[109] M. Raibert, "Atlas, the next generation." Available: `https://www.youtube.com/watch?v=rVlhMGQgDkY`, Feb 2016. 83

[110] I. Fantoni, R. Lozano, and M. Spong, "Energy based control of the Pendubot," *IEEE Transactions on Automatic Control*, vol. 45, no. 4, pp. 725–729, 2000. 84

[111] X. Xin, J. H. She, T. Yamasaki, and Y. Liu, "Swing-up control based on virtual composite links for n-link underactuated robot with passive first joint," *Automatica*, vol. 45, no. 9, pp. 1986–1994, 2009. 84

[112] S. Collins, A. Ruina, R. Tedrake, and M. Wisse, "Efficient bipedal robots based on passive-dynamic walkers," *Science*, vol. 307, pp. 1082–1085, 2005. 84

[113] Microbot Inc., *Operation of the Five-Axis Robot Model TCM*. Microbot Inc., 2 ed., 1982. 86

[114] F. Duvallet, "RI Thesis Template." Available: `https://github.com/felixduvallet/ri-thesis-template`, 2017.